Design and Modelling of a Magnetic Fluid Based Artificial Muscle for Gait Rehabilitation

by

Thomas Harry Scone

A thesis submitted to the University of Birmingham for the degree of
DOCTOR OF PHILOSOPHY

Department of Mechanical Engineering
School of Engineering
College of Engineering and Physical Sciences
The University of Birmingham July 2022

Abstract

Robotic gait rehabilitation systems have seen a plateau in functional gait rehabilitation outcomes for hemiparetic stroke survivors over the past 5 years, particularly when using improvements in walking speed as a key metric. Research continues into various types of robotic systems, and many have been seen to increase rates of independent walking. Why then have improvements in users' walking speed remained sluggish? It is suggested that the issue may lie either in the design of the robotic systems themselves or in approach these systems take to providing training. A such a ground up approach is taken for this research into improving robotic gait rehabilitation techniques. This first required a closer look at how hemiparetic gait patterns vary with walking speed though this in turn necessitated consideration of the targeting effect. Caused by the presence of a distinctly marked shape along their path, this effect was found to have no significant impact on the kinematic parameters of hemiparetic stroke survivors. This allowed gait analysis into the kinematic gait patterns of stroke survivors to be carried out and relationships between said pattern and the participants walking speed to be obtained. It was found that there existed compensatory gait techniques that related to walking speed and it was suggested that these could be encouraged as beneficial traits to improve functional rehabilitation outcomes. This still left the consideration of the robotic system itself though. Soft robotics and smart materials had been suggested as a potential avenue for designing improved robotic systems that would allow for high user engagement and autonomy while removing the tethering common in current designs. A magnetic fluid muscle design and FEA model was proposed and validated. The design was iterated on using the FEA model to improve its functionality and gather details about its potential for use in gait rehabilitation.

Acknowledgements

I wish to express my gratitude to my supervisor, Dr. Mozafar Saadat, for his continued support throughout what was, on occasion, an arduous and difficult project. His willingness to support my decisions and ability to keep my head up and my focus on the end goals of my PhD have helped me through to this point.

I would also like to thank my secondary supervisor for his support, Dr. Marco Castellani. His technical help and his ability to listen to my problems and his belief in my work was much appreciated. In addition, the smaller talks, recommendations and help from Dr David Punt and Dr Daniel Espino were valuable and not forgotten.

Throughout this work my partner Hannah Barton has been my most steadfast supporter. Her friendship, love and invaluable insight have time and again helped me through the most difficult periods in this project.

Finally, my parents, Catherine and Steven Scone have always been behind me unwaveringly throughout all my studies for which I will always be grateful. They have never ceased to offer their love, time, and support. I would not be half the person I am today without them.

Table of Contents

List of Illustrations

List of Tables

Chapter 1 – Introduction

1.1.1. Background

An array of current robotic systems meant for gait rehabilitation have been shown to have no significant impact on key gait rehabilitation outcomes, in particular walking speed (1). While effective at improving outcome rates of independent walking, which is itself an important milestone, robotic gait rehabilitation requires continued research to achieve the full range of benefits that were initially expected (2, 3).

One of the key concerns that has been raised is lack of user engagement, i.e. the system moving the stroke survivor's limbs without any actual input on their part (4). The Path Control technique was developed for use on the Lokomat (shown below in Figure 1.1) partially to alleviate these issues and encourages active user participation by allowing the user to influence the timing, and to some extent the path, of their leg movements (5, 6). This form of user conscious robotic rehabilitation has seen continued development but a question that should be asked is how is this optimal gait pattern decided for a user?

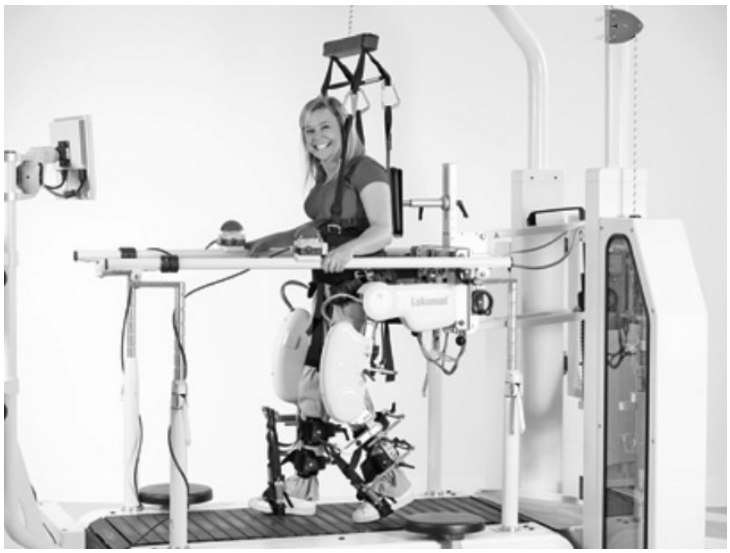

Figure 1.1: The Lokomat robot (6)

Traditionally, the asymmetry of hemiparetic gait has been seen as a key evaluation criterion, and sometimes part of the problem that must be addressed (7). Indeed, when the self-selected walking speed and step lengths were evaluated a broad correlation was found between increased walking speeds and greater step symmetry (8). Interestingly though, when broken down by impairment severity it was found that stroke survivors classified as severely hemiparetic were still able to achieve improvements in their walking speeds even with a non-symmetric gait pattern.

While full recovery is of course the highest aim that gait rehabilitation can achieve an equally important outcome is functional recovery, potentially best exemplified by self-selected walking speed. Studies have shown walking speed to be closely linked to increased ambulatory levels, reduction in the occurrence of post-stroke depression, and improved Quality of Life (9-13).

Some studies have already found that functional gait recovery does not always align with the healthy baseline (14, 15) suggesting that there are other methods of improving gait rehabilitation beyond those that are commonly targeted. Producing an examination of the gait kinematics of stroke survivors by comparison to a measure of functional gait recovery, in this case walking speed, could therefore provide a valuable insight into new avenues for gait rehabilitation.

Gait analysis efforts can be hampered by the targeting effect however, which occurs when a target is presented to the participant being examined. Commonly this target is a force plate placed in the centre of the walkway that the participant is expected to walk, placed there to collect kinetic data as shown in Figure 1.2. There is concern that participants may shorten or

lengthen their steps to ensure they hit the force plate which has led to studies being carried out on volunteers without any gait abnormalities (16, 17).

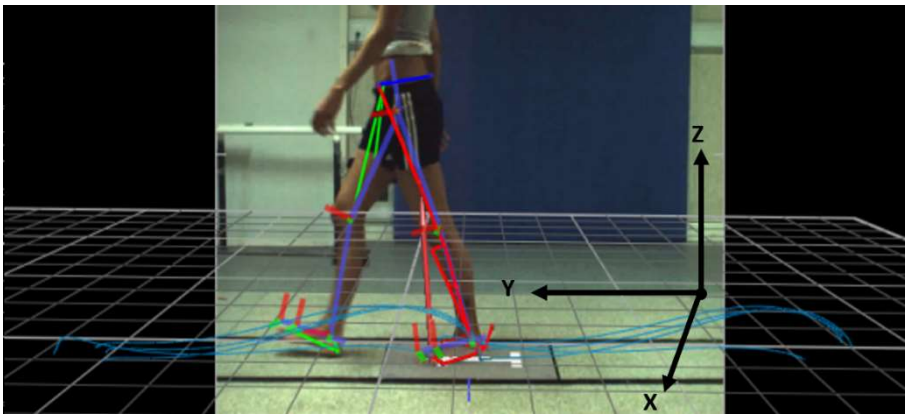

Figure 1.2: A participant walking along a marked out walkway as part of a gait analysis study with the force plate labelled and obviously marked

These studies primarily showed that there were little to no effects from the targeting effect on the participants gait patterns. However, to best ensure any gait analysis of hemiparetic stroke survivors is representative of their normal gait patterns a similar study with hemiparetic participants should be carried out.

Even after a potential target is found to improve functional gait recovery for stroke survivors there remains the issues of constructing a system that can be best utilised in helping reach said target. Soft robotic devices have been suggested as a promising field for use in rehabilitation with several soft robotic exoskeleton systems already under research (18-22) with a schematic of the Myosuit shown below in Figure 1.3. However, reviews have noted that these systems still tend to be tethered to base systems due to the requirements of their robotic systems (23), reducing the environments that they can be used in and creating issues for the user.

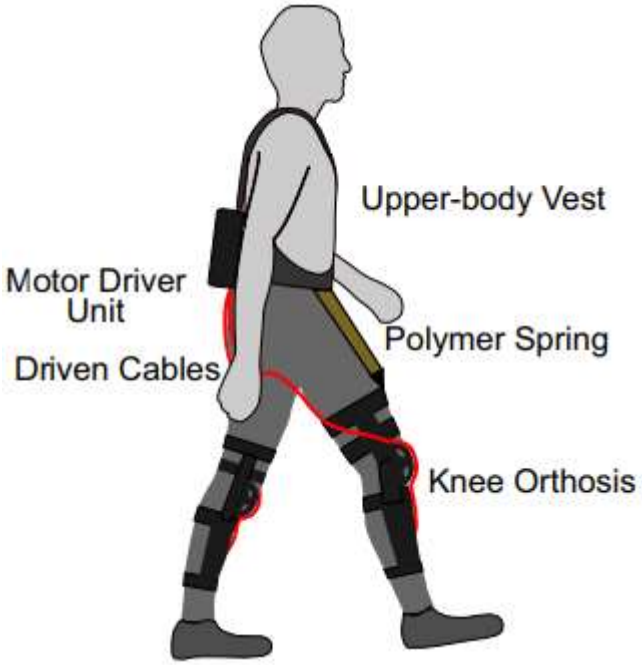

Figure 1.3: A schematic diagram of the soft robotic exoskeleton Myosuit (18)

Many current devices make use of the classic Pneumatic Artificial Muscles (PAM's), these muscles often utilise high powered pumps and are the reason that many systems remain tethered. Smart materials by comparison have seen many recent developments for use within the field of soft robotics and have many different methods of activation, e.g. direct electric current, heat, and magnetic fields (24, 25).

A design that utilises the well explored principles of PAM's while taking advantage of smart materials could therefore be one method of attempting to reduce the reliance of robotic gait systems on tethered stationary power supplies.

1.1.2. Aim and Objectives

The aim of this research was to identify areas of the hemiparetic gait pattern that could be tied to higher functional gait recovery and design a novel system that could be used to target said areas.

This aim was supported by the following objectives:

Objective 1 (Obj. 1): Investigate the impact of the targeting effect on gait analysis for hemiparetic stroke survivors by comparison to a healthy baseline.

Objective 2 (Obj. 2): Identify any significant kinematic patterns within the gait of stroke survivors that corresponds to higher walking speeds.

Objective 3 (Obj. 3): Develop a soft robotic method of actuation that utilises smart materials to reduce the size of necessary power supplies and may be integrated into a self-contained orthosis.

1.1.3. Thesis Outline

Chapter 1 presents a general outline on the role of robotic systems within gait rehabilitation while highlighting key areas that could be explored to facilitate better functional recovery of gait. The overall aim of this research along with the associated objectives are also detailed.

Chapter 2 presents a literature review that goes into detail on the targeting effect, hemiparetic gait analysis and robotic gait rehabilitation. Specific focus is placed on how the current trajectory of gait rehabilitation has been critically evaluated and used to inform what is expected of robotic systems.

Chapter 3 presents study into the importance of the targeting effect in gait analysis on a sample group of hemiparetic stroke survivors and compares this against existing studies. These results fulfil **Objective 1** and are used to inform the study design and considerations of Chapter 4**.**

Chapter 4 details gait analysis of a group of hemiparetic stroke survivors using the Linear Fit Method to provide novel insights into how particular joint kinematics vary with walking speed. This data forms the outcome of **Objective 2**.

Chapter 5 introduces the design of a magnetic fluid muscle. An FEA model is validated against experimental data to evaluate the supporting theory and facilitate future work using the model.

Chapter 6 builds upon the work presented in Chapter 5 and improves the initial design of the magnetic fluid muscle using the validated FEA model. This improved design's suitability for use in an orthosis informed by **Objective** 2 is then evaluated, exploring how well **Objective 3** has been achieved.

Chapter 7 provides a conclusion to the research before presenting the overall findings, contributions and suggesting the direction future works might take.

Chapter 2 – Literature Review

2.1. Introduction

Robotic gait rehabilitation systems are, by their very nature, a multidisciplinary endeavour. Rehabilitation studies and gait analysis can examine what is believed to benefit rehabilitation outcomes and formulate tasks that they wish to put a stroke survivor through to overcome their hemiparetic gait. However, unless this information is conveyed effectively to an engineer then any robotic system that is designed may come from a place of ignorance.

The further information is shared between the Engineering and Rehabilitation areas of research the more tailored systems can become for the specific needs of the user. Thus, building an understanding of what a robotic rehabilitation gait systems needs to achieve by first examining evidence from gait analysis studies will provide a solid foundation for approaching the robotic side, in which there are already many, many concepts and ideas being trialled. Even then walking speed improvements have seen a plateau across robotic gait systems which is a key challenge to be explored.

2.2. Targeting Effect in Gait Analysis

Quantitative gait analysis is a useful tool in the research and treatment of pathological gait patterns and studies in sport biomechanics. It allows the person conducting the gait analysis to assess spatiotemporal, kinematic and ground reaction force (GRF) parameters at a specific point in the subject's gait or over several steps to supplement their own observations. Most

commonly this is recorded by attaching reflective markers to the anatomical landmarks and using equipment such as a motion capture system, force plates, and EMG sensors.

Current professional level equipment such as the VICON 3D motion capture system have been proven to provide accurate and reliable results and are often used as the standard by which other motion capture equipment are tested (26, 27). The reliability such systems confer is of key importance to their use in research and clinical settings as it ensures that less trials are unusable due to poor or missing data. This reduces the overall time an experiment takes. Within research this means that a larger sample size can be used; it also benefits clinical analysis where time and expertise may be in limited supply for each patient to be analysed (28).

Considering this, one of the major issues present in gait analysis is the reliable acquisition of the force data. Generally, most gait analyses use one or more small force plates embedded in the walkway. To provide useful data, the participant's footfall must land solely within the boundaries of the force plate and their next step must not land even partially on the same force plate; anything other than this leads to unrepresentative and unusable kinetic data which often means that the trial must be performed multiple times. To minimise this issue, the force plate might be clearly marked in the walkway and the participants instructed to aim to step within this marked area.

This method of providing explicit instruction to the participants speeds up data acquisition, reducing the number of trials necessary during an experiment. However, treating the force plate as a target that must be hit can affect the participants gait; they may shorten or lengthen their steps to hit the force plate as centrally as possible as investigated in previous

research (16, 17). This research has identified that the targeting effect involves a separate control scheme employed by the brain during gait. Regular gait, without obstacles/targets, occurs under the motor programming scheme (normative). When an obstacle/target is introduced, the control scheme employed switches to visual control (targeting) which assists the person in ensuring that their foot lands in the right place to ensure balance and safety.

This control scheme shift should be thoroughly investigated to understand its effects on gait analysis and whether it is producing any systematic or random error in experimental results. Additionally, whether the targeting effect will manifest purely from instruction or visual guidance should also be investigated. Similar concerns had been expressed nearly two decades ago by Oggero et al (29). who suggested that targeting effects are not fully representative and that hidden force plates should be used instead to ensure normative gait is captured.

Despite this, there is limited research into this area with literature mostly offering restricted overall conclusions. Early studies focused mostly on the kinetic parameters from the force plate with only general spatiotemporal information being looked at. These found that there were no significant effects of targeting gait on the kinetic parameters by comparison to normative gait (30, 31).

Since 3D camera capture systems have become the industry standard, there has been only one recent study utilising these systems to observe this targeting effect (32). Verniba et al. found that there was evidence of targeting during the trial, the participants exhibited decreased variability in step length leading up the force plate. However, it produced no significant differences in the spatiotemporal, kinematic or kinetic gait parameters or their

variability for a young and healthy population. Their paper made suggestions for further study to be undertaken in this field, specifically looking at the effect of targeting in populations of people who suffer from pathological gait conditions, i.e. special populations.

To add to this area of research, gait analysis records from a healthy population were compared against records from the stroke afflicted population for this study using statistical methods to observe any significant differences that could be attributed to the targeting effect. As the previous studies gave conclusions that indicated that the kinetic parameters were not affected by targeting in the healthy population particular emphasis was put on the spatiotemporal and kinematic parameters.

Stroke survivors were chosen as the special population of interest for this study as stroke has been found to be a leading cause of disability in adults (33), leaving 72% of survivors suffering from lower limb weakness (34). This increases survivors' dependence on others to perform basic daily activities (35) and can be a contributing factor to the prevalence of long-term depression in survivors (36). Thus, research into this condition and its associated effects, particularly hemiparesis, is of considerable importance and as such must be thoroughly understood.

Quantitative gait analysis has had a long history with researching issues surrounding stroke such as investigating the effects of orthopaedic devices on the users gait (37) or to investigate whether audio cueing can help improve the gait patterns of stroke survivors (38). Additionally, it has been used within clinical settings to compare and choose between different training methods (39) and as tool to help predict the likelihood that a stroke

survivor would be at risk of a fall (40). Reliable and representative data are key to the success and clinical usefulness of this type of research.

2.3. Hemiparetic Gait Analysis

2.3.1. Current Compensatory Gait Analysis Outcomes

Designing improved hemiparetic gait rehabilitation devices and programmes is an ongoing effort that often utilises gait analysis to inform methods and targets. Past studies, using a wide variety of gait analysis techniques, have focused on either identifying the limiting factors in hemiparetic gait patterns or finding aspects of the pattern that correspond with improvements of the stroke survivor's walking abilities.

Self-selected walking speed has often been chosen as a parameter to assess overall gait rehabilitation effectiveness for studies. Higher self-selected walking speeds have previously been shown to correspond with overall higher ambulatory activity levels and community interaction (11-13, 40, 41). This in turn has been linked to a reduction in the occurrence of post-stroke depression (10), increases in the survivor's reported Quality of Life (9), and reducing predicted hospital costs (42) and as such is a valuable indicator of the wider outcomes of the effectiveness of gait rehabilitation.

Previously, a large focus has been placed on the asymmetry of hemiparetic gait which, being a key trait of healthy gait patterns, made it an important evaluation criterion in rehabilitation studies (7). Balasubramanian et al examined the relationship between self-selected walking speed and step length asymmetry and found a broad correlation between increased walking speeds and greater symmetry (8).

However, when breaking down the participants by impairment severity it was demonstrated that survivors with severe hemiparesis could still achieve high walking speeds via an asymmetric gait pattern. This leads to a more complex picture of the improvement of hemiparetic gait which becomes difficult to summarise.

Research by Kim et al. touched upon this topic with their study finding evidence of survivors achieving faster walking speeds by adopting non-normal gait patterns. These featured a prolonged hip abduction in the paretic limb which was presented as compensating for insufficient peak flexion at the paretic knee and hip joints (43). While presenting a detailed look at walking speed and kinetic parameters such as power generation, this work used representative parameters such as the mean and range of joint angles when examining kinematic data. These representative parameters can be extremely useful when performing gait analysis but by their very nature they lead to some data, particularly time dependant data, being overlooked.

For instance, even in thorough reviews on stroke survivor's gait the kinematics of joint angles are often described in a qualitative way which is supported by specific angles pulled out at set gait pattern events (44), examples of gait events are shown below in Figure 2.1 (45). This leaves it difficult to look at the exact behaviour between gait events quantitively, especially if they consist of complex waveforms, which is a barrier to more advanced forms of analysis on larger data sets, i.e. statistical.

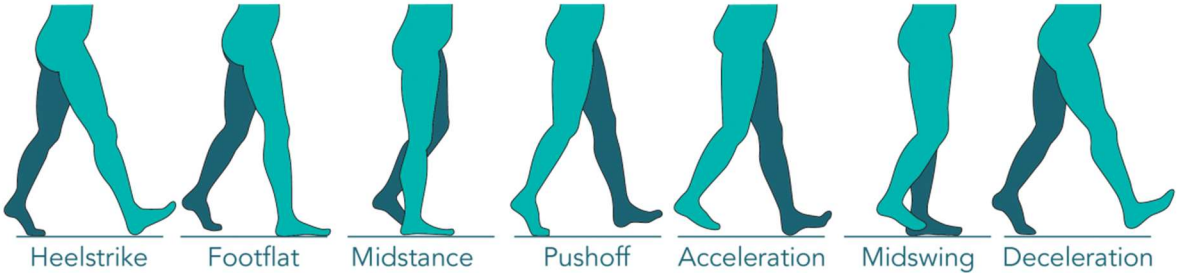

Figure 2.1: Gait cycle pattern as defined by major gait events (45)

2.3.2. Time Inclusive Gait Analysis Techniques

Time dependant data may instead be analysed as a waveform to preserve further data resolution. To allow for ease of comparison between trials, previous studies have taken each parameter plotted against time, e.g. spatial position or joint angle, and normalised it with regards to specific gait events (46).

Numerous methods have been suggested to compare this form of waveform data from Principal component analysis to neural networks (47, 48). These methods have the benefit of reducing information loss and can provide detailed outcomes, but these outcomes vary significantly in their ease of application and can be difficult to attribute direct physiological meaning for those not well versed in their use.

The fairly recent presentation of the Linear Fit (LF) Method as a simple and effective alternative to previous analyses brings up an interesting prospect in going back to analyse hemiparetic gait relationships in more depth (49). The LF Method assess the similarity between a reference waveform and the waveform of interest via three parameters that describe the shape, amplitude and offset differences in an intuitive, easy to explain manner.

The LF method considers the entirety of the gait analysis waveform data and has been shown to appropriately and reliably highlight difference in gait between healthy baseline gait

and abnormal gait patterns. In addition, its ability to examine even small variations in the waveform data has been utilised in previous gait analyses and compares favourably with coefficients of multiple correlation analysis methods while maintaining easy to read physiological based outcomes (50).

The LF method has also seen use in the validation of gait analysis technologies and has proved useful in allowing for clear understanding of variations between emerging technologies and the current "gold standard" of gait analysis, the gait plug-in within the Vicon Nexus system (51, 52). Proper use of the method can thus allow an effective analysis of gait patterns down to small variations.

2.4. Robotic Rehabilitation for Gait

Robotic rehabilitation has previously been seen as an obvious improvement over conventional gait rehabilitation methods. Many different designs have been introduced that can generally be broken down as shown below in Figure 2.2. One of the commonly touted advantages of robotic rehabilitation is how it reduces the effort of leading the training for the physiotherapist by providing the mechanical assistance to move and position the patient's limbs (3, 53, 54). This can ensure that only one therapist is needed to run the therapy, whereas in some cases multiple therapists may have been needed to properly support, and ensure the safety, of the patient.

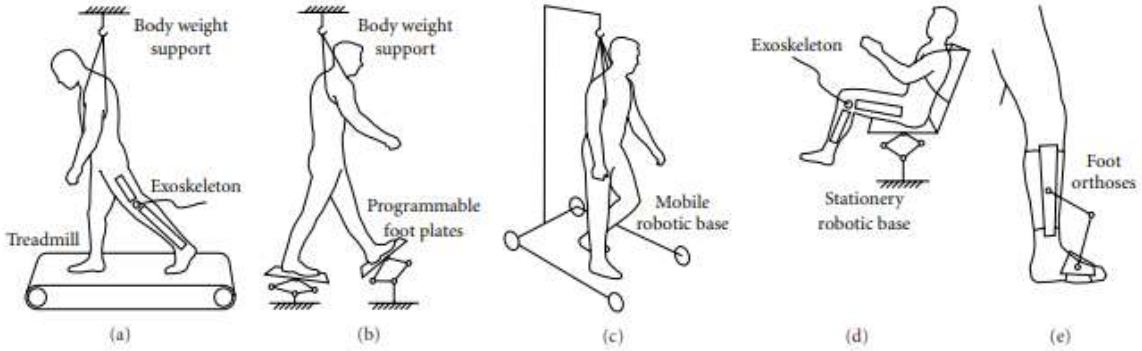

Figure 2.2: Robotic system types for lower-limb rehabilitation: (a) treadmill gait trainers, (b) foot-plate-based gait trainers, (c) overground gait trainers, (d) stationary gait and ankle trainers, and (e) active foot orthoses. (53)

Reducing the effort of the therapist helps increase the intensity of rehabilitation that is available to the user (3). The user can train for longer due to the combination of body weight support and robotic assistance which means the therapist does not become fatigued. Lowering the number of therapists required per rehabilitation patient should also increase the available resources of the clinic and thus the potential therapy time available.

Intense training has been shown to correlate with improvements in rehabilitation outcomes (55) and has been one of the focuses of neuro-rehabilitation efforts over the last decade (56, 57). While intense training can be a somewhat generalised term, it will be defined here as training that has active engagement/effort on the patient's part and longer times spent performing tasks which actually challenge the user, both of which have strong supporting evidence behind their effectiveness (57-59).

Early Lower Limb Robotic Rehabilitation System's (LLRRS's) struggled to meet these criteria as they were designed to carry the user through a set gait pattern (60-62) which, while generally beneficial, can allow the patient to remain passive during training (4) and does not adjust the challenge to suit the user's level of recovery.

LLRRS's have been commended for their ability to deliver task specific training to the user (2, 3, 63). This is due to the fact that they reproduce the complete gait cycle, a complex series of motions, in a repetitive manner. The major benefit of task-specific training is that the outcomes of the training should better prepare the user to be able to accomplish activities of daily living, thus achieving functional benefits (64, 65).

In the acute phase of stroke the stroke survivor's major goal is to achieve independent walking if they are not able to walk following the stroke event (3). Current devices are most successful for stroke survivors that fit this criterion and are under 3 months post stroke event according to a Cochrane review of 62 trials (specifically for people in the first 3 months after stroke) (1). Accordingly, the next goal for someone who has achieve independent walking should then be to improve their walking speed and capacity, self-selected walking speed being of the most obvious indicators of gait improvement (11-13, 40).

The Cochrane review found no significant increases in walking speed of stroke survivors using robotic training devices by comparison to those who received training without the devices (1), which is supported by the findings of other reviews (2, 4). Thus, it can be said that current LLRRS's in use do not set any better training or challenge to encourage further rehabilitation than traditional physical therapy.

This is a key area where the robotic systems could improve as once independent walking is achieved by the stroke survivor the system has no substantial benefits over physical therapy. This would explain why the advice most often given in reviews of robotic rehabilitation is to utilise robotic systems as a tool to complement traditional methods (66).

2.5. Soft Robotics in Gait Rehabilitation

2.5.1. Artificial Muscles

The design and implementation of soft robotic devices is an extensive area of research with broad applications, including producing collaborative robotic systems for manufacturing (67), designing highly specialised “biomimicry” robots inspired by nature (68), and in exoskeleton devices to assist a person’s motions (22). There have been many designs presented which utilise various mechanisms to provide the power and compliance necessary for a device to fall under the category of soft robotics.

One of the most common subsets of these soft robotic devices are artificial muscles. As the name implies these devices mimic muscle fibres, being able to produce tensile forces and change their stiffness while maintaining a level of compliance not seen in most other forms of actuators. A recent review noted 2 main branches in artificial muscles, Flexible Fluidic Actuators (FFA), McKibben, Hydraulic Muscles etc., and Smart Material based actuators, Electro-Active Polymers, Shape Memory Materials etc. (25).

Among these, one of the simplest and still widely discussed design is the FFA McKibben's Artificial Muscle also known as Pneumatic Artificial Muscles (PAMs) (69) as demonstrated below in Figure 2.3. A thin-walled rubber tube in a braided sleeve, the McKibben's muscle contracts when filled with a pressurised gas. Initially designed for use in artificial limbs, the muscle, and other designs like it, have also long been considered a potential solution to producing more effective rehabilitation devices (70) and continue to be pursued (71).

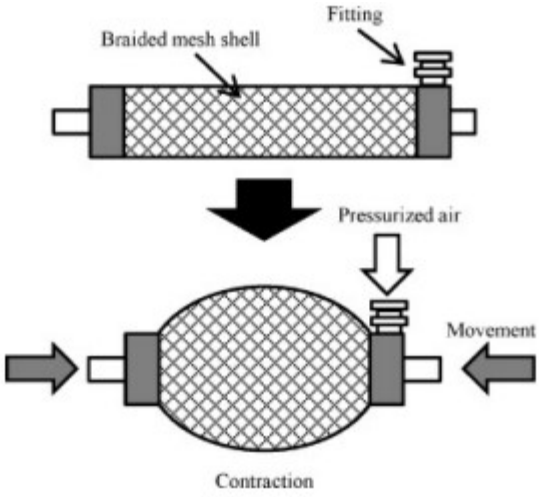

Figure 2.3: The contraction behaviour of a McKibben Artificial Muscle (71)

Current commercial pneumatic muscles have the potential to provide forces of around 700N (72) and numerous robotic rehabilitation designs incorporating PAMs targeting various joints have been put forward (20-22). Recent research highlights the benefits of soft robotic designs in rehabilitation with it being suggested that their compliant nature removes excessive constraints on the targeted joint and reduce joint alignment issues, mitigating potential damage and encouraging improved rehabilitation outcomes (73). However, even the more portable designs still incorporate power supplies/pump systems that can weigh around 4kg and can be reasonably complex (22). Other designs still require connection to a static source of actuation which has been cited as a challenge for soft robotics in general (23, 74).

2.5.2. Smart Materials

While fluid based actuation methods remain popular, see Figure 2.4 below, devices based off of smart materials such as dielectric elastomers (DEA's) and magnetorheological elastomers are being explored which can require comparatively simple mechanisms to activate their smart properties which can reduce the necessity of bulky support systems that keep rehabilitation systems tethered (75).

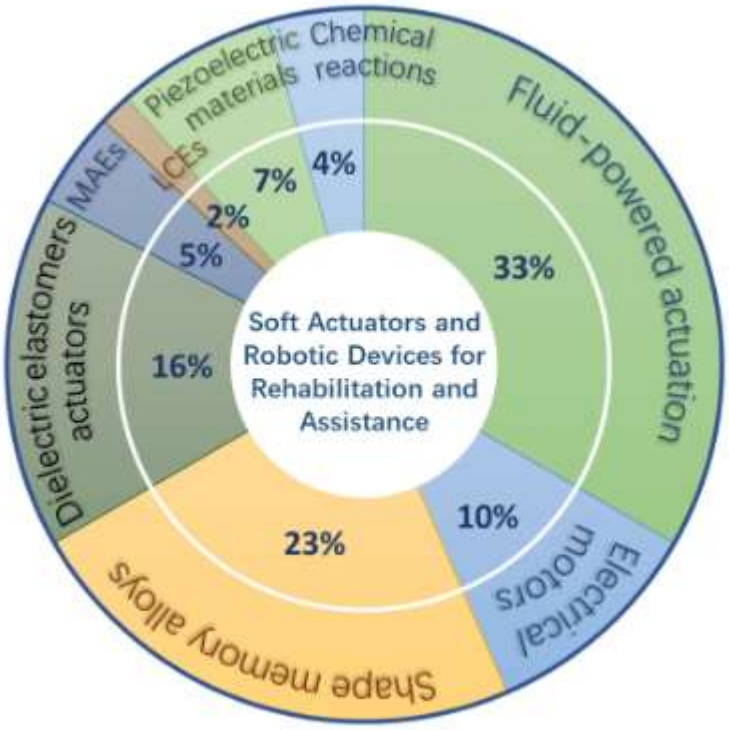

Figure 2.4: Overview of current split in mechanisms utilised by soft robotic systems for rehabilitation and assistive purposes. MAE's = Magneto-Active Elastomers, LCE's = Liquid Crystal Elastomers (75)

DEA's are a good example of the potential benefits of utilising smart materials. For example, a glove using twisted and coiled type polymer muscles made from silver coated Nylon 6,6 threads was able to allow users to grasp a variety of everyday objects while weighing only 90 g (76). Systems for use with gait rehabilitation have also been proposed with a hip joint

orthosis for hemiparetic stroke survivors being able to produce 94 N at a weight of 2 kg (77). While still a significant weight, this device was able to be facilitate outdoor walking due to its compact power and control systems.

However, reviews have noted that DEA based devices often require high driving voltages which in turn can cause very high temperatures in their di-electric components and requiring heat resistant materials to be built into their design to keep their users safe (75). Magnetic elastomers by comparison have the advantage of few inherent dangers with their operation though they have relatively low force outputs by comparison to other soft robotic mechanisms considered for rehabilitation and their characteristics have now always been fully modelled/explored (78). Shape memory alloys also have their own issues, often requiring heat to activate and having relatively slow response times (75).

Some soft robotic designs have been proposed using traditional electromagnet actuator design applied to across novel materials. This relies on the effect between a permanent magnet and an electromagnet, and the force generated by their interacting electromagnet fields. To facilitate the compliance necessary in this field, conductive fluids are used in place of the wires that would usually make up the coil of the electromagnet component (79).

This is the same principle as using a magnetic fluid with an electromagnet to produce a controllable motion. Magnetic fluids have been a widely discussed type of smart material that has seen much development since they were first introduced. When a magnetic field is applied, magnetic fluids can be manipulated to perform useful work and have the potential for high force densities in easily realisable conditions, in excess of 50 times the force density

of gravity (80). Studies have found that these fluids can be accurately modelled within FEA software and designs built and optimised around this (81, 82).

Current designs that utilise magnetic fluids in soft robotics tend to focus the producing simple systems that can move themselves. The ability of magnetic fluids to be manipulated by an external field that requires no actual physical contact with the power source, unlike DEA's, allow small and simple designs to be put forth and their motion controlled by more complex external electromagnet setups. For example, systems range from those based on the movement of individual cells (83) all the way up to Soft-Ball, a 5cm across ball of ferrofluid in a soft shell that can overcome various obstacles (84).

Given the viability of soft robotic devices based on magnetic fluids already demonstrated it is suggested that many of the current designs for fluidic muscles could potentially be adapted for use with the smart material with relatively simple adjustments. A design that utilises a fluidic muscle filled with a magnetic fluid might have unique characteristics that are worth examining in more detail.

Chapter 3 - Targeting effect on gait parameters in healthy individuals and post-stroke hemiparetic individuals

3.1. Introduction

As part of this research, data will be gathered that allows for comparison against previous studies in this area and investigation of the general effects of targeting on stroke survivors helping improve the designs of future gait analysis experiments. If the targeting effect is shown to be significant then this indicates that gait analysis experiments that make the participant target the force plate are producing data that is unrepresentative of normal gait. In this case, it would be recommended that experiments use a hidden force plate to be a representative study. This would generally lead to more gait trials having to be performed due to a likely increase in steps outside the force plate area.

If there are no significant effects of targeting found then it would indicate that participants could be told to specifically target the force plate without compromising the data produced. This could significantly reduce the number of invalid trials during an experiment and increase its efficiency.

The objective of this study is to assess whether the targeting effect has a significant impact on the gait of a stroke survivor. This will be compared against a healthy control group and findings from previous studies. The hypothesis being tested can be stated as:

Having a target in a gait analysis setup (i.e., a clearly marked force plate) has no statistically significant effect on the gait parameters of a participant by comparison to if there was no target present, regardless of whether the participant was healthy or had suffered a stroke.

3.2. Methodology

3.2.1. Participants

The experiment conducted was carried out on a group of eight males, including four healthy participants (age: 28 ± 4 years, height: 168 ± 3 cm, weight: 78 ± 4 kg) and four stroke participants (age: 32 ± 3 years, height: 167 ± 2 cm, weight: 8 ± 3 kg). All participants were recruited via local advertising. The stroke survivors selected for the experiment were suffering from right side hemiparesis due to the stroke event and all healthy participants had no history of neurological disorders or brain damage. Ethical approval for the methods used in this study was sought and obtained from West Midland Rehabilitation Centre (WMRC), Birmingham.

3.2.2. Experimental Equipment and Set-Up

The experiment was conducted using a VICON MX System for motion measurement and analysis. The system used 12 cameras situated around the testing area, 6 were MX3+'s and 6 were MX T40's, both of which were capturing at 100 Hz. These cameras captured positional data using reflective markers that had been placed upon the participants' lower body based on the Oxford foot model. All the cameras were calibrated by an Active Wand before starting the experiment.

Participants were asked to wear clothing that was tight to the body to ensure the markers remained close to their anatomical landmarks. The markers were positioned such that the upper leg, lower leg and foot all contained at least three markers. This allowed the markers to be used to define a distinct plane for each section of the leg. The system was able to

report the kinematic positioning data of each of these sections by comparing against a set of normative trials that were done for each participant.

Two additional digital cameras were used to capture each gait trial, one focused along the walkway to record the frontal view and one records the lateral view. These cameras captured data at 50 Hz and were used to assist data processing and data syncing.

The path set up for the subject to walk down was 10 m long and a Kistler force plate (collecting data at 100 Hz) was situated at the centre of the walkway. The dimension of the target was 600 mm 400 mm. The force was measured in X, Y and Z axes and the magnitude of the force vector was considered in this study. The width of the walkway was indicated by lines to help ensure the participant did not step off to one side of the plate, invalidating the trial. The force plate was marked so that its boundary was clearly visible to the participant as shown in Figure 3.1.

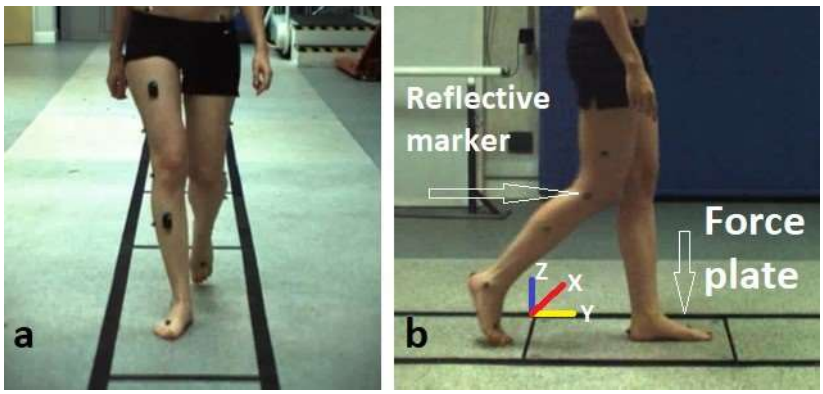

Figure 3.1: Two different views of a healthy participant during targeted walking along the walkway in the gait lab; (a) Frontal view, (b)

3.2.3. Procedure

All post-stroke participants had the ability to walk without assistance. Each participant performed at least six trials in total, three with their left leg leading and three with their right leg leading. Trials were repeated until there were three trials recorded for each leg in which the participant stepped completely within the force plate boundaries. Before starting the experiment, static tests, where the participant stands still on the force plate, were performed in order to calibrate the force plate and to measure the participants' body mass and height.

Participants were informed about the presence and location of the force plate before beginning the trials, but they were not told to step on the force plate necessarily, and there were normally a couple of trials per participants in which they missed the target, or they did not step on the force plate completely.

This form of instruction was chosen as it presents the condition where the force plate is an obvious target for the participant to aim for but avoids using direct instruction which have already been suggested to add variability to gait analysis (85). This keeps the focus on the targeting effect manifesting from visual cues. As mentioned previously, the instruction would also have an effect but for this experiment, a single focus was chosen.

Participants were not stopped if they missed the target or if they did not step on the target completely. However, these failed and non-usable trials were discarded from the analysis at the end. There was no psychological pressure on the participants and participants did not have to remain at constant speed in all the trials.

3.2.4. Data Processing and Analysis

The data from each gait trial were captured and processed using VICON Nexus 1.8 Gait Analysis Software. For each subject, the trials were examined and trials which had foot placement outside of the force plate were set aside. From the remaining trials, six were selected for further analysis. Half of the selected trials had the left foot stepping on the force plate and the other half had the right foot stepping on the force plate.

Using the regular cameras, the frames in which the toe-off and heel-strike gait events occurred were noted allowing the 3D positioning data to be synchronised with the visual recording. This was performed over a three-step section of the participants' gait, i.e., 1.5 gait cycles. This period began with the toe-off of the foot that would connect with the force plate as shown in Figure 3.2.

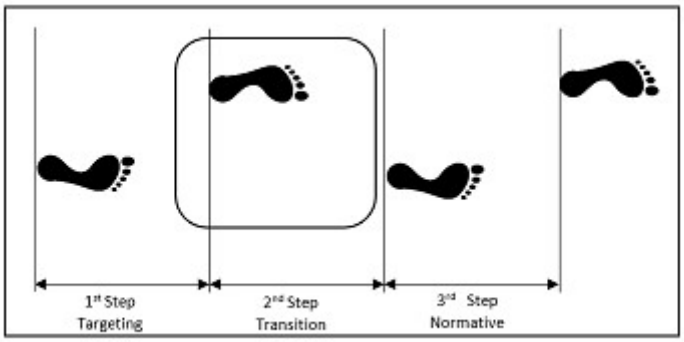

Figure 3.2: One step before the force plate and two steps after the force plate are the control zones that gait parameters have been studied and compared to each other. The first, second and third steps are considered as targeting step, transition step and normative step, respectively.

Verniba (32) showed how a small difference in the variability of the step was present immediately after the force plate targeting step. While Verniba did not mark this as a significant difference, it would comply with the known theory of targeting that after the

target has been achieved, the participant would revert to normative gait. Thus, for the data analysis within this paper, the comparison will be made within trials between the targeting step landing on the force plate, the first step and the third step that is assumed to be representative of normative gait.

The spatiotemporal parameters that were calculated for the first and third steps included step speed, step length and step time. The step length was calculated from the change in position of the heel marker in the Y axis between the toe-off and heel-strike gait events. The difference in time between these two events gave the step time and was used to find the step speed. The coordinate system is shown in Figure 3.1.b.

The kinematic parameters were found by the VICON system which calculated the angles of the planes created by the markers at the thigh and shank referenced against the participants standing posture. The parameters that were used in the statistical analysis were the sagittal plane angles between these limb segments at the moment of heel strike to give a snapshot of the position of each leg at each crucial gait event.

The positional data were then exported from the VICON software into an excel file and a code was then created in MATLAB R2016A which would isolate the relevant sets of gait data over the relevant period and output the chosen parameters. The length and weight parameters were normalized to percentages of the participants' height and body weight as these parameters have a large impact on the variations of gait; normalized values are more comparable to inter and intra groups (86).

3.2.5. Statistical Analysis

Statistical analyses were conducted on the experimental data using the IBM SPSS Statistics 22 program. A three-factor ANOVA was performed to compare each of the spatiotemporal and kinematic parameters between groups. The three grouping variables used were control versus stroke, left trials versus right trials and first step versus third step. This test indicated whether any significant difference is present and what effect the grouping variables or interaction effects between the grouping variables had.

A two-way ANOVA was used to compare the peak GRFs between groups. The means and standard deviations were then compared against values obtained in a previous study conducted using foot-scan technology (87). As the foot-scan technology is packaged in a shoe, it means there is no obstacle for the participant to target during the trial, hence removing its effect from the trial. This has been shown to be comparable to regular kinetic measurement methods (88) and as such can be used as an example of a non-targeting set of trials for comparison to this experimental data. Statistical significance level was set at $p < 0.05$.

3.3. Evidence of Targeting Effect in Gait Analysis Results

The results of the ANOVA tests are listed in Table 3-1 for descriptive statistics.

Table 3-1: Descriptive Statistics of Recorded Gait Parameters

Parameter	Mean (SD)							
	Control				Stroke			
	Left		Right		Left		Right	
Spatiotemporal	1st Step	3rd Step	1st Step	3rd Step	1st Step	3rd Step	1st Step	3rd Step
Step Speed (%h/s)	95.56 (17.65)	107.39 (16.53)	95.57 (19.99)	107.39 (21.84)	67.53 (14.11)	78.12 (15.59)	67.34 (12.24)	80.86 (14.72)
Step Length (%h)	40.16 (5.81)	42.73 (5.33)	39.15 (5.85)	42.74 (5.49)	30.63 (5.43)	33.63 (5.35)	30.09 (5.23)	33.41 (6.25)
Step Time (s)	0.42 (0.02)	0.40 (0.02)	0.41 (0.03)	0.40 (.04)	0.46 (0.05)	0.42 (0.03)	0.45 (.05)	0.41 (0.04)
Kinematic								
Ankle Angle (°)	0.3 (1.5)	1.5 (1.7)	2.9 (2.9)	3.6 (2.8)	1.1 (7.9)	0.5 (7.0)	3.4 (7.6)	4.5 (6.1)
Knee Angle (°)	7.6 (2.7)	6.9 (1.6)	7.9 (3.7)	7.2 (3.0)	10.4 (12.6)	10.7 (12.2)	17.8 (14.4)	17.2 (14.8)
Hip Angle (°)	33.5 (3.5)	32.8 (3.5)	32.0 (5.1)	31.7 (5.2)	29.2 (5.0)	28.9 (5.4)	34.6 (7.6)	35.2 (7.4)
Kinetic	Foot Scan	Force Plate	Foot Scan	Force Plate	Foot Scan	Force Plate	Foot Scan	Force Plate
Peak GRF (%)	118.96 (1.63)	141.08 (18.37)	118.96 (1.63)	145.45 (21.03)	100.10 (2.96)	109.56 (5.69)	97.45 (2.55)	117.19 (7.15)

3.3.1. Spatiotemporal Parameters

Step speed. As shown in Figure 3.3, a three-factor ANOVA showed no significant interaction effects between any of the factors on step speed and no significant main effect for trial type,

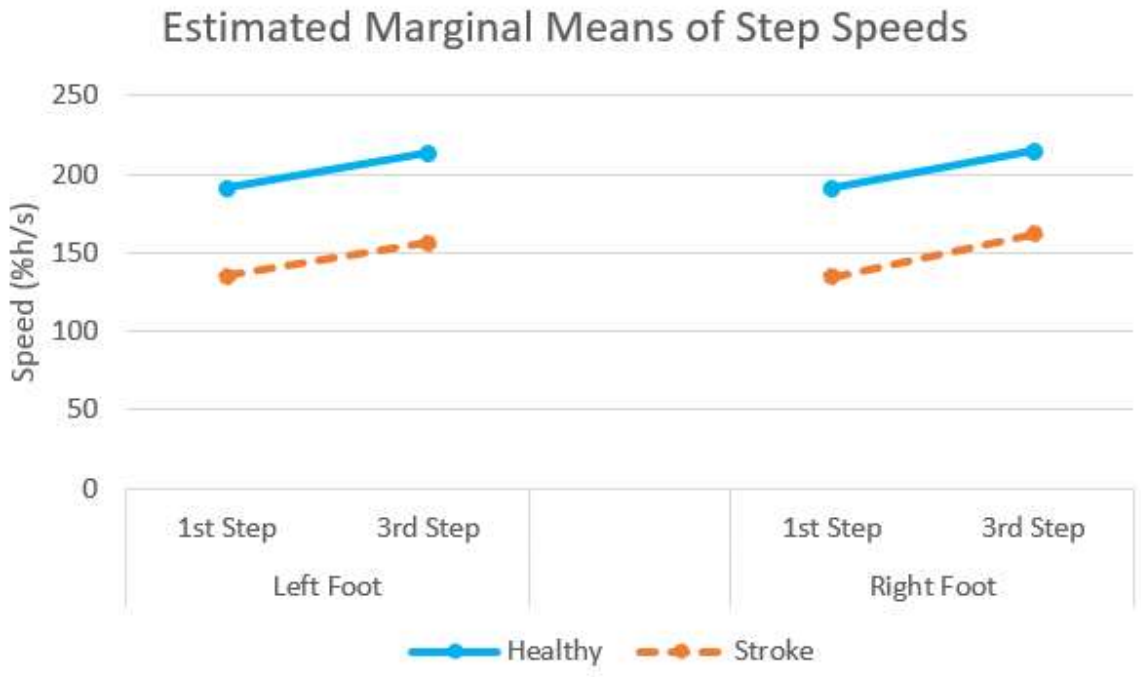

Figure 3.3: Interaction effects of targeting/normative on step speed.

F(1,88) = 0.052, p = 0.820. Subject group and step number were found to have a significant effect on the parameter, F(1,88) = 66.11, p < 0.001 and F(1,88) = 11.85, p = 0.001.

It can be seen that the estimated marginal means of step speed differ consistently between the healthy group and the stroke survivors for the left and right leg trials with the stroke survivors having a slower step speed. Additionally, for both groups and both legs, there is seen a similar gradient between the data for the first and third step speeds indicating that the step number is a significant variable which effects both groups in a similar manner and as such no interaction effect exists.

Step length. As shown in Figure 3.4, three-factor ANOVA showed no significant interaction effects between any of the factors on step length and no significant main effect for trial type, F(1,88) = 0.143, p = 0.706. Subject group and step number were found to have a significant effect on the parameter, F(1,88) = 65.49, p < 0.001 and F(1,88) = 7.49, p = 0.008.

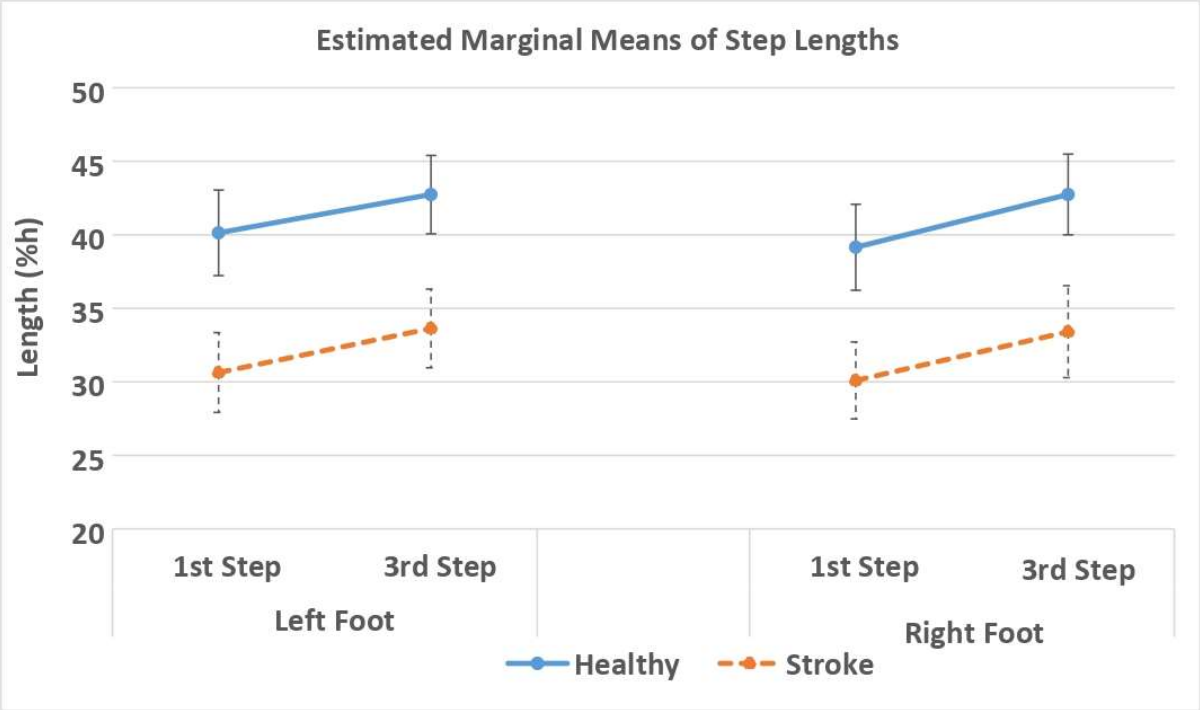

Figure 3.4: Interaction effects of targeting/normative on step lengths.

Similar to step speed, the estimated marginal means of step length show clear differences between the healthy group and the stroke survivors with the stroke survivors taking shorter steps. This is consistent over both left and right leg trials showing that the group has a significant effect on this parameter but left versus right does not. In both legs, a positive gradient was seen between the first and third steps demonstrating that the step number had a significant effect. As the gradient is similar between both groups and for each leg, this shows that there was no significant interaction effect.

Step time. As shown in Figure 3.5, the three-factor ANOVA showed no significant interaction effects between any of the factors on step time and no significant main effect for trial type, $F(1,88) = 0.822$, $p = 0.367$. Subject group and step number were found to have a significant effect on the parameter, $F(1,88) = 13.36$, $p < 0.001$ and $F(1,88) = 12.52$, $p = 0.001$.

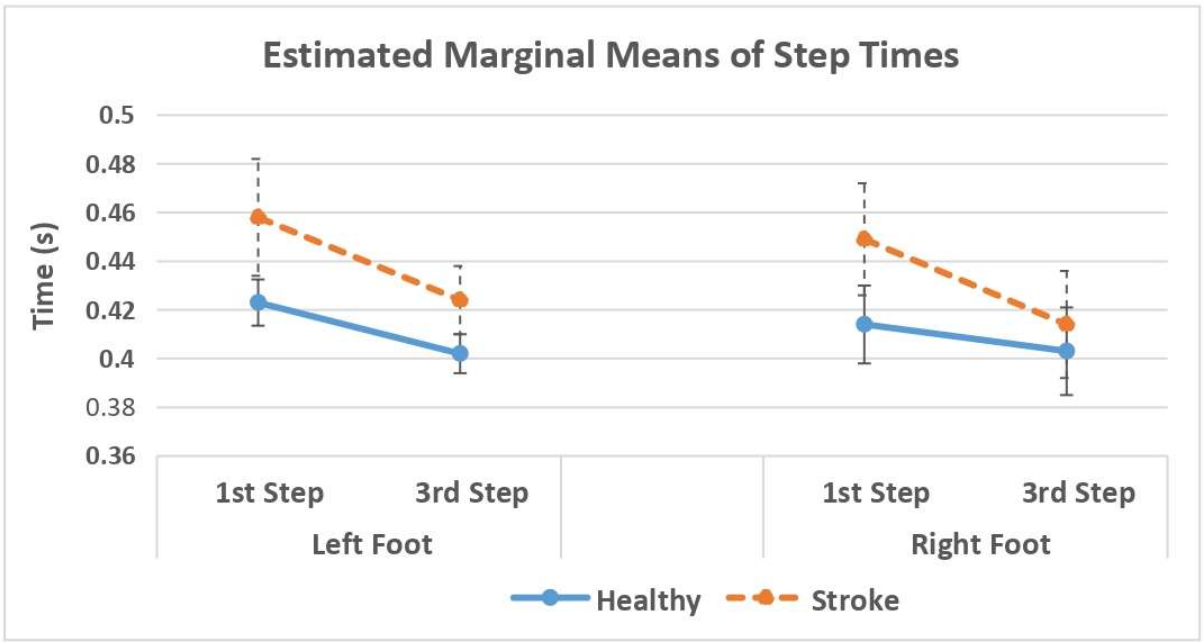

Figure 3.5: Interaction effects of targeting/normative on step time.

The estimated marginal means of step time show significant differences between the healthy group and the stroke survivors with the stroke survivors showing slower step times for both right and left legs. In both groups, there was a negative gradient between the first step and the third step which was seen in both legs. While the gradient differs between the two groups in the right foot this is over a very small scale and overall is not considered significant. Similarly, while there were minor differences between the left and right legs, these were determined to not be significant leaving only group and step number as the significant grouping variables.

Averaged foot velocity profiles. To compare the foot velocity profiles in the direction of motion (Y-Axis) between groups, step side and the targeting and normative steps, the positions of the marker on the back of the participants' ankle were exported from the VICON data. The changes in position between each frame were then compared to find the speed of the foot during each step. This speed profile was then normalized over the three steps of the trial for each foot such that they could be compared against each other. The profiles were then averaged within the healthy and stroke groups and the targeting and normative steps were plotted against each other. These averaged profiles are shown in Figure 3.6(a) and (b).

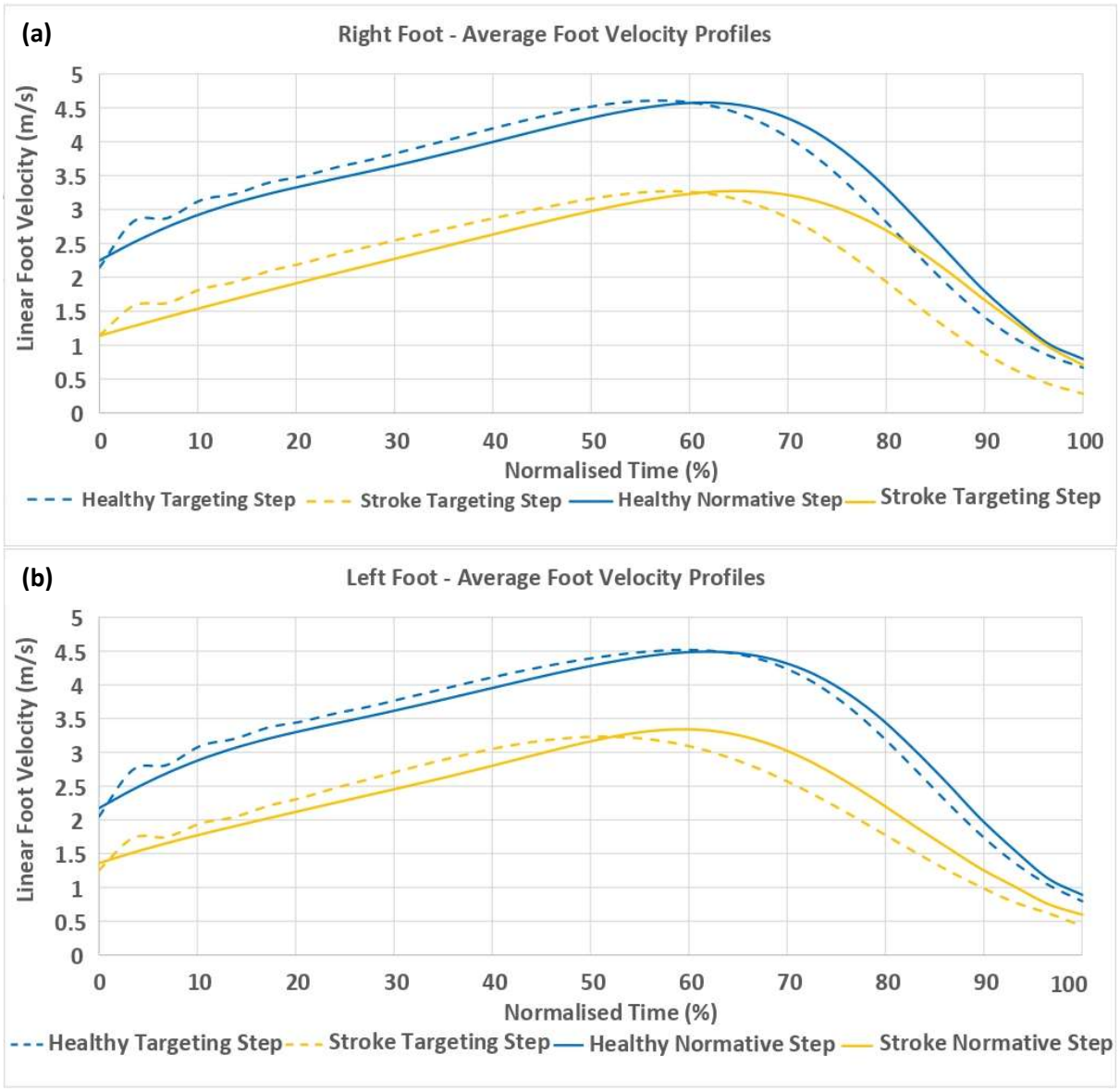

Figure 3.6: Average velocity profiles of the participants' foot during the trials

3.3.2 Kinematic Parameters

Ankle angles. As shown in Figure 3.8, the three-factor ANOVA showed no significant interaction effects between any of the factors on ankle angles and no significant main effect for group and step number, $F(1,88) = 0.001$, $p = 0.978$ and $F(1,88) = 0.108$, $p = 0.744$. Trial side was found to have a significant effect on the parameter, $F(1,88) = 7.528$, $p = 0.007$.

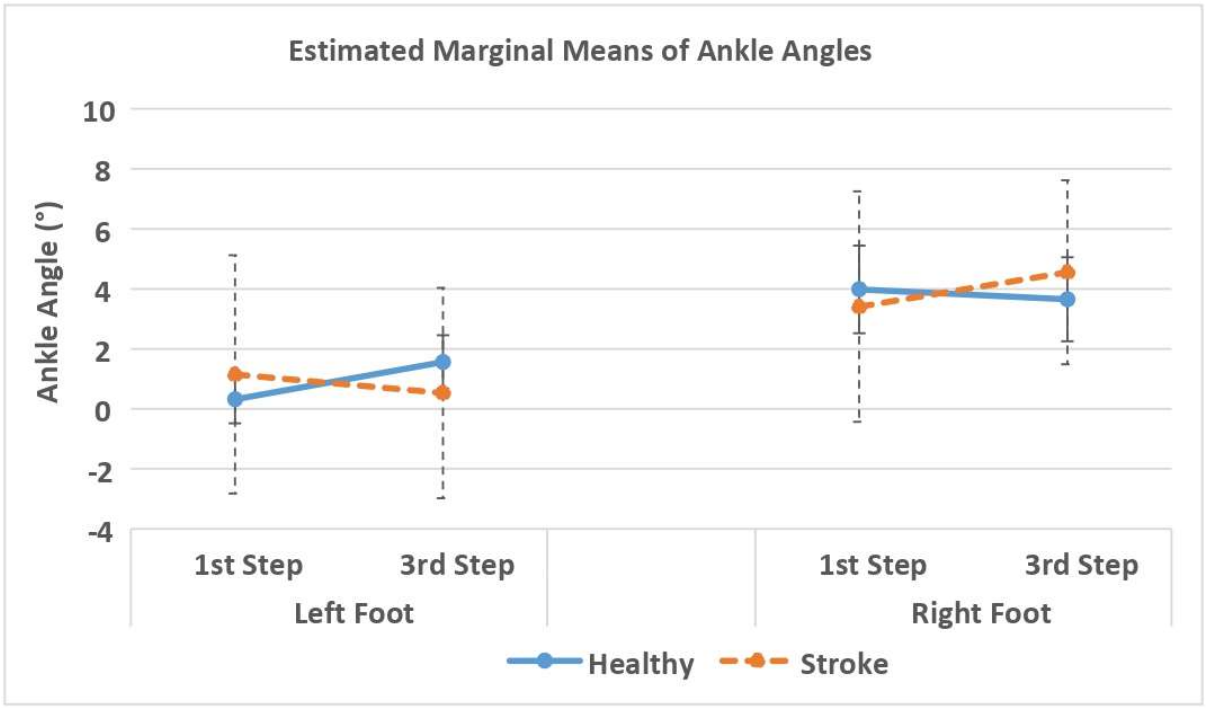

Figure 3.7: Interaction effects of targeting/normative on ankle angles at heel strike.

The estimated marginal means of the ankle angles show a slightly more complex relationship but over a fairly small set of angles. There is a clear difference between the left and right legs; however, while in the left leg trials the healthy subjects went from a low angle to a higher angle between the first and third steps, they showed the opposite behaviour in the right leg trials albeit with overall higher angles. This was nearly exactly opposite to the relationships shown by the stroke survivor group. From this, no major conclusions were taken aside from the obvious effect of trial side.

Knee angles. As shown in Figure 3.9, the three-factor ANOVA showed no significant interaction effects between any of the factors. However, the interaction effect between group and trial was much closer to significance, $F(1,88) = 2.77$, $p = 0.099$. Trial side and step number were found not to have a significant effect on the parameter though trial was also close to significance, $F(1,88) = 3.223$, $p = 0.076$ and $F(1,88) = 0.039$, $p = 0.844$. Group was found to have a significant effect on the parameter, $F(1,88) = 10.87$, $p = 0.001$. Figure 3.9 demonstrates this graphically.

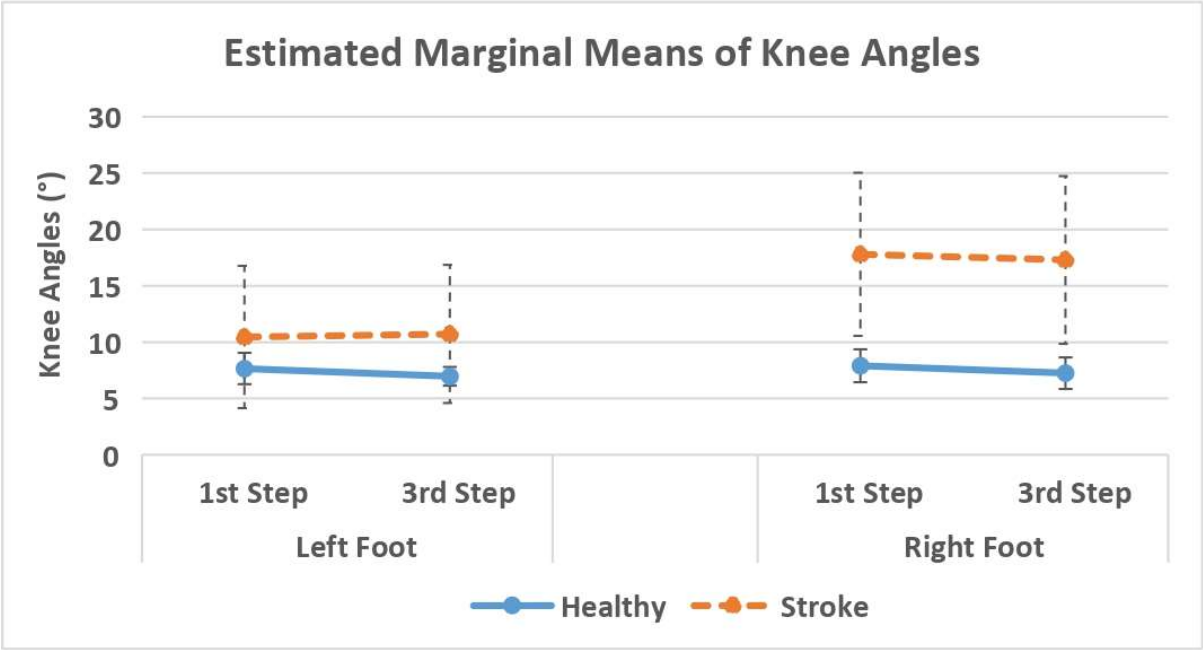

Figure 3.8: Interaction effects of targeting/normative on knee angles at heel strike.

The estimated marginal means of the knee angles show clear differences between the control group and the stroke survivors with the stroke survivors showing a higher angle across both legs. The differences between the left and right legs for the stroke group were pronounced by comparison to the minor differences in the control group which led to a near significant interaction effect between the group and trial and the significant impact of group.

The change in knee angle between the first step and the third step was minor for both groups.

Hip angles. As shown in Figure 3.10, the three-factor ANOVA showed a significant interaction effect between the group and trial side on hip angles, $F(1,88) = 9.93$, $p = 0.002$. There were no other significant interaction effects between any of the factors. Step number and group were found to have no significant main effect on the parameter, $F(1,88) = 0.024$, $p = 0.876$ and $F(1,88) = 0.222$, $p = 0.639$. Figure 3.10 demonstrates this graphically.

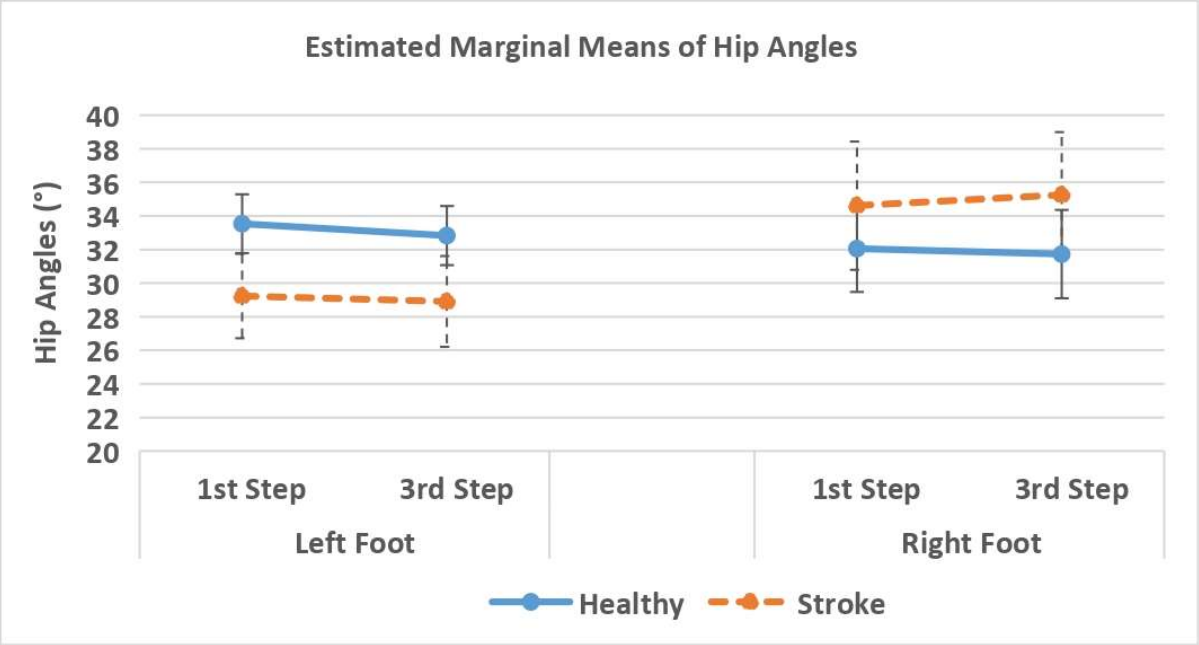

Figure 3.9: Interaction effects of targeting/normative on hip angles at heel strike.

The estimated marginal means of the hip angles show that there is a side-specific difference between the healthy group and the stroke survivors with the healthy group having larger hip angles during left leg trials and lower hip angles during right leg trials. This shows the significant interaction effect between the group and trial side. There are minor observable differences between the first and third step, but these were not significant.

3.3.3 Kinetic Parameter

As shown in Figure 3.10, the two-factor ANOVA showed no interaction effect between group and trial on peak GRF and there was no significant main effect from trial side, $F(1,88) = 0.501$, $p = 0.483$. Group was found to have a significant effect on the parameter, $F(1,88) = 12.43$, $p = 0.001$. This is in-line with the differences that would be expected between a stroke population and a healthy population.

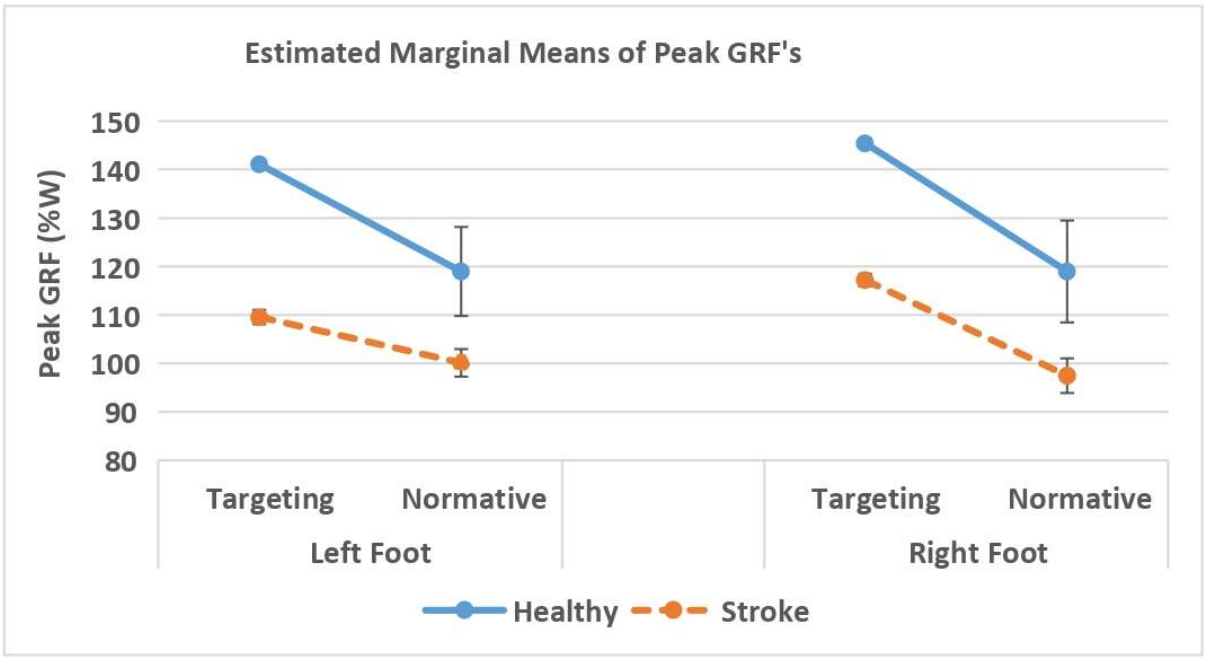

Figure 3.10: Interaction effects of targeting/normative on peak GRF's. GRF: ground reaction force.

The mean values of the peak GRF were then compared against the values found in a study conducted by HyunDong et al (87). for a superficial comparison that may be used to inform and direct further studies. The results for the targeting step showed significantly higher values of peak ground force within the control group. Additionally, within the stroke group, there was higher peak GRFs found in the study for both legs, while the other study found that there was a higher peak GRF in the unaffected limb and it was found that the opposite was true in this study.

3.4. Discussion

3.4.1. Spatiotemporal data

During the experiment, some trials were rendered invalid due to the participants not stepping wholly within the area of the force plate. Additional trials then had to be performed until there were enough usable trials for later analysis. The stroke group had a higher failure rate than the healthy group, 37% as opposed to 24% necessitating that more trials had to be performed. This is in line with what is expected for the stroke population.

In order to improve the validity of gait studies, the importance of the targeting effect for human gait must be quantified. To this end, the data from this gait analysis experiment was analysed statistically using ANOVA tests and by comparing averaged profiles of the foot velocity. These tests showed two major trends. Firstly, in the test conducted, there was an observable effect of targeting behaviour in both groups. Secondly, the differences were observed in the spatiotemporal parameters but not within the kinematic parameters. The differences in the peak GRF require further study.

Contrary to what was expected from Verniba et al.'s (32) recent study, the analysis showed significant statistical differences attributable to a targeting effect within the control group. The targeting step, the first step, of the control group was on average slower and shorter than that of their non-targeting step, the third step. These effects were found in similar proportions in both sides of the healthy participants' gait. This is closer to the effects presented in the prior study by Wearing et al. (31).

As found in the Wearing et al.'s study, there was an effect on the total variability of each step in the control group. An overall reduction in standard deviation in step speed and a slight decrease in standard deviation of step length was observed. This indicates that the healthy participants had a slightly more consistent step speed when aiming for the force plate but an increase in variability for their step length.

These findings are consistent with the theory of targeting control leading a person to make subtle adjustments to their step length during the targeting step to ensure they were within the marked area. During this process, they seem to slow down and take longer to complete their step, also reducing the variability of this speed.

The stroke-survivor group took smaller steps and had longer step times than the control group as was expected due to their impairment. This was confirmed as significant by the statistical tests. The ANOVA results also indicated that there were significant differences between their targeting and normative steps spatiotemporal parameters similar to that exhibited by the control group.

The stroke-survivors group had, on average, slower and shorter targeting steps by comparison to the normative step. These effects were similar across both sides of the stroke-survivor participants' gait. The ANOVA found no significant effect on the spatiotemporal parameters due to any interaction effects between the three factors. This shows that while there are minor differences between the left and right legs of the stroke participants between each step, this is not dissimilar to the overall effect exhibited in the control group. Thus, it can be said that the targeting effect acted in a consistent way between each leg regardless of whether the participant had suffered a stroke or not.

However, the similarities between the groups did not extend to standard deviations. The right step length deviation increased on the normative step for the stroke survivors and the left step length deviation barely changing at all. This could be related to the nature of hemiparetic gait. As all of the stroke-survivor participants were impaired on their right-hand side, it is suggested that they had to focus on controlling their right leg motion more during the targeting step to compensate for their impairment. Their left leg also had a reduced standard deviation between the two steps, but this was very minor.

Comparing the two groups' spatiotemporal parameters there were obvious differences due to the impairments of the stroke-survivors as was expected. However, both groups exhibited similar differences between the targeting step and normative step which was similarly significant for both groups by the statistical analysis. There was an overall decrease in step speed, shorter step lengths and longer step times for the targeting step in both groups. The only notable difference that was observed was the stroke survivors' right leg targeting step length standard deviation being lower than that of the normative step as opposed to the control group where the reverse was observed. This would suggest a small change in the ways that the impaired subjects compensated for targeting the force plate. This is in contrast to Verniba et al.'s (32) findings which showed little difference between normative and targeting spatiotemporal parameters.

In addition to the statistical analysis, a further investigation was made of the speed profiles of the participants' foot during the trials. The graphs produced, Figure 3.6 (a) and (b), showcased the major difference between the two groups that was expected. The stroke survivors had significantly lower peak step speeds during the experiment and there also had

a greater variation in profiles between their left and right legs. It was also found that once normalised for the time period, the profiles between the groups took on a similar shape indicating a degree of similarity between how the two groups shifted their weight forwards. This is inferred by the velocity variation corresponding to progression in the swing phase and therefore the movement of the centre of mass of the participant. This could be subject to further study in and of itself however.

It was also observed that the targeting step consistently peaked in step speed earlier than the normative step for both groups and between both legs. This supplements the findings of the ANOVA analysis and indicates that the targeting effect changes the swing phase of the gait cycle, making the participant slow down earlier before making contact with the force plate. This could be linked with the theory that the participant is taking additional time during this targeting step to correct the foot's placement. This effect seems to be present regardless of whether the participant had had a stroke.

3.4.2. Kinematic Data

The analysis of the kinematic angles of both groups focused on the moment of hitting the force plate. Within the control group, the statistical analysis found no significant influence from step number on any of the parameters. The major differences present in the group were between left and right steps with the left leg showing slightly smaller ankle angles. Additionally, there was little change in any of the standard deviations of the parameters between the targeting and non-targeting step. Thus, it is suggested that this study found no effect on the kinematic properties of the healthy control group due to targeting effects confirming Verniba et al.'s findings (32).

By comparison, the stroke group showed similar ankle angles but significantly different knee angles for both legs and leg-dependent differences in hip angles. These values correspond with expected characteristics of hemiparetic gait (89). However, there were no significant differences attributed to the targeting step versus the normative step. Additionally, standard deviation was found to be similar across steps. The statistical analysis showed that there was no significant effect on kinematic angles at heel strike due to targeting present in either group for both legs.

3.4.3. Kinetic Data

During the initial stages of the experiment planning, it was found that using multiple force plates while still ensuring accurate comparison across normative and targeting steps was beyond the available resources. Instead, it was decided that the available kinetic data would be compared to previous studies of similar nature. This allowed broad conclusions to be drawn though their use is limited to being a stepping point for further studies.

Comparing the peak GRF value found during the targeting step in this study with data from previous gait analysis experiments shows that higher average peak GRF values were exhibited in both the healthy and stroke-survivor populations within this study (32, 87). The control group showed no statistical difference between the left and right legs which was as expected for the population. By comparison, the stroke group showed asymmetrical peak GRF values but rather than showing a larger GRF for the unaffected limb as was shown in HyunDong et al.'s study, it was found that there was a larger GRF for the affected limb.

It is suggested that there may have been a side dependent effect on the peak GRF due to targeting within the control group because of the stark contrast shown between these two

studies. To confirm this, further studies would have to be conducted within the test population. This should be done with a much longer experiment involving a series of normative trials where the presence and location of the force plate are unknown followed by a series of trials, where the force plate is clearly marked, and the participants are instructed to step within its boundaries.

Alternatively, as the findings of this experiment have shown, the rate at which a participant changes their spatiotemporal gait parameters after the targeting step onto the force plate back to what is suggested to be a normal non-targeting gait may be taken advantage of in further experiments. It would be possible to have a visible targeting force plate followed by a hidden force plate. The advantage of this set-up would be that the position of the participants' footfall should be fairly easy to approximate following on from the visible force plate and as such this should increase the reliability of getting valid kinetic data from a trial.

Lastly, kinetic data could also be collected in a normative manner by use of insole pressure sensors as used in HyunDong et al.'s (87) study. However, currently the sensitivity and usefulness of these devices are limited when compared with existing force plates. If the technology were to be developed further, the ability to record GRF without the use of a force plate would limit the number of trials necessary while removing the targeting effect as there would be no visual cues influencing the participant.

3.5. Conclusion

This study found that hemiparetic stroke survivors exhibit a noticeable targeting effect for their spatiotemporal and potentially kinetic parameters whereas kinematic parameters were not significantly affected. Some similar effects were also found in the healthy baseline comparison group in contrast to some previous studies. Until wearable sensors see wider adoption, the most common method of gait analysis will likely still use force plates. To improve the methods that researchers and clinicians use with these set ups, it is suggested that gait analysis experiments report the total number of trials that were failures to help determine more reliable procedures. During the experiment, it was found the failure rates for stroke survivors to be significantly higher than for healthy participants. This value was not in the author's opinion excessive, but more work could be done to establish reliable standards for analysing gait.

Chapter 4 Effects of Variations in Hemiparetic Gait Patterns on Improvements in Walking Speed

4.1. Introduction

The Linear Fit (LF) method is suggested to be a useful tool for analysing the kinematic data that is commonly overlooked in gait analysis studies. Often, kinematic data is taken as a range or sample points at particular gait events which leaves out key information about the "path" the joint angles take between these two points including acceleration and lag/lead. Using the LF method on hemiparetic stroke survivors and comparing their data against a healthy baseline would allow for the variations in gait between the two populations to be described by reference to the healthy baseline and produce outcomes that clearly describe the variations and more importantly can be utilised to perform more in-depth statistical analysis.

The aim of this study is to identify any significant patterns in the 3D kinematic gait profiles of hemiparetic gait that correspond to variations in self-selected walking speed. The study will then help identify common elements of hemiparetic gait patterns that correspond to higher self-selected walking speeds. These elements could then be used to inform targets for rehabilitation therapies focusing on functional gait recovery.

4.2. Methodology

4.2.1. Methodology Overview

This pilot study took experimental gait analysis data from a group of healthy participants as a baseline gait pattern against which to compare clinical gait analysis data from a small selection of hemiparetic stroke survivors as covered in Figure 4.1. The stroke survivors exhibited a range of self-selected walking speeds, a useful parameter for assessing gait functionality. This data was then prepared for further assessment by normalising each gait trial based off of key gait events.

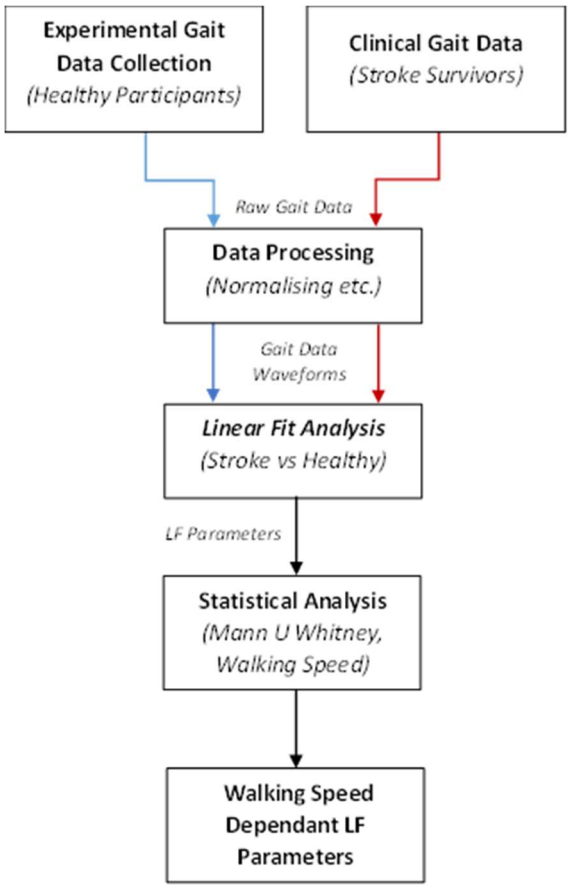

Figure 4.1: Methodology flow chart showing how gait data was handled and assessed

A comparison between the two groups was made using the Linear Fit Method which compares the gait data as continuous waveforms. This method produces 3 parameters that describe how the hemiparetic gait pattern varied from the healthy reference pattern for each of the recorded gait trials.

These variations, thus quantified, were then analysed with respect to the self-selected walking speed exhibited by the participants during each gait trial. This was achieved with a Mann-Whitney U Test to establish the relationship between self-selected walking speed hemiparetic gait pattern variations.

4.2.2. Participants

This study used clinical gait analysis data from stroke survivors at the Gait lab of the West Midland Rehabilitation Centre (WMRC), part of Birmingham Community Healthcare NHS Foundation Trust. All stroke survivors completed a consent form informing them of how their data could be used and the corresponding ethical approval was obtained by WMRC. From the data available, 4 chronic male stroke survivors were selected, all of whom had suffered right-hand side hemiparesis as the result of a stroke (age: 31+/- 3.7 years, height 168 +/- 5.5cm, weight: 59.8 +/- 12.4kg). The survivors were selected as they were able to walk unaided, had achieved a range of self-selected walking speeds and had all received physical therapy after their stroke event at the WMRC.

Further gait trials were performed on a locally recruited set of healthy participants, of which 3 male participants were selected that matched the stroke survivors for gender and approximately for age (age: 25.3 +/- 1.5years, height 172.3 +/- 5.5cm, weight: 74 +/- 7.1kg). All healthy participants had no history of neurological disorders or brain damage.

4.2.3. Experimental Procedure and Data Processing

The system that was used consisted of a VICON MX system with 12 cameras dispersed around a central walkway for motion analysis. Of the 12 cameras, 6 were MX3+'s and 6 were MX T40's, both sets of which were capturing at 100Hz. The VICON Nexus 1.8 Gait Analysis Software was used for capturing and processing the gait data. The cameras were calibrated at the start of each session using a Vicon "Active Wand" to ensure they were capturing correctly. The reflective markers that were used to track the participant's movements were applied according to the Vicon Lower Body marker set based off of the Newington-Helen Hayes model (90).

Participants were required to wear tight clothing in order to ensure that the marker was as close to the body as possible and stayed in position during motion. The participants were bare foot for the gait trials.

To help corroborate the data recorded by the VICON camera system and ensure processing was performed correctly, two digital cameras were used to record reference videos at 50Hz.

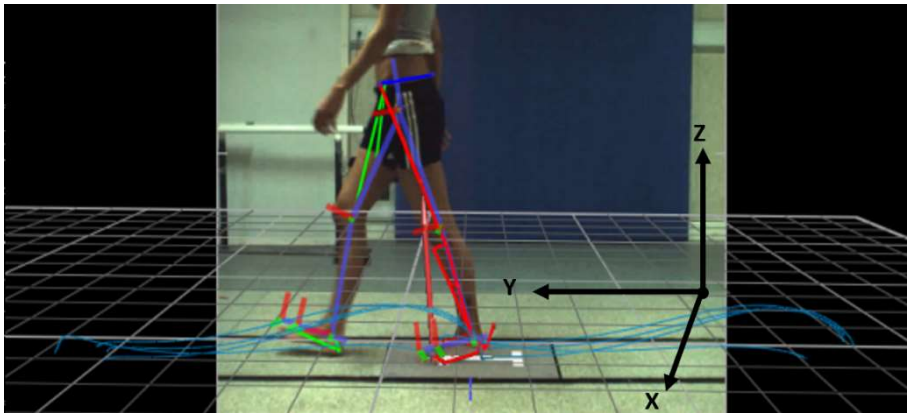

Figure 4.2: View of participants walking along walkway with attached markers around the ankle, knee and hip joints with the axis labels X,Y,Z corresponding to the Frontal, Sagittal and Vertical axes of movement respectively

One was placed at the end of the walkway, pointed down its length, and the other at its midpoint looking across it. Visuals from both camera sets are presented in Figure 4.2.

The walkway itself was 10m long and defined by a pair of parallel markings on the ground. Additionally, a force plate was present and outlined at the centre of the walkway as part of the standard equipment used for the gait analysis in the centre. Due to the format of the analysis, kinetic data was not included in this study.

After a series of calibration trials were completed, the participants were asked to walk along the walkway at their preferred, comfortable self-selected walking speed. The procedure followed the format specified by the WMRC for their clinical trials. The participants were made aware of the presence of the force plate but were not told to specifically target it. The presence of a clearly marked force plate has previously been found to slightly impact the step speed and length of both stroke survivors and healthy samples as seen in Chapter 3. However, this impact is similar across both groups and no evidence of effects on kinematic parameters were found. Other studies have shown that it does not affect healthy participants gait significantly (32) and as such is deemed to present a sufficiently low risk of effecting the significance of the study outcomes.

From the processed trials, six were randomly selected from each participant for further analysis. Each of the trials was then cut down to two consecutive steps representing a snapshot of the gait pattern, right (paretic) toe-off to left (non-paretic) heel strike.

The kinematic and spatiotemporal data for the left and right hip, knee, and ankle joints were extracted as sets of continuous 3D data from which additional basic gait parameters such as step lengths and step time were also calculated. The kinematic data gave the angles at each

of the joints in Flexion and Extension around the Frontal (X) axis, Abduction and Adduction around the Sagittal (Y) axis and Internal and External Rotation around the Vertical (Z) axis as highlighted in Figure 4.2.

The data was then normalised to allow for effective comparisons. The paretic (right) limb toe-off event was used to mark the beginning of the gait cycle, 0%, and the non-paretic (left) limb heel-strike occurred at completion of the period, 100%. This version of the gait cycle is due to the nature of data collection employed. Collected in a clinical setting, the resulting comparable data between stroke survivors was limited while still focusing on high quality, representative data. To account for variations due to the anthropometrics the step lengths were normalised against the participant's height giving units of percentage of height per second (%h/s).

4.2.4. Linear Fit Analysis of Gait Patterns

The Linear Fit Method (49) was chosen to compare the gait cycle between the healthy and stroke survivors' group to allow for a straightforward comparison between the data that does not rely on comparing values at specific gait events or the minimum and maximum values.

The proposed method uses 3 formulae which compare how a continuous dataset of interest and its average (P_a,$\overline{P_a}$) the stroke survivors' gait, varies from a reference dataset and its average (P_{ref},$\overline{P_{ref}}$), average gait of the 3 healthy participants, and produces 3 corresponding parameters. These parameters are:

a_1, or the **Amplitude Scaling Factor**, compares the rate of change between the data sets and is given by $Eq.4.1$. It is the factor for which the reference gait data should be multiplied such that its rate of change matches the dataset of interest. I.e if the stroke survivor data sees lower accelerations than the healthy average set then the expected value of a_1 would be <1.

$$a_1 = \frac{\sum_{i=1}^{N}(P_{ref}(\boldsymbol{i}) - \overline{P_{ref}}) \cdot (P_a(i) - \bar{P}_a)}{\sum_{i=1}^{N}(P_{ref}(i) - \overline{P_{ref}})^2} \quad Eq.4.1$$

a_0, or **Scalar Addition**, is the scalar addition needed to ensure that the data of interest's value is 0 when the reference data is 0 and is given by $Eq.4.2$. It can also be described as the average offset between the data sets.

$$a_0 = \bar{P}_a - a_1 \cdot \overline{P_{ref}} \quad Eq.4.2$$

R^2, or **Shape Similarity**, is the square of the Pearson's correlation coefficient R which establishes the strength of the linear relationship between the two waveforms that the data sets make such that their variance, or shape, matches. This is given by $Eq.4.3$. A value of 1 is a complete match.

$$R^2 = \frac{\sum_{i=1}^{N}(a_0 + a_1 \cdot P_{ref}(i) - \bar{P}_a)}{\sum_{i=1}^{N}(P_a(i) - \bar{P}_a)^2} \quad Eq.4.3$$

These parameters allowed for quick and convenient comparison between the stroke survivor's gait patterns and the healthy average over the full gait cycle. If the two gait data sets were identical, the LF parameters would be a_1=1, a_0=0 and R^2=1. These parameters can thus be used to assess where hemiparetic gait differs by comparison to a healthy average gait pattern for a given gait speed.

To give a benchmark of deviations that could be accounted for within healthy gait, the healthy participants gait patterns were also analysed against the healthy average using the Linear Fit Method.

There are however limitations, as raised within the original outline of the method which highlighted that for larger variations from the shape similarity the LF method can lose definition (49) and as such care should be taken when assessing which data is significant. As suggested in the paper that originally introduced the method, if a set of joint angle waveforms had average values of R^2 below 0.50 then the data for a_0 and a_1 was not included in the discussion. Exceptions were made for cases where R^2 showed a strong positive correlation and the higher end of data was deemed comparable.

4.2.5. Statistical Analysis of the Linear Fit Parameters

The program used to conduct the statistical analysis was IBM's SPSS Statistics 22. The LF parameters that described the variations in the kinematic waveforms between the data set of interest and the healthy average comparison over the course of the selected gait cycle were examined using walking speed as the independent variable for the statistical analysis.

The analysis was performed in two stages, the values of R^2 of the healthy participants and the stroke survivors were directly compared to assess whether the variation from the average was significantly different and what could be accounted for by normal fluctuations in healthy gait. After testing for normality found that a significant portion of the data did not fit the parametric assumptions a Mann Whitney-U test was selected as the method to compare the groups.

The second stage was to select a test that would assess whether the variation in LF parameters was related to the Survivor's self-selected walking speed. A linear regression analysis was considered as it would effectively determine whether a linear relationship existed between the LF parameters and walking speed and its relative strength.

In order to test if the data was fit for a regression analysis a selection of scatter plots between the LF parameters and walking speed were produced using a sample taken from across various parameters and participants. Few of the plots had significant outliers and various parameters showed visual evidence of linear relationships with gait speed. An example set of scatter plots are shown below in Figure 4.3. The same visual analysis also looked for homoscedasticity with no clear patterns in the distribution of the data being found. Based off of the back of these preliminary analysis a Linear Regression test was found to be suitable method of analysing the LF parameters with respect to walking speed. Statistical significance level was set at $p<0.05$ for both the Linear Regression and Mann-Whitney U analyses.

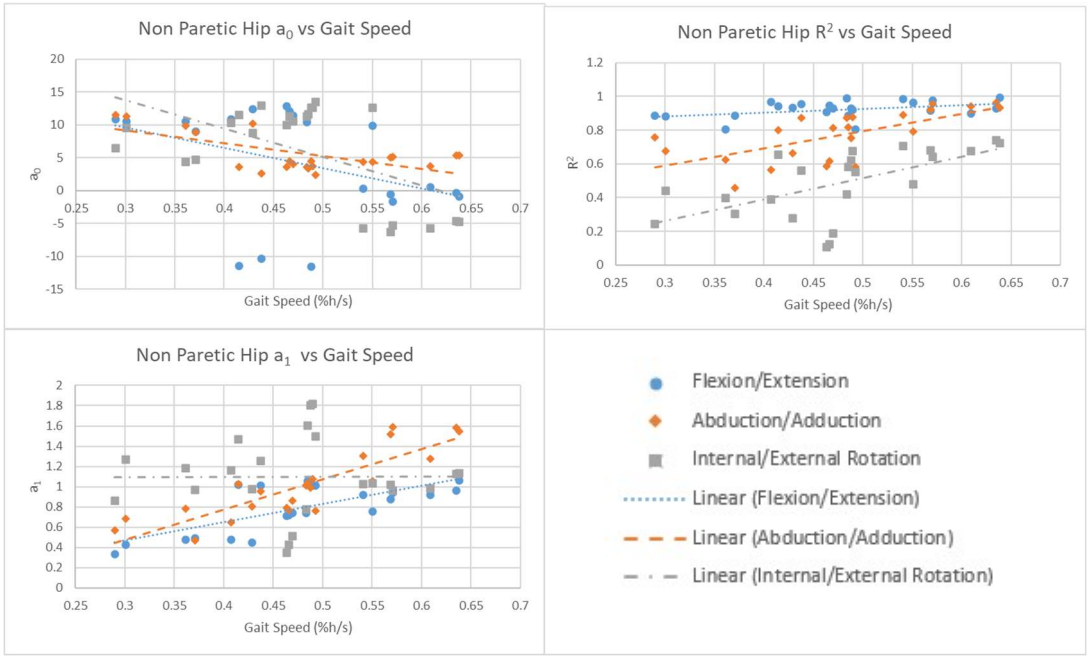

Figure 4.3: Scatter plots between LF parameters and gait speed for the left (non-paretic) hip for stroke survivors

4.3. Walking Speed and Hemiparetic Gait Variations

Additional gait parameters are presented and analysed separately to further inform the LF analysis. The average values and standard deviations of these overall parameters are given in Table 4-1: Average values and standard deviations of gait parametersTable 4-1.

Table 4-1: Average values and standard deviations of gait parameters

	Average Value (Standard Deviation)		
Gait Parameters	**Healthy**	**Stroke Paretic**	
Gait Speed (%height/s)	0.607 (.018)	0.479 (.094)	
Double Support Time (s)	0.112 (.010)	0.098 (.028)	
Step Length (%height)	32.60 (.021)	22.00 (.037)	
Step Time (s)	0.414 (.022)	0.402 (.025)	
Cycle Time (s)	0.939 (0.053)	0.940 (.063)	

The regression analysis was carried out on 3 of the gait parameters and are presented in Table 4-1 with their significance and regression coefficients. Gait speed was omitted as it was used as the independent variable while the cycle time was made up of the double support and step times. The survivor's self-selected walking speed for each trial was taken as the independent variable and the LF parameters produced from the data waveforms as the dependant variable. The healthy group showed no significant regression relationship with any of the gait parameters whereas the stroke survivors' showed relationships in the step length of both legs along with the double support time between the steps.

Table 4-2: Linear regression results of basic gait parameters with gait speed as the independent variable

	p-Value (Standardised Correlation Beta Coefficient, Regression Coefficient)		
Gait Parameters	**Healthy**	**Stroke Paretic**	**Stroke Non-Paretic**
Double Support Time (s)	.420 (-.203, -.107)	**.002 (-.598, -.176)**	
Step Length (%height)	.941 (-.349, -.032)	**.000 (.677, .027)**	**.002 (.594, .025)**
Step Time (s)	.156 (-.019, -.341)	.594 (.114, .030)	.198 (-.272, -.198)

The LF method was applied to the kinematic waveform data for the stroke survivors with the resulting average and standard deviation for each of the kinematic LF parameters being listed in Table 4-3. These values describe the differences between the stroke survivors and the healthy participants gait waveforms.

Table 4-3: Kinematic Stroke Survivor average LF parameters derived from comparison to established healthy baseline gait pattern

Kinematic	**Average LF Value (Standard Deviation)**					
	Non-Paretic			***Paretic***		
Flexion/Extension (x)	**Ankle**	**Knee**	**Hip**	**Ankle**	**Knee**	**Hip**
a0	1.36° (9.98°)	2.47° (15.77°)	3.54° (6.46°)	3.84° (6.46°)	11.17° (18.84°)	4.60° (8.69°)
a1	0.784 (0.227)	0.767 (0.203)	0.752 (0.296)	0.840 (0.142)	0.709 (0.305)	0.892 (0.155)
R2	0.616 (0.209)	0.885 (0.084)	0.886 (0.183)	0.740 (0.143)	0.842 (0.158)	0.835 (0.090)
Abduction/ Adduction (y)	**Ankle**	**Knee**	**Hip**	**Ankle**	**Knee**	**Hip**
a0	-2.16° (2.12°)	-1.91° (3.65°)	5.81° (2.95°)	-1.28° (1.90°)	-3.91° (6.57°)	0.89° (0.16°)
a1	0.796 (0.636)	1.136 (0.591)	0.986 (0.334)	1.197 (0.503)	1.182 (1.111)	0.954 (0.463)
R2	0.464 (0.271)	0.626 (0.272)	0.743 (0.194)	0.451 (0.280)	0.492 (0.301)	0.611 (0.230)
Internal/External Rotation (z)	**Ankle**	**Knee**	**Hip**	**Ankle**	**Knee**	**Hip**
a0	10.56° (7.31°)	-3.71° (14.26)	5.02° (9.20°)	6.51° (8.25°)	-2.86° (15.02°)	1.90° (5.36°)
a1	0.632 (0.493)	0.936 (0.366)	1.049 (0.439)	0.841 (0.420)	0.379 (0.559)	1.001 (0.464)
R2	0.450 (0.273)	0.616 (0.176)	0.466 (0.220)	0.458 (0.264)	0.228 (0.302)	0.444 (0.166)

The waveforms for the kinematic joint motion are also presented in graphical form with comparisons between the healthy average waveform along with the upper and lower quartiles, Q3 and Q1 respectively, of the stroke survivors' average waveform with regards to gait speed. These graphs are contained within Figures 4.4, 5 and 6 which correspond to the hip, knee and ankle joints respectively.

Within each of these 3 figures there are 6 sub-figures, each representing rotation about one axis across either the left (non-paretic) or right (paretic) joints:

- [a] = Non-Paretic Flexion/Extension
- [b] = Paretic Flexion Extension
- [c] = Non-Paretic Abduction/Adduction
- [d] = Paretic Abduction/Adduction
- [e] = Non-Paretic Internal/External Rotation
- [f] = Paretic Internal/External Rotation

To test that the two populations are significantly different, the values of R^2, waveform similarity, were compared between the stroke survivors' and healthy participants' data sets using the Mann-Whitney U test with all data split between left and right limbs, that being non-paretic and paretic for stroke survivors, and compared separately. It was found that the populations differed significantly in their waveform shape across all joints and axes in both limbs.

The regression analysis outcomes of the LF parameters of the kinematic dataset with respect to walking speed are presented in Table 4-4 Table 4-5. Table 4-4 contains the p-values for each LF parameter and represents where significant relationships were found. The strength of these relationships is conveyed in Table 4-5 with the standardised correlation coefficients and the regression coefficients. Significant regression results are presented in bold font.

Table 4-4: Linear regression analysis p-values of the LF parameters which highlight statistically significant regression between LF parameters and the independent variable, gait speed. Results below 0.05 are presented in bold.

Kinematic	p-Value					
	Non-Paretic			***Paretic***		
Flexion/Extension (x)	**Ankle**	**Knee**	**Hip**	**Ankle**	**Knee**	**Hip**
a_0x	.246	**.035**	.415	.471	**.019**	**.040**
a_1x	**.007**	**<.001**	**.018**	**.014**	.104	**<.001**
R^2x	.103	.340	.925	.610	.910	**.002**
Abduction/ Adduction (y)	**Ankle**	**Knee**	**Hip**	**Ankle**	**Knee**	**Hip**
a_0y	**.002**	**.020**	**.002**	**.011**	**<.001**	**<.001**
a_1y	**.002**	.889	**<.001**	.641	**<.001**	**<.001**
R^2y	**.006**	.274	.058	**.008**	**<.001**	**<.001**
Internal/External Rotation (z)	**Ankle**	**Knee**	**Hip**	**Ankle**	**Knee**	**Hip**
a_0z	.066	.425	**.009**	.512	.839	.167
a_1z	**<.001**	**<.001**	.747	**.004**	**.001**	**<.001**
R^2z	**.004**	.107	**.022**	**.005**	**<.001**	.098

*Table 4-5: Linear regression analysis correlation and regression coefficients for LF parameters which describe the strength of the hemiparetic gait pattern variations from the established healthy baseline by comparison with self-selected walking speed. Results in **bold** correspond to a significant outcome (p<0.05)*

Kinematic	Standardised Correlation Beta Coefficient (Regression Coefficient)					
	Non-Paretic			***Paretic***		
Flexion/Extension (x)	**Ankle**	**Knee**	**Hip**	**Ankle**	**Knee**	**Hip**
a_0x	-.246 (-26.14)	**-.431 (-72.29)**	-.175 (-22.42)	-.154 (-10.60)	**-.476 (-95.36)**	**-.421 (-38.91)**
a_1x	**.532 (1.282)**	**.764 (1.648)**	**.479 (1.507)**	**.497 (.748)**	.340 (1.102)	**.772 (1.273)**
R^2x	.341 (.757)	.204 (.183)	-.020 (-.039)	.110 (.167)	.024 (.041)	**.589 (.567)**
Abduction/ Adduction (y)	**Ankle**	**Knee**	**Hip**	**Ankle**	**Knee**	**Hip**
a_0y	**.596 (13.41)**	**.471 (18.27)**	**-.596 (-18.72)**	**.511 (10.32)**	**.789 (55.15)**	**.864 (23.82)**
a_1y	**.606 (4.096)**	-.030 (-.189)	**.795 (2.821)**	-.100 (-.536)	**-.828 (-9.781)**	**.689 (3.396)**
R^2y	**.542 (1.563)**	.233 (.672)	.393 (.812)	**.528 (1.573)**	**-.737 (-2.359)**	**.707 (1.729)**
Internal/External Rotation (z)	**Ankle**	**Knee**	**Hip**	**Ankle**	**Knee**	**Hip**
a_0z	-.382 (-29.69)	-.171 (-25.91)	**-.518 (-50.73)**	.141 (12.33)	-.044 (-6.98)	.292 (16.61)
a_1z	**.696 (3.650)**	**.736 (2.867)**	-.069 (-.324)	**.563 (2.516)**	**.645 (3.839)**	**-.776 (-3.826)**
R^2z	**.571 (1.659)**	-.337 (-.632)	**.466 (1.092)**	**.557 (1.561)**	**.666 (2.141)**	-.346 (-.612)

The other results sections examine the LF parameters from Table 4-1 and Table 4-3 and their respective regression coefficients from Table 4-2, Table 4-5 and Table 4-5, focusing on those whose p-values indicate that there are significant relationships with walking speed. This is supported using the graphical waveform representations in Figures 4.4, 5 and 6 where appropriate.

4.3.1. Step Length and Step Time

The recorded step lengths showed a positive relationship with speed for both limbs in Table 4-2. The paretic limb (right) exhibited slightly higher improvements in the step length - 7% more than the non-paretic limb (left) - over the range of walking speeds observed. The non-paretic leg maintained a higher stride length than the paretic leg as walking speed increased, but this gap did narrow.

The time taken per step did not see any relationship with walking speed in either the paretic or non-paretic limbs. The double support time did see an overall decrease with walking speed with a regression coefficient of -.176. The higher walking speeds were therefore accomplished due to an increase in average step length and a decrease in the amount of time between steps while the time taken for each individual step remained similar.

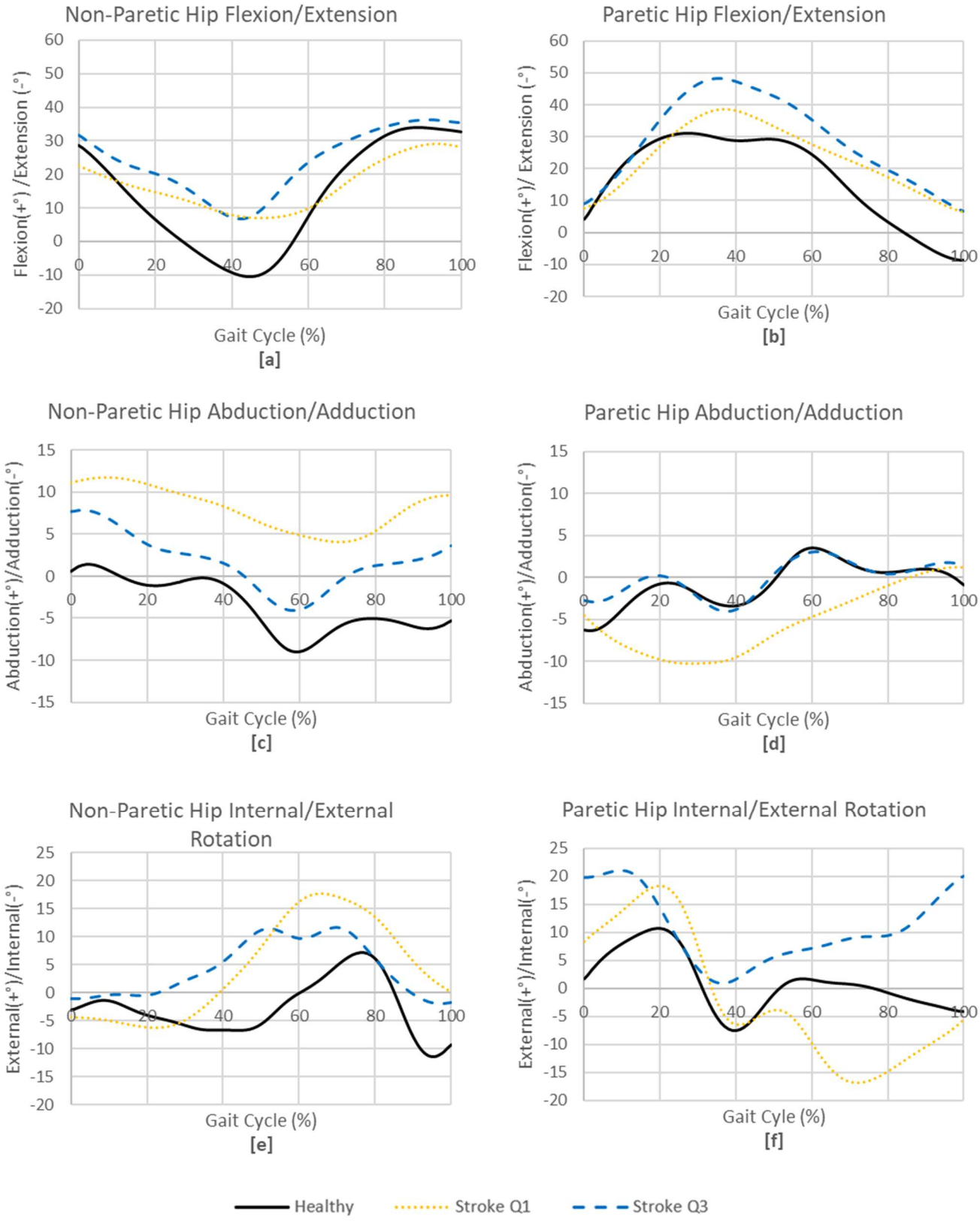

Figure 4.4: Kinematic waveforms describing the variation in joint angles for the left (non-paretic) and right (paretic) hip joints over the extent of the gait trial for the average healthy gait pattern along with the lower (Q1) and upper (Q3) quartiles of average hemiparetic gait patterns for walking speed

4.3.2. Circumduction in Paretic and Non-Paretic Hip Joints

At slower speeds, the abduction and adduction pattern of the paretic hip had low similarity to the healthy average with a kinematic $R^2y < 0.611$. This similarity, the rate of change, a_1y, and offset, a_0y, all increased with higher speeds though, with relatively strong correlation coefficients of .707, .689 and .864 respectively. This presents a paretic hip circumduction pattern that became more similar to the healthy pattern as the self-selected walking speed increased, as can be seen in Figure 4.4d.

The non-paretic hip on the other hand saw higher average similarity to the healthy comparison, $R^2y = 0.743$, for abduction and adduction but no relation to the walking speed. There was, however, a significant increase in rate of change as walking speed increased for the non-paretic hip, similar but weaker than that of the paretic hip, with a regression coefficient of 2.821 for a_1y and a strong correlation coefficient of .795.

It was also noted that there was a steady decrease of average abduction in both hip joints (kinematic a_0y), increasing for the paretic hip and decreasing for the non-paretic, as gait speed increased. This led to a smaller average angle between the two limbs, which may indicate a shift in the degree of loading between limbs though the non-paretic hip was still left with a noticeable abduction offset as can be seen in Figure 4.4c.

The faster walking speeds coincided with an increase in flexion of both hip joints of the stroke survivors, a_1X correlation (and regression) coefficients of .772 (1.273) and .479 (1.507) for the non-paretic and paretic hip respectively, indicating a stronger relationship for the non-paretic hip. Overall, this led to the non-paretic hip still showing reduced peak flexions as

shown in Figure 4.4a while the paretic hip had increased peak flexions and decreased peak extensions which can be seen in Figure 4.4b.

The average waveform similarity for both hip joints was low, $R^2z \approx 0.45$, leading to difficulties in accurately assessing their relationship with walking speed. However, the value of R^2z of the non-paretic hip joint was found to correlate with increased walking with a regression coefficient of 1.092 though this relationship was weaker than some others seen in the analysis with a correlation coefficient of .446. This led to a non-paretic hip joint rotation with a reduced average offset and more familiar waveform pattern when compared against the healthy baseline.

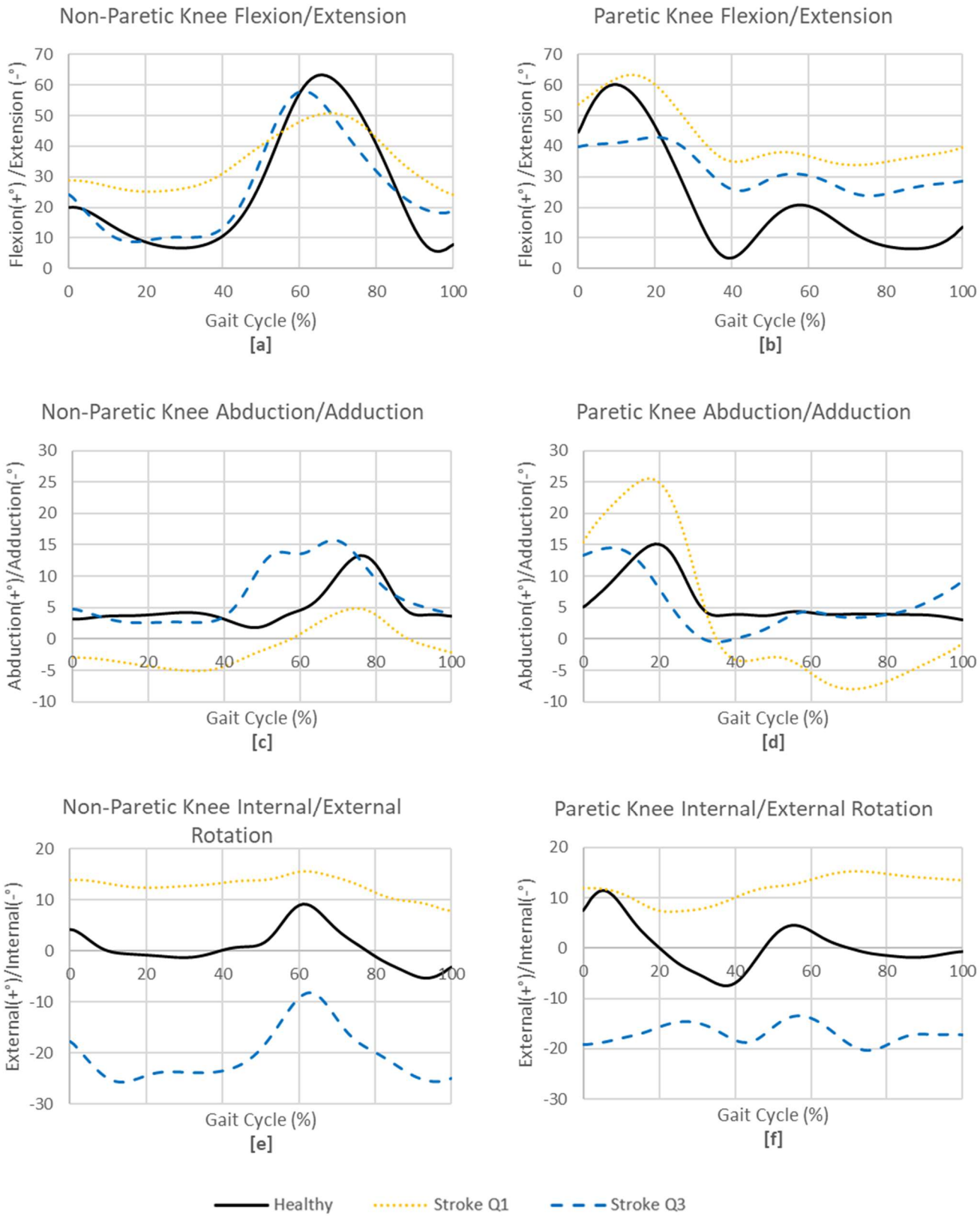

Figure 4.5: Kinematic waveforms describing the variation in joint angles for the left (non-paretic) and right (paretic) knee joints over the extent of the gait trial for the average healthy gait pattern along with the lower (Q1) and upper (Q3) quartiles of average hemiparetic gait patterns for walking speed

4.3.3. Overextension of Paretic Knee at Higher Walking Speeds

One of the major causes of limb lengthening - a lower degree of flexion in the paretic knee joint - was found to be exacerbated in higher speed trials with the value of the kinematic a_0X showing a general trend towards a decrease in average flexion with regards to the healthy average (a regression coefficient of -95.36° and a correlation coefficient of -.476) as can also be seen in Figure 4.5b. The acceleration of the joint angle, a_1x - and, therefore, the overall range and acceleration of motion - saw no relationship with gait speed and was lower on average than the healthy sample, mean paretic knee kinematic $a_1x = 0.709$. This data shows that the paretic knee had particularly reduced flexion during the toe-off and subsequent swing phase of the paretic leg at higher speeds (Q3), increasing its effect on limb lengthening.

The non-paretic knee also saw a decrease in overall flexion (a_0x) at faster gait speed. Unlike in the paretic leg, an increase was also observed the rate of change of flexion/extension, a_1x. This led to a relatively similar kinematic pattern of flexion and extension to the healthy comparison as can be seen in Figure 4.5c.

For rotation around other axes the paretic knee had very low similarity scores, averages of $R^2y=0.492$ and $R^2z=0.228$, leading to difficulties in making clear comparisons. Of note though is that each similarity score did see a relationship with walking speed. While the internal and external rotation of the paretic knee joint showed a strong positive relationship with walking speed (moving closer to the healthy waveform), the Abduction/Adduction waveform actually drifted further away from the healthy pattern which can be seen to an extent in Figure 4.5f and d respectively.

The non-paretic knee joint did not see any relation between the waveform shapes and walking speed and the similarity scores were low on average, around 0.45, with fairly large standard deviations of 0.27. This makes it difficult to compare via the statistical analysis though Figure 4.5c and e can be used to observe the large offsets that were present.

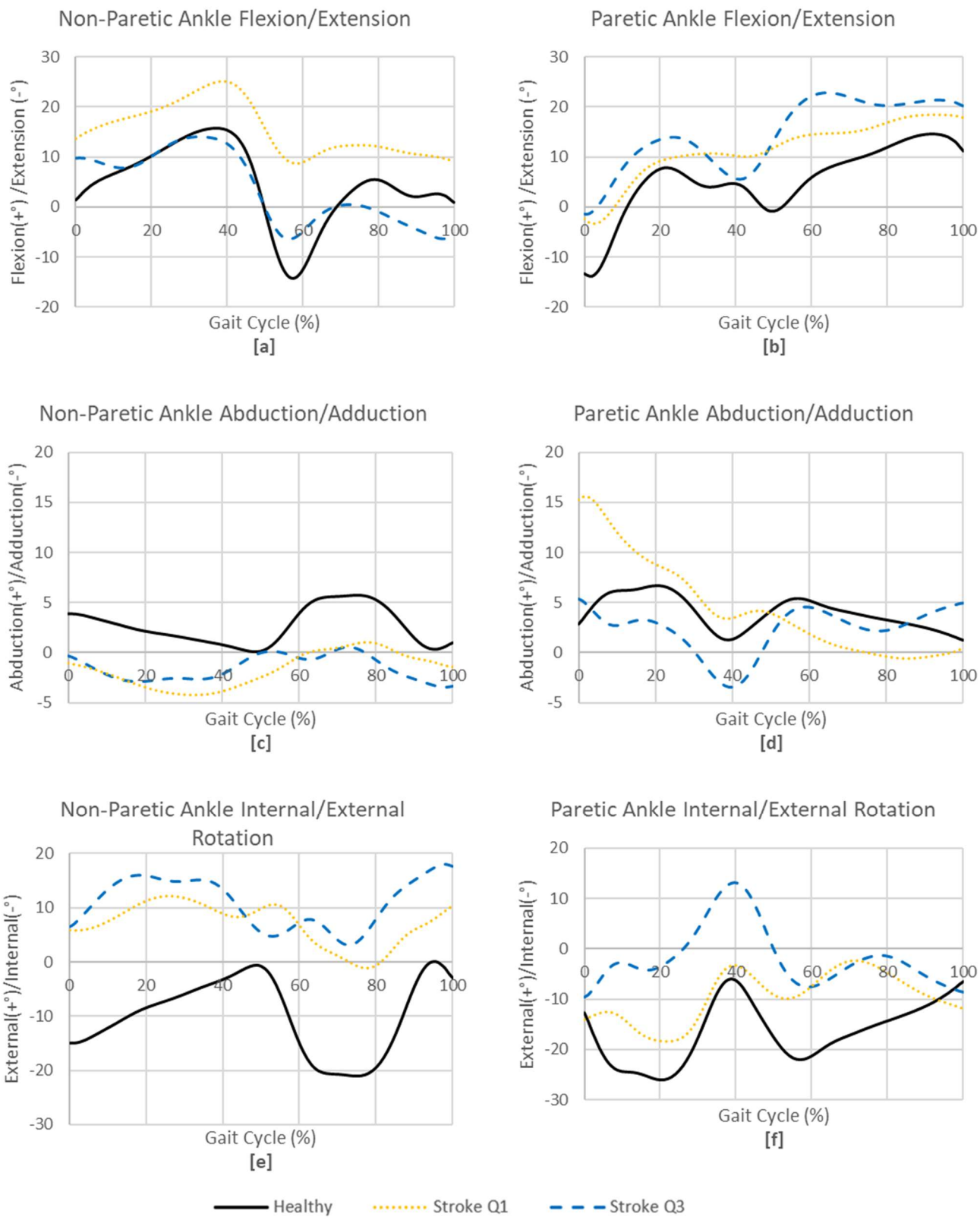

Figure 4.6: Kinematic waveforms describing the variation in joint angles for the left (non-paretic) and right (paretic) ankle joints over the extent of the gait trial for the average healthy gait pattern along with the lower (Q1) and upper (Q3) quartiles of average hemiparetic gait patterns for walking speed.

4.3.4. Foot Drop in Paretic and Non-Paretic Ankle Joints

The analysis found that both the paretic and non-paretic ankles had surprisingly similar kinematic relationships with walking speed. Both exhibited a slight average flexion offset, a_0x = 3.84° and 1.36° for the paretic and non-paretic ankle joints respectively, and large standard deviations which didn't vary significantly with walking speed.

Additionally, both ankle joints exhibited an increased rate of change with larger peak dorsiflexion angles (flexion) at higher walking speeds. For slower speeds both joints had values of a_1x below 1 indicating lower peaks than the healthy comparison but strong positive regression coefficients, particularly in the non-paretic ankle, led to the non-paretic ankle approaching near healthy flexion levels and the paretic ankle developing a distinct peak in flexion and extension as can be seen in Figure 5a and 5b respectively. The faster paretic ankle waveform does not match the healthy waveforms shape though and instead peak extension occurs approximately 10% earlier in the gait cycle.

The rotation in other axes for both ankle joints showed lower average similarity to the healthy baseline, $R^2 \approx 0.45$, though all showed increasing similarity to the healthy pattern as walking speed increased.

The internal and external rotation in both ankle joints also showed increases in peak accelerations, a_1z, though without a shift in offset both feet remained pointing away from the sagittal plane as can be seen in Figure 4.6e and f. The ankle joints also showed significant relationships between increasing abduction offset and walking speed, a_0y, though this

remained below the healthy baseline as seen in Figure 4.6d and c. Lastly, the non-paretic ankle joint also saw increasing peak accelerations in abduction and adduction behaviour, a_1y.

4.4. Discussion

This pilot study examined the evidence describing common hemiparetic gait disturbances and how they changed with respect to walking speed. The combination of these patterns shows that, while the stroke survivors adjusted their gait to compensate for the effects of hemiparetic gait as speed increased, the changes made did not end up matching the average pattern.

Instead, as the stroke survivors' walking speed increased a compensatory gait pattern emerged with peak paretic knee flexion reducing by 20° as gait speed increased between the lower and upper quartiles of gait trials while its ab/adduction pattern drifted away from the healthy baseline. It was also note there was increasing paretic ankle flexion acceleration though the pattern of flexion and extension did not relate to walking speed. The hip joint saw peak paretic abductions reducing to a nearly normal pattern while peak paretic hip flexions increased by 10°.

The non-paretic limb also exhibited compensatory elements with hip flexions never increasing from peak extensions 10° below the healthy comparison and peak ankle flexions reducing by up to 10°. The non-paretic hip also reduced the hip abduction offset but this remained at nearly 2.5° to 5° from the healthy comparison over the course of the gait cycle.

This pilot study therefore suggests that while certain aspects of the hemiparetic gait pattern may move towards the healthy baseline as walking speed increases there remains compensations in some joint kinematics that allow for these improvements.

Some detail has been lost though. The average shape similarities of the rotation in the Sagittal and Vertical axes were often fairly low and without a significant relationship being established between this value and the walking speed led to the LF parameters no longer representing the variations accurately. Potentially, a combined analysis method could prove even more effective in a future study - or a refinement of the Linear Fit Method that allowed for additional information on waveforms that deviate far away from the comparison.

It is suggested that this research may benefit future rehabilitative robotic designs which have seen a plateau in gait speed outcomes recently (1). This may be achieved by either assisting or constraining the movement of each joint or providing training which emphasises adaption of compensatory gait patterns. Suitable robotic designs for the later method are already in development, one such design being developed in the University of Birmingham being potentially capable of both dynamic support and rendering of various surfaces (91, 92).

4.5. Conclusion

This pilot study set out to establish the relationships between the kinematic waveforms of stroke survivors and their chosen walking speed. The Linear Fit method, along with a linear regression analysis, was able to highlight these relationships and communicate their impact on the gait pattern effectively for small to moderate variations from the healthy pattern. The results suggest that non-normal compensatory gait patterns have the potential to lead to

positive rehabilitation outcomes. However, the causation and impacts of these relationships would require further study, and there is the question of the effects of long-term use of abnormal gait patterns.

Chapter 5 Design and Model of a Magnetic Fluid Based Fluidic Muscle

5.1. Introduction

The possibility of a pneumatic style muscle which is actuated using a magnetic fluid is explored within this study. Pneumatic muscles have seen significant developments within the field of soft robotics and are commonly applied in robotic rehabilitation. However, they are often limited by large, stationary power supply systems. Utilising a smart material like magnetic fluid allows alternative methods of actuation to be explored that utilise more compact designs.

To establish the feasibility of powering a fluidic muscle with a magnetic fluid this study seeks to design a simulated version of a simple muscle design and compare it against an experimental set-up. Presenting this model and proving its validity will allow for further muscle designs to be tested via simulation and allow for future optimisations to be performed.

The proposed muscle design is a simple rubber tube filled with a magnetic fluid and subjected to a non-uniform magnetic field. This is expected to cause a boundary stress in the targeted area of the muscle, forcing a majority of the magnetic fluid in the muscle to flow to this point and expanding the rubber tube. This expansion could then be converted into more useful work with a braided sleeve as in the McKibben's Actuator design.

5.2. Methodology

5.2.1. Experimental Set-Up and Procedure

The design of the initial Magnetic Fluid Muscle proposed is fairly simple in its construction. A latex rubber tube of 7 mm diameter is filled with a magnetic fluid, EMG-901, produced by Ferrotech. Each end of the tube is capped with an insert and sealed with a zip tie. One end is suspended from a lab stand leaving the muscle suspended between a pair of commercially available electromagnets that are suspended on a stationary rig. In addition, a thin SingleTact brand capacitive force sensor of 8mm diameter was placed between the Magnetic Fluid Muscle and the electromagnet to examine the contact forces at this point. This set-up can be seen in Figure 5.1.

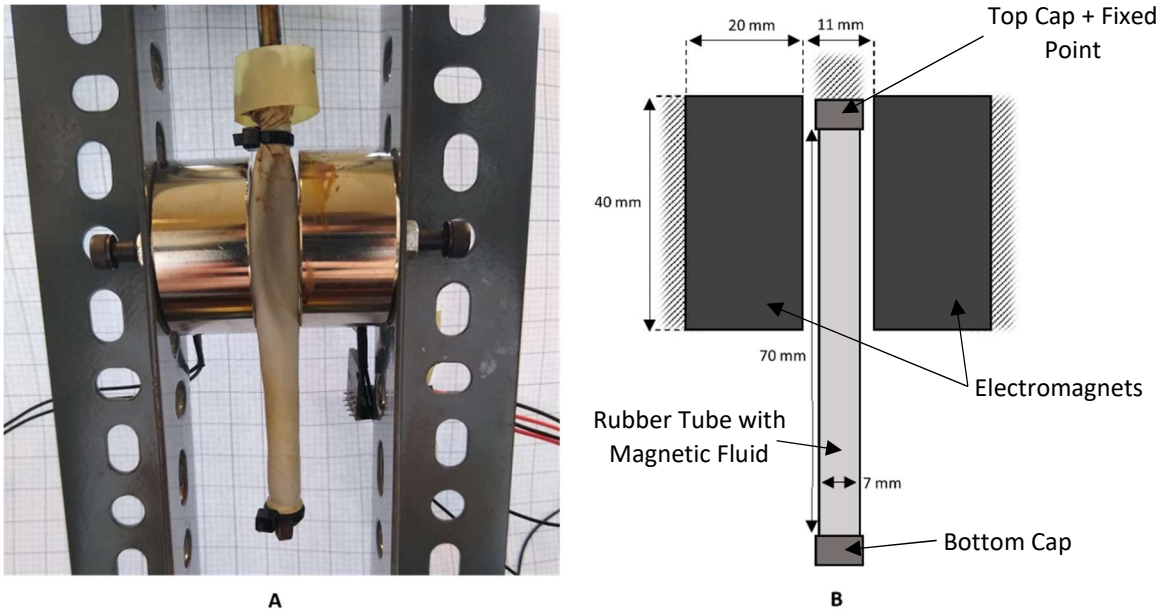

Figure 5.1: Image (A) and diagram (B) of the magnetic fluid muscle experimental set-up including key dimensions

The current supplied to the electromagnets will be varied over the course of the experiment from the maximum, 0.30 A, down to 0 A in 0.02 A increments. At each of these increments readings will be taken from the force sensor along with the maximum dimensions of the current muscle deformation in terms of its minimum thickness below the area targeted by the electromagnets.

5.2.2. COMSOL Model

The problem presented in modelling a Magnetic Fluid Muscle is two-fold. First, a magnetic field simulation must be produced to simulate the magnetic field produced by the 2 electromagnets. Second, a fluid structure interaction that uses this electromagnetic field data to predict the stresses induced in the magnetic fluid and the effect this has on the hyperelastic rubber muscle wall.

Magnetic Field Study

The magnetic field model was developed in the COMSOL Multiphysics software using the Magnetic Fields interface. The magnetic field study was set up as a pair of electromagnets suspended such that they are facing each other. Their centre points are 20 mm below the top of the Magnetic Fluid Muscle and they are 11 mm apart as laid out in the experimental set-up in Figure 5.1b with similar dimensions. The electromagnets were modelled with a soft iron core with a diameter of 18mm and a series of 2000 copper windings around this core with a maximum internal diameter of 36mm.

Magnetic Fluid Stress

To connect the magnetic field model to the Fluid Structure Interaction model requires understanding the behaviour of a magnetic fluid subject to an external magnetic field. This can be predicted via equations derived from the Macroscopic Maxwell Theory. In work published by Stierstadt and Liu, these equations are rederived and expanded upon to create a useful set of Maxwell Equations, including the Maxwell Stress, that describe the forces in a magnetic fluid in equilibrium along with a more in depth look into off-equilibrium effects, utilising principles of thermodynamics (80).

This study is initially concerned with determining the equilibrium of a magnetic fluid inside a deformable bladder with an applied stationary magnetic field. As such the static Maxwell equations that are used in an example put forward by Stierstadt and Liu can be utilised. This example demonstrates how the stress tensor can be applied to the boundary of a manometer immersed in magnetic fluid. This can be seen as a parallel to the conditions at the boundary of deformable container filled with magnetic fluid (80):

$$\tilde{\sigma}_{nn}^{LCR}(T, \xi_\alpha, H) = j_0(m) + P_0(V) - \frac{\chi}{2\mu_0\mu_r} B_n^2 - \frac{\mu_0}{2}\chi H_t^2 \quad Eq. 5.1$$

Where:

- $j_0(m)$ = Field Independent Grand Potential of medium
- $P_0(V)$ = Pressure of vacuum beyond medium
- χ = Magnetic Susceptibility
- μ_0 = Vacuum Permeability
- μ_r = Magnetic Permeability
- B_n = Normal component of the Magnetic Induction Field
- H_t = Tangential component of the Magnetic Field

The grand potential summarises the effects related to the internal energy, chemical potential, and temperature of the medium. In this the system is considered over a short

period of time and at an equilibrium. As such, there are assumed to be no significant density variations that would affect the chemical potential and no significant temperature changes. Thus, the grand potential term will not significantly change between the initial state of the system and the end equilibrium state. The remaining term, internal energy, represents the energy present at initial conditions which is solved and accounted for by the COMSOL simulation.

In many circumstances the magnetic system will not be under vacuum like conditions and in these cases additional stresses must be added to the electromagnetic stress as separate terms, but this may be handled with additional boundary conditions in the FEA software. By equating the electromagnetic stress and the external terms acting on the boundary the point of equilibrium may be found. In addition, the pressure term $P_0(V)$ becomes equal to the atmospheric pressure of the surrounding system, P_{atm}, which is already included in the COMSOL study. The equation may therefore be used to act as the magnetic fluid boundary stress component may be written as:

$$\tilde{\sigma}_{nn}^{LCR}(H) = \frac{\chi}{2\mu_0\mu_r} B_n^2 - \frac{\mu_0}{2}\chi H_t^2 \quad Eq. 5.2$$

Solid Mechanics Study

The Magnetic Fluid Muscle model was developed in the COMSOL Multiphysics software using the Solid Mechanics module. The behaviour of the magnetic fluid volume and the surrounding air domain were simplified, and their deformation controlled via the moving mesh module which is paired to the solid mechanics outputs. The magnetic properties of internal fluid, EMG – 901, were taken from the manufacturers provided data sheet (93).

The overall geometry of the initial muscle design is very simple, a thin wall connecting a bottom and top end caps and a pair of electromagnets in close proximity.

The muscle wall material is a hyperelastic latex rubber using the material properties provided in COMSOL's "Inflation of a spherical balloon" example model which itself uses information from Holzapfel's "Nonlinear Solid Mechanics" (94). As the endcaps and electromagnets are made from a significantly stiffer material than the muscle wall they are set as rigid domains and their stress and deformation therefore do not need to be considered for this study. The top cap will be the fixed point for the study.

In addition, the contact between the rubber muscle wall and the electromagnet stand in components was added to the model using a Contact Pressure Penalty Factor with a contact surface offset of 0.25 mm and an increase penalty factor multiplier to account for the low stiffness of the hyperelastic rubber. The offset protects the air domain moving mesh from collapsing as it is pinched between the deforming muscle and the electromagnet.

The magnetic fluid boundary stress was added to the model as a pressure on the internal boundary faces and is calculated from Eq.5.2. This equation draws on the constant parameters, the magnetic field data from the electromagnet model, and the normal vectors of the elements that make up the internal boundary faces to provide the local magnetic fluid stress at each boundary point. To maintain a constant magnetic fluid volume, a global equation is applied that regulates an internal pressure along the boundary walls that maintains the constant volume.

There were some difficulties for the solver as wrinkles would sometimes form within the hyperelastic muscle wall. These were found to be difficult to fully develop without some

form of outside perturbance, a computational case that has been widely covered in other studies (25). In the case of this study a minor boundary load was applied to the outer edges of the muscle and swiftly removed which proved sufficient to allow the deformation to take place.

Lastly, the study was set-up using a parametric stationary study with a set of spring foundations constraining the motion of the muscle that were subject to an exponential decay while, at the same time, the magnetic fluid boundary load was linearly ramped up. This linear ramp up, along with the decreasing distance between the muscle and the electromagnet, led to a composite exponential ramp in magnetic boundary load.

5.3. COMSOL and Experimental Outcomes for Magnetic Fluid Muscle

The COMSOL model was compared against the experimental results across 2 major measured outcomes: deformation and contact pressure. The contact pressure results were expanded with the addition of a set of single electromagnet tests. The COMSOL model was also further analysed with the distribution of the magnetic fluid boundary stress and propagation of the magnetic fields mapped out and presented.

5.3.1. Deformation of Muscle Bladder

As shown below in Figure 5.2, The magnetic fluid muscle underwent a radial expansion in the area suspended directly between the two electromagnets (A) until it made contact with the electromagnet faces. This expansion tapered off near the bottom edge of the electromagnets and then rapidly narrowed as the section below the electromagnets had flattened as the magnetic fluid had moved up the muscle into the expanding upper section

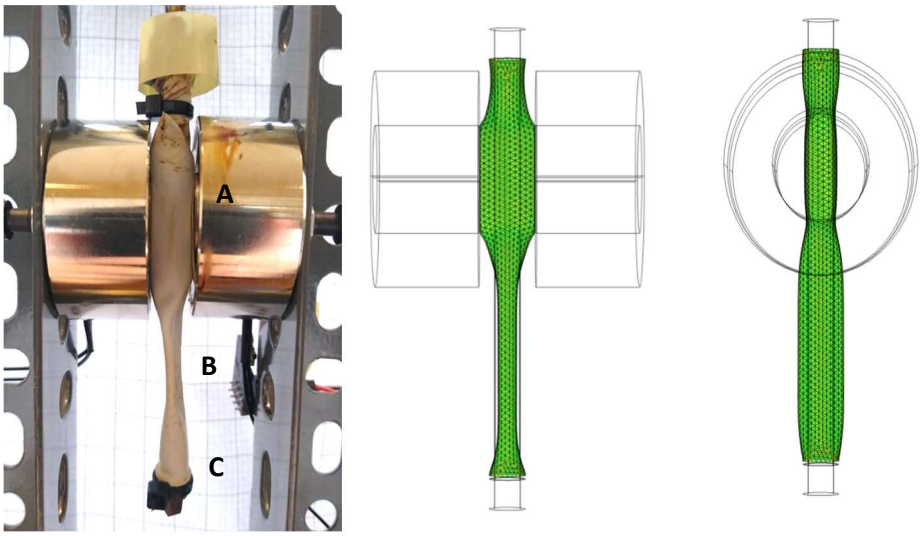

Figure 5.2: Magnetic Fluid Muscle Deformation due to a pair of Electromagnets under 0.30A, Experimental and COMSOL Model

(B). This narrow section eventually began to expand back into the original cylindrical shape of the muscle for the last ~10mm before the bottom plug (C).

The COMSOL simulation showed similar behaviour to the experimental set-up. The muscle expanded radially until contact conditions were reached with the electromagnets. There was a small section above and below the electromagnet core where the muscle expansion tapered off. Additionally, the behaviour in the side-on view was similar to the experimental muscle but easier to demonstrate visually, with the muscle flattening into a wide but thin section. Finally, the simulation muscle transitions back to the original shape at the plug but noticeably does so further down than the experimental muscle.

To further check the deformation behaviour between the two cases the thickness of the muscle at area B, where the muscle flattened, was measured and compared for currents between 0.22 A and 0.30 A as seen in Figure 5.3 below. Below 0.22 A the COMSOL model showed a different form of deformation as being dominant; a much more asymmetric

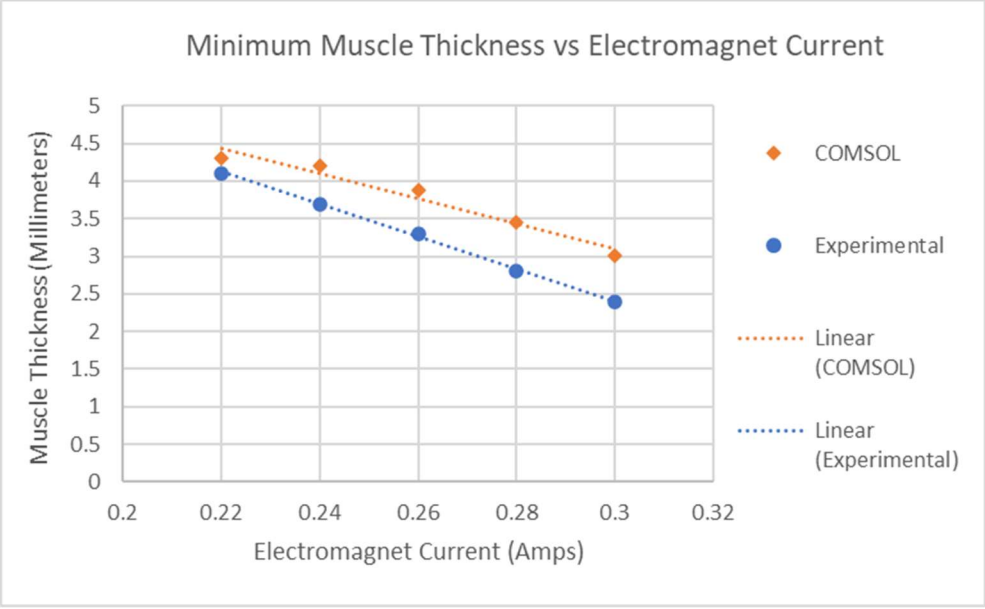

Figure 5.3: Graph showing the Experimental and COMSOL muscle thicknesses along its lower length

movement with only one part of the muscle making significant contact and causing convergence issues

The experimental results showed a slightly lower thickness than the COMSOL results for the highest currents. This gap closed as the current was reduced with the experimental results showing a slightly steeper gradient though both trends remain approximately linear over the available range of current.

5.3.2. Contact Pressure

Single Electromagnet Set-up

The contact pressure between the magnetic fluid muscle and the powered electromagnets was measured using a thin force sensor. This pressure was recorded for a short period of contact, approximately 5 seconds, and then averaged over this time frame to reduce the impact of noise on the reading. The COMSOL contact pressure is derived from the average

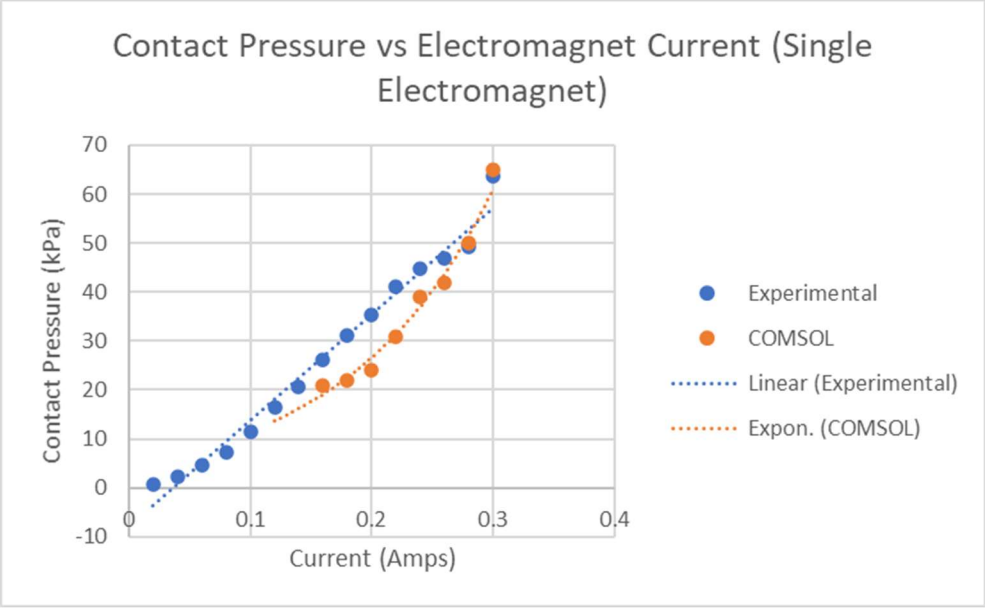

Figure 5.4: Graph of contact pressure against electromagnet current for a single electromagnet

value around the most prominent pressure peaks. The results are contained within Figure 5.4.

Experimental results showed a relatively linear relationship between the contact pressure and the electromagnet current, varying most significantly at limits of the current range. By comparison, the COMSOL simulation results showed a slightly looser trend that appears exponential rather than linear. Notable, is the close agreement between the simulation and experiment for currents of 0.3A and 0.28A.

Figure 5.5 shows the contact pressure stress pattern for the single electromagnet set-up. Peaks occurring towards the edges of the surface contacting the electromagnet core, particularly near its top and bottom. Smaller local pressures peaks were also noted near the bottom of the contacting surface that may be due to small variations in the muscle mesh and its distance from the surface of the electromagnet core.

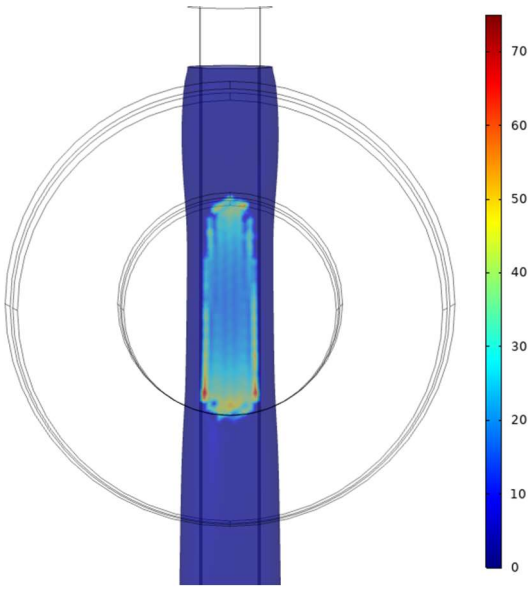

Figure 5.5: Contact pressure surface data for single electromagnet set-up, 0.3A

Dual Electromagnet Set-Up

Similar to the single electromagnet tests, the contact pressure between the magnetic fluid muscle and one of the electromagnets was measured using a thin force sensor and averaged

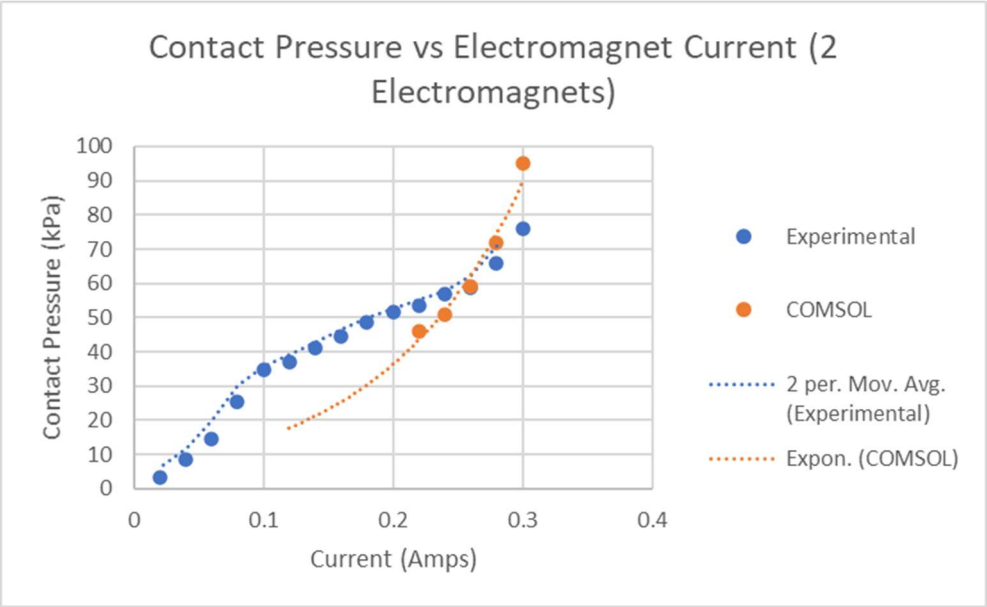

Figure 5.6: Graph of contact pressure against electromagnet current for dual electromagnets

over a short time period while the COMSOL contact pressure derived from the values around the peak pressure spots. These results were plotted within Figure 5.6.

The experimental results showed that the contact pressure did not have a simple, clear relationship. Plotting a two-point moving average shows a gentle exponential increase for upper and lower bands of the current range while between 0.1 A and 0.2 A the contract pressure increased roughly linearly. Comparable data from the COMSOL model was limited to the upper current range, 0.22 A onwards, as the expansion of the bladder did not follow the deformation seen in Figure 5.2 at lower currents. Instead, non-symmetrical expansion forced issues that affected solver convergence. The available data from the Dual Electromagnet COMSOL model shows fairly close agreement, particularly around 0.26 A,

though at 0.3A the model suggests a significantly higher contact pressure than the experimental results.

Figure 5.7 shows the contact pressure stress pattern for the dual electromagnet set-up. The contact surface is more limited than in the single electromagnet set-up, Figure 5.5, and shows a higher distribution of stresses with stronger peaks along all edges of the contact surface.

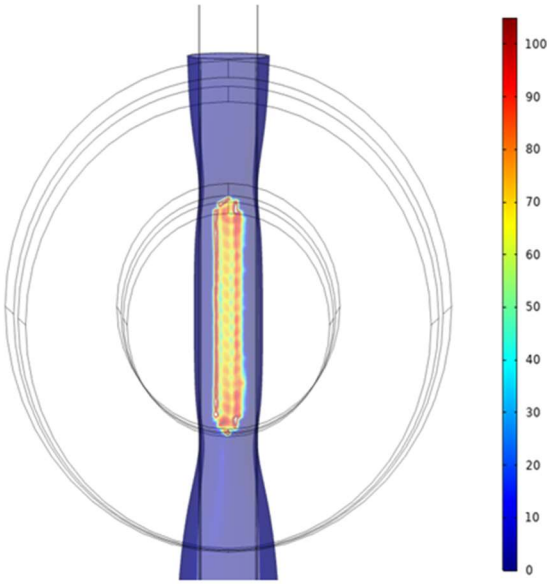

Figure 5.7: Contact pressure surface data for dual electromagnet set-up, 0.3A

5.3.3. Magnetic Fluid Boundary Load

To understand the internal forces acting on the muscle from the magnetic fluid the magnetic boundary stress load was presented along the internal surfaces for the muscle at full contact in Figure 5.8, below.

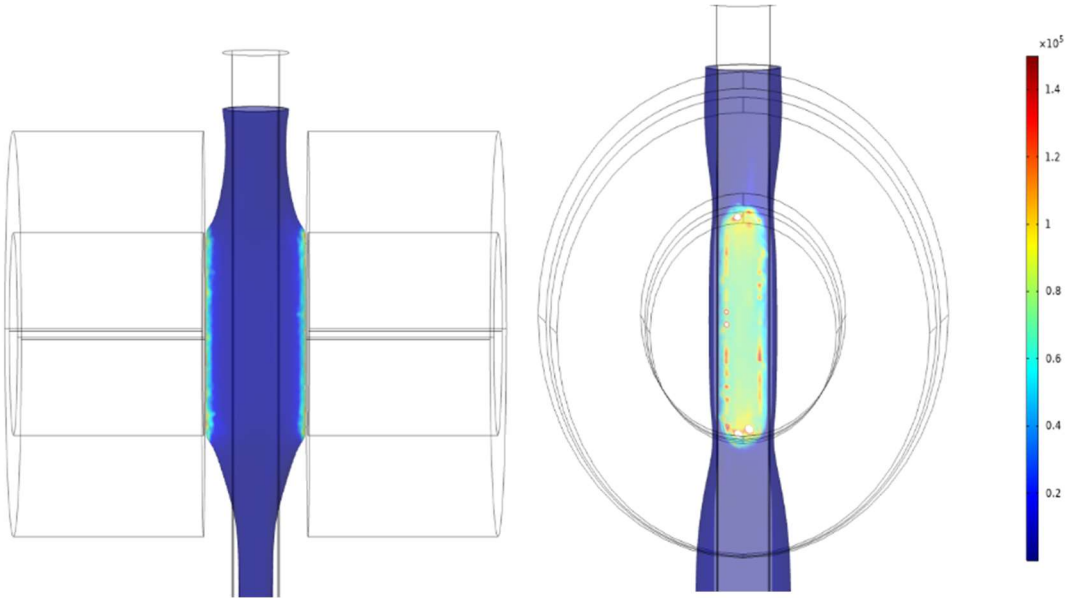

Figure 5.8: Surface plot showing the boundary load stress (N/m^2) generated by the Magnetic Fluid with dual electromagnets at 0.3 A

As can be seen on the figure, the magnetic boundary stress is highest at the faces of the muscle parallel to the electromagnet core face and reduces quickly with distance and orientation of the surface. This is reinforced in Figure 5.9, below, where the magnetic boundary stress is shown for the muscle prior to full contact being established. Peak stresses occur across the closest face of the muscle and the electromagnet with the stresses dropping off quickly for the faces perpendicular to the electromagnet.

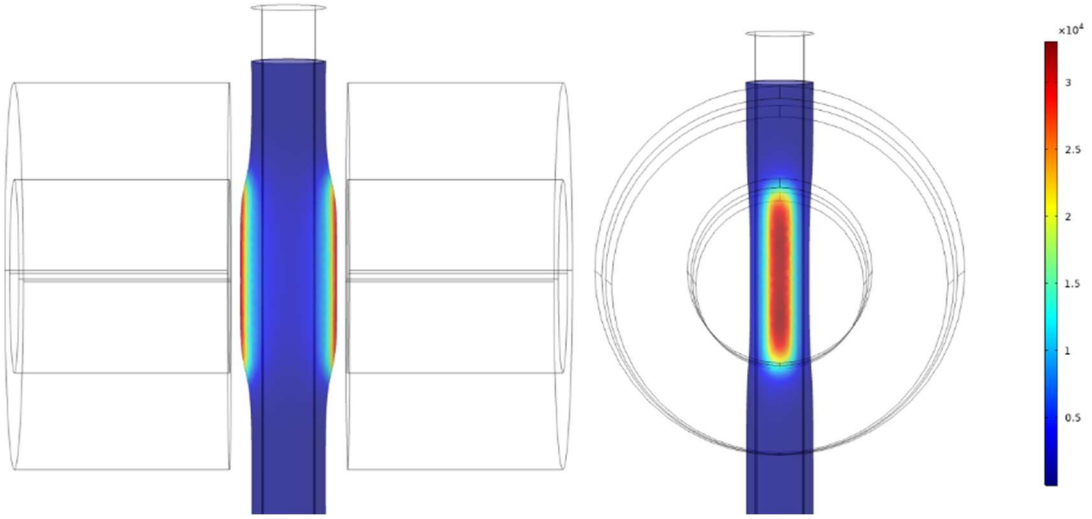

Figure 5.9: Surface plot showing the boundary load stress (N/m²) generated by the Magnetic Fluid with dual electromagnets at 0.3A, part way through the solution

Of note in Figure 5.8 by comparison to Figure 5.9 are the more localised stress peaks within the surface plot. These correspond with the mesh and highlight the where the contact condition is struggling to maintain the mesh integrity of the two domains. The peaks themselves could correspond to minor changes in the distance between the muscle and the electromagnet leading to different boundary stresses or where the muscle walls themselves are "pinching" due to its hyperelastic behaviour.

5.3.4. Magnetic Field Pattern

To better visualise the interaction between the magnetic fluid muscle and the acting magnetic field, the magnetic flux density norm, B^{norm}, and magnetic flux streamlines were plotted for each plane intersecting the centre line of the muscle and the electromagnets and are shown below in Figure 5.10.

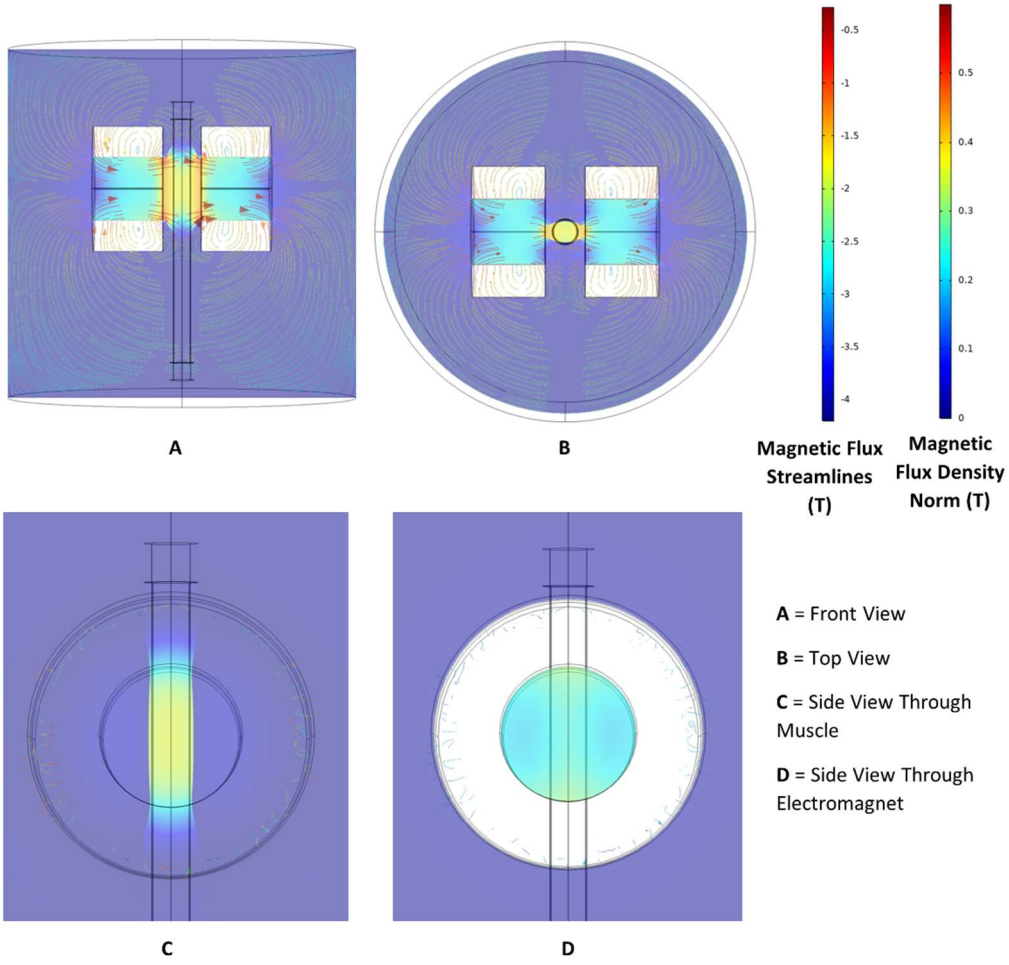

Figure 5.10: The magnetic flux density norm and streamlines shown across the planes intersecting the centre line of the muscle and electromagnets

As shown by the magnetic flux density norm, the magnetic fluid allowed the magnetic field to propagate for a short distance, creating a region of particularly high magnetic flux within the fluid which quickly dissipated outside of the region contained by the electromagnet cores. However, despite the fairly high magnetic flux density present perpendicular to the electromagnet faces within the muscle there was significantly less deformation in this direction. This is somewhat explained by the magnetic field lines which show that the direction of the magnetic field vectors primarily acted between the two electromagnets, tangential to the front and back of the muscle. This tangential magnetic field flux does not

influence the magnetic fluid stress as significantly as the normal component as shown in Eq.5.2.

5.4. Discussion

This study evaluates the potential of using magnetic fluid to create actuated muscles made from hyperelastic rubber. Establishing the design of a COMSOL model that can be compared against an experimental set of data and shown to accurately predict the behaviour of these magnetic fluid muscles goes some way to demonstrating how magnetic fluids can be controlled to perform actuation within soft robotics.

It was found that the COMSOL models deformation matched the experimental set-ups fairly well. The simulation predicted a radial expansion in the area between the two electromagnets which tapered immediately above and below this point. This causes the majority of the magnetic fluid to flow into this region causing the lower section to constrict.

The constriction occurred primarily in one plane in the experimental set-up. While building the initial model, early results showed a set of wrinkles that were more radially distributed around this lower section that accounted for the lower volume. However, this was quickly deemed to be unlikely to occur under experimental conditions and was a by-product of the near-perfect symmetry of the computer-generated mesh. Via the introduction of a minor force disturbance in this section that was then removed over the course of the parametric study the model quickly showed behaviour much more similar to the experimental muscle.

The thickness of this lower section was measured and, while varying more significantly at higher current, there was fairly close agreement between the COMSOL and experimental

results, suggesting a roughly equal distribution of fluid in the internal volume. The slightly lower thickness measured for the experimental results could be accounted for by the larger amount of fluid gathered at the bottom of the experimental magnetic muscle as can be seen in Figure 5.2c.

Contact pressure measurement showed a wider degree of variation between the experimental and COMSOL models over certain sections of the range of currents indicating limitations with the model or the experiment. Some sections of data did show close agreement, indicating that the use of the magnetic fluid boundary stress equation is a good fit and can be implemented effectively within COMSOL. Integrated with the magnetic field module and a moving mesh, a magnetic fluid stress can be placed over a solid boundary and the static equilibrium deformation and stresses of a hyperelastic material predicted to a useful degree of accuracy.

As shown in Figure 5.5 and Figure 5.7, the contact pressure varies over the contact surface, with peaks around the edges. This could potentially have led to the sensor reading being hard to reconcile with the COMSOL outcomes. While the sensor was placed as close as possible to the centre of the electromagnet and was nearly fully obscured by the muscle contact surface during each experiment, it is possible that were the sensor to contact the outer edge of the muscle surface, it may produce a higher contact pressure reading.

The resultant magnetic fluid boundary stress acting on the interior of the muscle is demonstrated clearly within the results along with its relationship with the magnetic field. In areas of magnetic field lines which cross perpendicularly with the muscle surface there are areas of high stress. By comparison, even with the magnetic field propagating though the

fluid, the field lines towards the faces of the muscle that are perpendicular to the electromagnet are still almost parallel. This represents an area of potential work that is being lost in the current magnetic field set-up and if a more radial field is introduced then a wider band of magnetic fluid boundary stress may be applied.

While the current set-up is able to adequately show how the forces and stresses in a magnetic fluid muscle may behave under a magnetic field, this design does not produce a usable tensile force. Room is left for further iteration and improvement, particularly in the application of the magnetic field. If a radial magnetic field were applied to the muscle then expansion would also occur radially, leading to more significant swelling in a manner more akin to traditional pneumatic muscle. Then, applying a braided mesh sleeve around the muscle could capture the work produced by this expansion as a useful tensile force to provide a soft robotic muscle suitable for use areas such as rehabilitative robotics. This work can be achieved using a similar COMSOL model designed to that presented in this study.

5.5. Conclusion

A COMSOL model of a hyperelastic rubber muscle filled with magnetic fluid and suspended between two electromagnets has been made and compare against an experimental version. While some differences were found, overall, there is close agreement with the expected deformation and reasonably close agreement between the measured forces involved. The proposed experimental set-up worked well for demonstrating the concept proposed. However, there are several aspects that can be further explored and improved, primarily the application of the magnetic field and the impact of using the design with the intended braided sleeve.

Chapter 6 Optimisation of the Design of a Magnetic Fluid Based Muscle

6.1. Introduction

In the previous chapter a design for a Magnetic Fluid based muscle introduced and examination carried out to see how such a device may be simulated using FEA software, namely COMSOL. It was found that the magnetic fluid boundary stresses that resulted from an electromagnet and the magnetic fluids own magnetisation contribution could be found and applied to a hyperelastic material model to a relatively accurate degree.

Further physical experimentation is possible but with the wide range of existing designs already outlined in literature for pneumatic and hydraulic muscles it is suggested that further development using the COMSOL simulation may prove more useful in allowing the potential of a magnetic fluid-based muscle to be fully explored in a manner available to a wider scientific community.

The set-up as proposed in Chapter 5 was relatively simple as the focus was on producing an experimental set-up that allowed for ease of comparison between the physical and simulated designs. As such, the system produced a localised stress within the rubber muscle that was not fully suitable for conversion into a working force. In addition, the set-up of the electromagnets, one fixed either side of the magnetic fluid muscle, would not be suitable for a device meant to be mounted on a more mobile system, such as a robotic rehabilitation device.

The first step in producing a device more suitable for a functional application was to consider the source of the actuating force, the electromagnets, and how it may be more conveniently

integrated into the muscle design. The issue with the current set-up was that to produce a significant magnetic field, acting on the normal of the muscle cylinder, at any significant distance away from the electromagnet required either an extremely strong electromagnet or the presence of two magnetic poles, one of each polarity. These paired electromagnets could create powerful boundary stresses, but the majority of their field vector was still orientated along a single axis.

A modified version of a simple one piece “pot” style electromagnet core is presented as a possible solution. Fitting over one end of the magnetic fluid muscle, the new electromagnet would produce a radial magnetic field leading to the magnetic field direction acting in the normal by comparison to the surrounding muscle bladder wall. This design could then be evaluated using a modified version of the previously introduced and validated COMSOL model.

6.2. Methodology

6.2.1. Electromagnet Design

The requirements for the magnetic field produced by the magnetic fluid muscles' electromagnet were that the majority of the magnetic field vector must be directed at a normal to the boundary it is acting on. The proportion of a magnetic field vector that could be broken down into a tangential contribution at that current point on the boundary would effectively not contribute to the magnetic fluid stress generated at this point as explored by Stierstadt and Liu in their submerged manometer example (80).

For the maximum amount of the magnetic field strength to be captured and converted into useful work by the magnetic fluid muscle, the magnetic field must be radial in nature. The design proposed utilised a single coil design, harnessing the polarity induced in the core material. Normally this dipole moment goes unused or unwanted in many commercial electromagnets but in a single piece electromagnet "pot" shaped core the central pin and the surrounding walls of the pot end up with opposite magnetic charges. By utilising only half of the regular interior space that is usually taken up by the windings, the rest of the internal space produces a radial magnetic field between the central pin and the external walls.

Placing a portion of the magnetic fluid muscle over this pin and inside part of the electromagnet core would allow for this radial magnetic field to act upon the muscle walls and capture the majority of the magnetic field vector as a useful radial stress. This design is shown below in Figure 6.1.

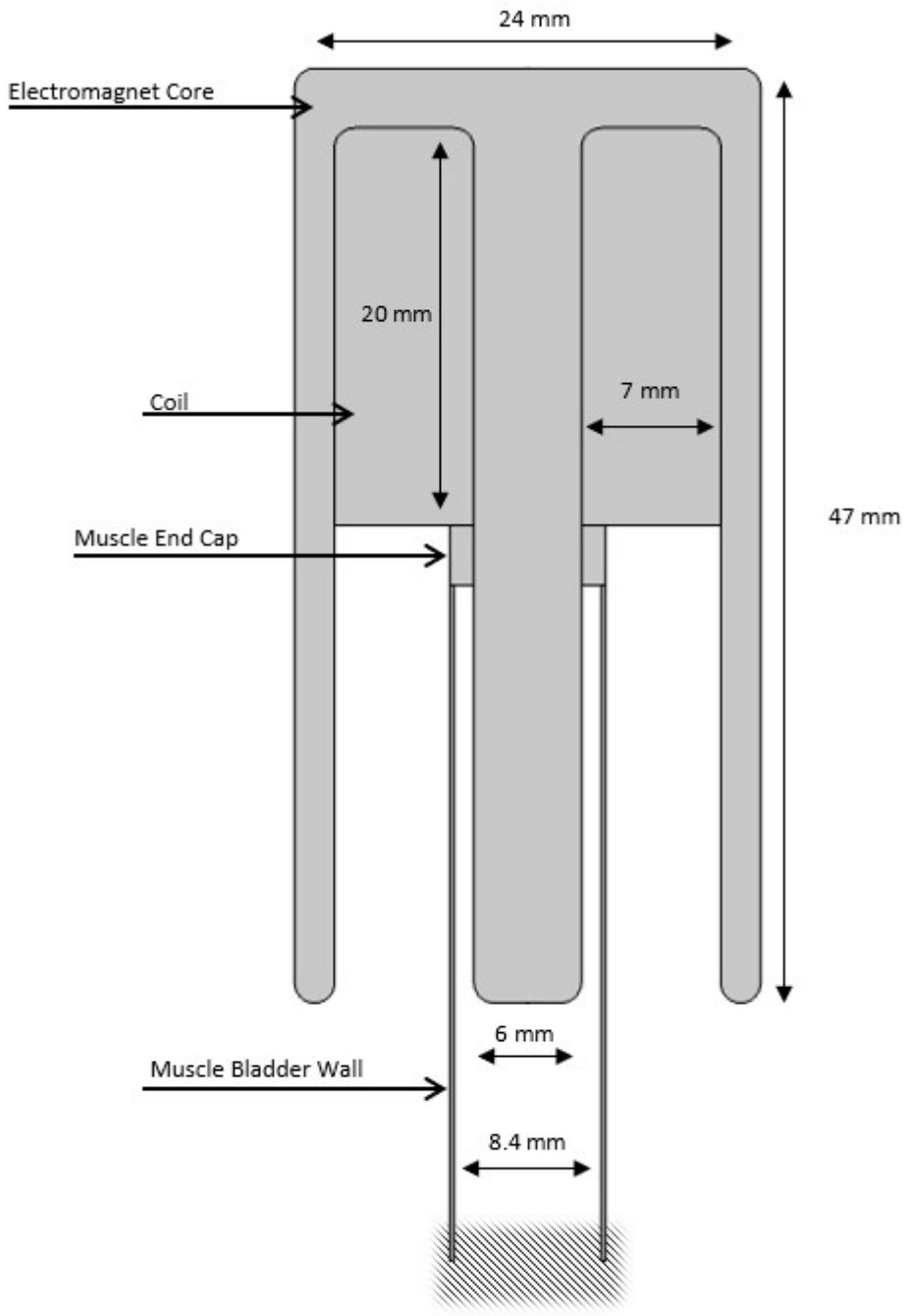

Figure 6.1: Cross Section Diagram of Electromagnet for Optimised Magnetic Fluid Muscle Design with key dimensions

The major limiting factor for the magnetic field strength that can be generated in this electromagnet will be the current density. Current passing through a wire produces heat and the tightly bundled wires needed to form an effective electromagnetic coil leads to a significant heating effect. This heating effect is dependent on the number of windings packed into the coil's cross-sectional area and the current across each of those windings.

The current density of an area can be found by multiplying the number of windings in that area, N, by the current they are carrying, I, divided by the total area, A_c:

$$J = \frac{IN}{A_c} \quad Eq. 6.1$$

The current density limit varies between designs and purpose. A coil that is in use constantly and without access to cooling will have a lower limit than a coil used for brief periods of time and with proper cooling as the heat is given the opportunity to dissipate. Works on the matter have suggested a maximum of around 2 A mm^{-2} for current carrying wire in compact constantly active set-ups with a maximum of 4 A mm^{-2} for wires that have no air circulation (95).

Taking the standard cross section area of a AWG29 wire and the available cross section area of the coil a maximum number of windings can be found. A packing efficiency of 78% was chosen which corresponds to simple, non-optimal, square packing. Then, based off of the number of windings and an average radius of the coil the necessary length of wire can be found along with a total resistance. These parameters are summarised below in Table 6-1.

Table 6-1: Electromagnet Design Variables for Optimised Magnetic Fluid Muscle

Electromagnet Design Variables			
Variable	**Symbol**	**Units**	**Value**
Wire Cross Section Area	A_w	mm^2	0.0642
Coil Cross Section Area	A_c	mm^2	140
Square Packed Circles Efficiency	η	%	78
Maximum Number of Windings	N_{max}	1	1700
Average Coil Radius	r_c	m	0.0065
Maximum Length of Wire	L_{max}	m	69.7
Wire Resistance per Metre	Ω_m	Ω/m	0.2685
Total Wire Resistance	Ω_{max}	Ω	18.715

From here the maximum current that the windings can carry within the safe current density bounds can be found. The total allowable current through the area is given by multiplying the safe current density by the total area, 560 A. Then this value is divided by the number of windings to find the maximum current per winding, 0.329 A.

Given these are maximum allowable values both the number of windings and the maximum current were reduced to 1500 and 0.3 A respectively. This gave a total current density of 3.214 A mm^{-2}. Given that the device is not intended to run continuously this was deemed a suitable starting point for the COMSOL model.

6.2.2. COMSOL Model

The COMSOL model was constructed as a 2D axisymmetric geometry to simplify the model complexity as all relevant forces in the system act radially from the central pin of the electromagnet. The electromagnet consisted of the custom extended pot core shape and the embedded coil. This was placed within a surrounding domain of air to allow the propagation of the magnetic field and its associated magnetisation.

The magnetic fluid muscle was constructed over the central pin of the electromagnet. However, rather than simulate the entire length of the muscle only the upper section, ending 13 mm below the tip of the electromagnet, was included within the model. This was done to aid solver convergence. As the muscle is made up of a thin sheet of hyperelastic material and is subject to non-uniform pressure loading wrinkling can be induced. These wrinkles can be very hard to accurately predict and model due to their rapid onset, large strains, and non-linear variations in component forces that lead to any computation seeking to model these behaviours becoming inherently complex and computationally expensive if not unstable (96).

The entire study was performed using a parametric sweep to apply the loads gradually and allow the model to utilise the previous steps deformations to account for the large final deformations.

Magnetic Field Study

The magnetic field model was developed in the COMSOL Multiphysics software using the Magnetic Fields interface. The electromagnet core was modelled as soft iron and the followed a halved version of the geometry laid out in Figure 3.3. Coil parameters were taken from section 6.2.1.

Magnetic Fluid Boundary Stress

As described in section 5.2.2 the model utilises a form of the Maxwell Stress Equation as laid out by Stierstadt and Liu (80). This equation was then simplified for application in COMSOL, with all of the parameters not directly tied to the Magnetic Field being accounted for by the

internal model parameters. The remaining terms form the Magnetic Fluid Boundary Stress as applied to the inside face of the magnetic fluid muscle and is given by Equation 5.2.

Solid Mechanics Study

The Magnetic Fluid Muscle model was developed in the COMSOL Multiphysics software using the Solid Mechanics module. The parameters of the solid mechanics module followed those laid out in the initial model design study however, there were some notable changes to account for the larger forces and 2D axisymmetric layout.

Firstly, due to the model only focusing on the actuating portion of the muscle the global equation controlling the constant volume with a global boundary load was removed. In addition, it was found that the spring foundations that allowed for the slow ramping of the ferrofluid boundary stress in the initial model were no longer suitable and a different approach was applied.

Due to the significantly higher magnetic field strengths involved and the larger deformations in the muscle the material would reach the hyperelastic point in its stress strain behaviour as the force was steadily increased. This led to a very large exponential increase in the rate of expansion as the magnetic field strength also increased exponentially as the muscle wall approached the outer electromagnet wall, compounding the acceleration and causing significant convergence difficulties.

Instead, a radial expansion was applied until the Muscle came into contact with the outer electromagnet wall surface. This radial expansion pressure was then gradually removed as the magnetic fluid boundary stress was introduced and ramped up allowing the muscle to

relax into a stationary equilibrium between the muscle elastic stress and the magnetic fluid force.

6.2.3. Idealised Muscle Tensile Force Calculations

Modelling of the braided mesh shell that makes up the actuating component of most common artificial muscles is difficult to implement with the current COMSOL model design. Instead, to consider the simulation results and give a generalised idea of the potential tensile forces that this design could generate an idealised model for a McKibben Artificial Muscle is used (97). The equations that govern the model are given below:

$$F_{ideal}(P, \varepsilon) = (\pi R_0^2)P[a - b] \quad Eq. 6.2$$

Where:

- P = Internal pressure
- R_0 = Initial muscle radius
- ε = Muscle strain
- a_0 = Initial braid angle

And:

$$a = \frac{3}{tan^2\alpha_0} \quad Eq. 6.3$$

$$b = \frac{1}{sin^2\alpha_0} \quad Eq. 6.4$$

This model only requires knowledge of the internal pressure and the maximum potential strain of the muscle which in turn depends on the initial angle of the braid of the sleeve.

6.3. Impact of New Magnetic Fluid Muscle Design

The COMSOL model was used to produce a series of figures that describe the magnetic field and resulting forces within the solid mechanics' study. The resulting forces were also used with Eq. 6.2 to calculate the potential tensile force that could be produced by a McKibben's style cylindrical muscle using this electromagnet setup.

6.3.1. Magnetic Field and Solid Mechanics Outcomes

Below is shown the Magnetic Flux Density Norm for the Magnetic Fluid Muscle at the instant of activation (a) and at its equilibrium state (b) in Figure 6.2. As can be seen in Figure 6.2a, the magnetic field strength is strongest at the tip of the central pin and propagates down through the magnetic fluid. However, by comparison the magnetic field is significantly weaker throughout the rest of the fluid in the enclosed space.

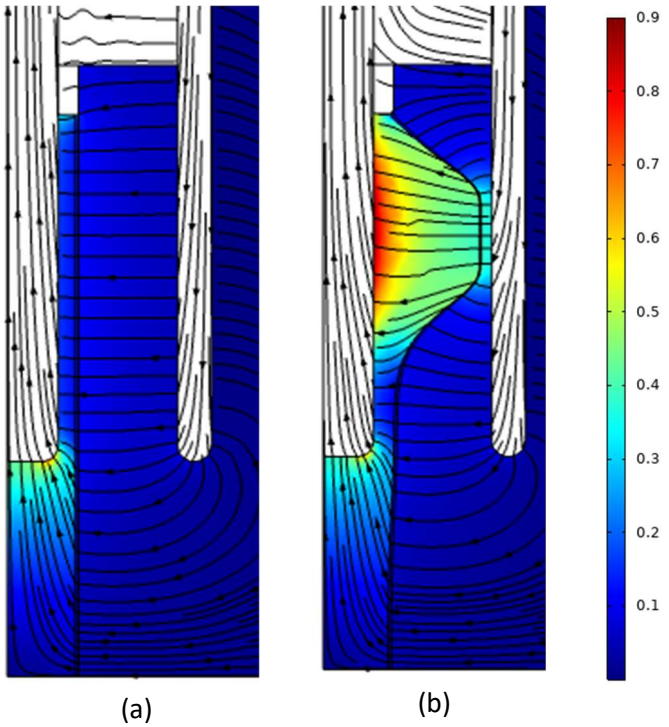

Figure 6.2: Surface plot of Magnetic Flux Density Norm with accompanying streamlines, Tesla (T)

The magnetic field quickly develops as the muscle begins to move. With a significantly higher magnetic susceptibility than the surrounding air domain, the magnetic fluid allows the magnetic field to form a region of much higher flux density between the internal pin and outer electromagnet wall as it moves to fill the space as seen in Figure 6.2b. This shifts the peak in magnetic flux density away from the electromagnet pin tip and creates a “bridge” of magnetic flux between the two domains which share opposing magnetic polarities. This leads to a change in maximum magnetic flux density from 0.69419 T in state a to 0.89002 T in state b.

The magnetic field’s effect on the muscle can be visualised in Figure 6.3a and b below, with each showing the muscle wall displacement and magnetic fluid boundary stress respectively. The expansion in the muscle can be seen to be concentrated around the centre of the

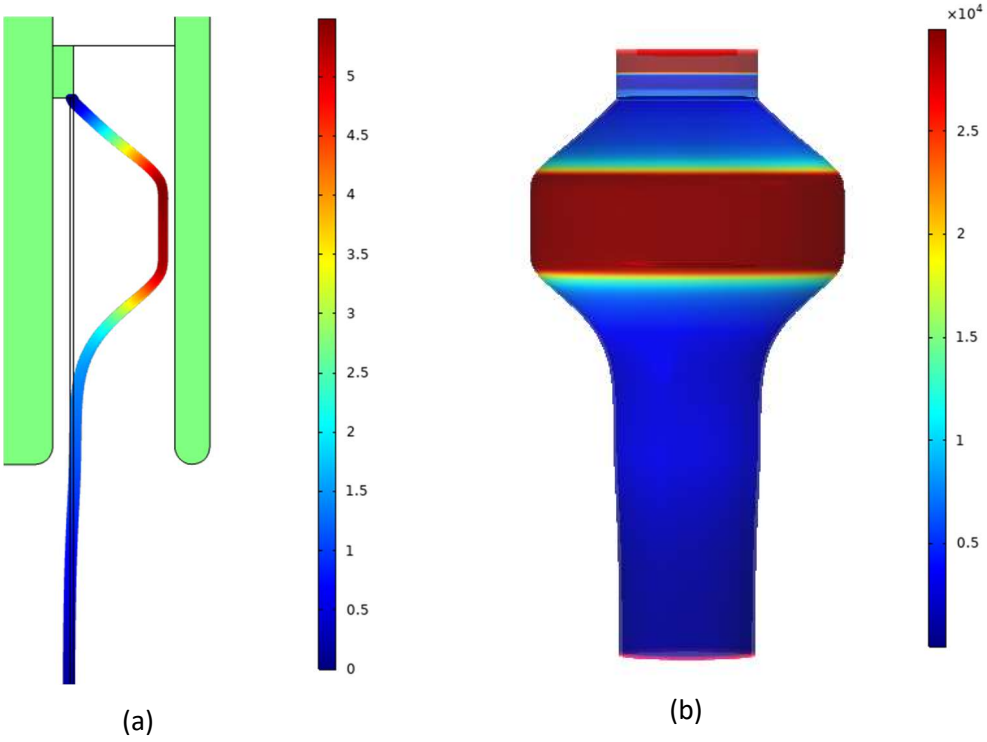

Figure 6.3: A line plot showing displacement in mm (a) and the concurrent magnetic fluid boundary pressure in N/m2 (b)

exposed portion of the electromagnet pin. This is likely due to the reduction in magnetic field strength away from the current source along with the elastic stress anchored around the fixed point in the muscle wall just below the electromagnet's coil.

As the distance between the magnetic fluid and the inner electromagnet wall decreases the magnetic fluid boundary stress increases dramatically with the region in contact with the outer wall seeing peak pressures of 30,000N/m2. This boundary stress has a very sharp gradient however, losing a quarter of its magnitude just 2 mm below the lower edge of contact. This leaves an area of expansion around 2cm long which can be used to capture work. While shorter than that of most other pneumatic muscles it still has the potential to generate a significant tensile force.

6.3.2. Potential Muscle Tensile Force

Using the idealised McKibben's Muscle equations with the data generated by the COMSOL model an estimation of the tensile force that could be generate a full version of this magnetic muscle design that includes a braided sleeve to capture usual work from the expansion of the elastic inner bladder. These equations utilise an internal pressure but as the pressure distribution inside of the muscle is non-uniform over most of its internal boundary two values are used to produce estimates. This pressure distribution is shown below in Figure 6.4.

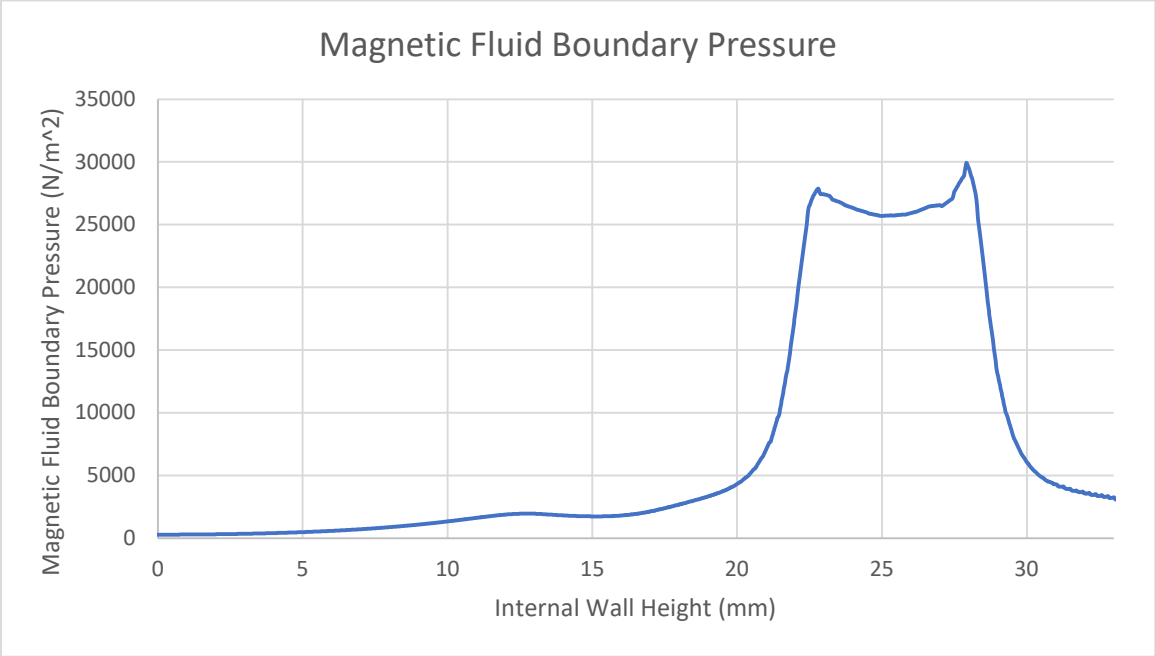

Figure 6.4: Graph of Magnetic Boundary Pressure along the internal bladder wall against vertical position from bottom of simulation space

Firstly, an average value is taken over the entire range of expansion, between 0.03m and 0.05m, which comes out to 9650.4 N/m^2. This represents a tensile force that is maintained over a majority of the contraction generated by the internal bladder expansion and as such is labelled as a contraction force, $F_{contract}$. The second is an average taken across just the peak of the expansion, 26664.34 N/m^2. This is the maximum tensile force that could be generated by the muscle, however as it is across a narrow area the contribution to contraction would be not as significant as the average. Instead, it could be seen as a holding force preventing full extension of the muscle, F_{hol} .

Respectively these give values of the potential maximum tensile force of a Magnetic Fluid Muscle of this design to be:

$$F_{contract} = 6.838\ N$$

$$F_{hold} = 18.894\ N$$

6.4. Discussion

Building on the initial design and validation of the COMSOL model presented in chapter 5 this study has considered an alternative design for the electromagnet powering the magnetic fluid muscle. The original experiment utilised a pair of electromagnets placed to either side of a bladder filled with magnetic fluid which was able to generate boundary stresses and deformation in the direction normal to the magnets.

However, this left a significant portion of the magnetic field potential underutilised as the magnetic boundary stress in a magnetic fluid relies on magnetic field lines intersecting along on the normal of the surface, with field lines along the parallel to the surface contributing little to nothing to the overall stress.

The design of the electromagnet in this study provided a radial magnetic field. When placed inside of this radial field, the cylindrical muscle surface was always kept at a normal to the field lines, leading to a significantly wider band of peak stresses and a larger muscle expansion. Over the working area the original magnetic fluid muscle setup saw an increase in volume of 61.45% whereas the radial electromagnetic field design saw a volume increase of 229.92% over the working area.

Notable though was that the original paired electromagnet set-up generated higher peak magnetic fluid loads, 120,000N/m^2 as opposed to 30,000N/m^2 for the new design. This shows the importance of the radial magnetic field in ensuring that the peak magnetic stresses were not contained in small stress peak spots but rather acted as a band of pressure, more akin to the uniform pressure applied within pneumatic muscles.

Additionally, this design utilised a single electromagnet which reduced the power needs for the device. The dual electromagnet set-up required 8 Watts per electromagnet while the initial design calculations for the radial electromagnet used in this study suggest a power requirement of 1.32 Watts though this is likely an underestimate based purely off the resistance of the total length of wire in the coil.

To fully convey the potential of this magnetic fluid muscle, the work transfer from the bladder through a braided sleeve is needed. Simple models have been proposed previously and were used here to estimate the potential of the magnetic fluid muscle presented. With potential tensile forces between 6.838N and 18.894N and an overall diameter of 2.4cm it is suggested that the system has the potential for use within gait rehabilitation in a limited fashion.

6.4.1. Magnetic Fluid Muscle Based Orthosis Design Potential

As demonstrated in Chapter 4 there are significant relationships between the walking speed of stroke survivors and their lower limb joints' kinematic waveforms across all axes of rotation. The study suggested that rehabilitation that explores targeting these joints and providing assistance with an aim towards encouraging the types of motion that have been noted to correspond with higher walking speeds could result in positive rehabilitation outcomes for stroke survivors.

To facilitate the user adjusting their gait pattern towards these compensatory patterns that have been found to hold beneficial outcomes for other stroke survivors the device would not necessarily need to provide enough force to complete the joint motions for the user but

simply enough to apply a guiding assistive force that guides the user to desirable motions and provides a corrective force to motions significantly outside of these determined goal parameters. This style of robotic rehabilitation training has seen significant discussion over the last decade and there have been designs implemented with control schemes which mirror these goals (98).

To this end the design of the magnetic fluid muscle for use in an orthosis was extrapolated for a test case, the flexion and extension of the paretic knee, which was shown to have a reduced average but higher accelerations in angular position as walking speed increased. Previous work has found the average offsets between paretic and non-paretic lower limb joint torques for certain motions (99). This work has been used to find the difference in torque which a device would have to account for to fully compensate for hemiparesis and are shown below in Table 6-2.

Table 6-2: Torque differences between a healthy average and an average stroke survivors' torque at the knee joint assuming a 70 kg participant.

	Paretic Knee Joint Torque	**Non-Paretic Knee Joint Torque**	**Torque Difference**
Flexion	0.12Nm/Kg 70kg person = 8.4 Nm	0.50Nm/kg 70kg person = 35 Nm	26.6 Nm
Extension	0.55Nm/Kg 70kg person = 38.5Nm	1.18Nm/kg 70kg person = 82.6Nm	44Nm

Each muscle can be constructed with an electromagnet at either end, providing twice the outlined tensile force. Then, each muscle can be closely packed to act in parallel with several other muscles. In this case 5 dual ended muscles are suggested. With a proposed leverage of 10cm, the total potential contraction and holding tensile forces generated by this muscle array can be calculated to be 6.838N and 18.894N respectively, or 15.54% and 42.94% of the

torque disparity across the knee for extension and 25.71% and 71.03% of the torque for flexion. The device could then be powered via a simple battery pack strapped somewhere discreet around the user's waist.

6.5. Conclusion

This chapter has taken the design presented within Chapter 5 and improved its function by designing an electromagnet intended to provide a strong radial magnetic field. It was found that the COMSOL model predicted a significant increase in the muscle bladder deformation such that it expanded to touch the inner wall of the electromagnet. While full details about the magnetic fluid muscle's function were not achieved additional analysis based off of research into McKibben's style pneumatic muscles have predicted potential tensile forces between 6.838 N and 18.894 N. While significantly lower than that of current commercial pneumatic muscles this level of force could be utilised in some rehabilitation applications and with the potential for a small power supply and further improvements, magnetic fluid muscles could find a role in soft robotics.

Chapter 7 Conclusions, Contributions and Future Work

7.1. Conclusions

The research reported in this thesis has detailed a ground up approach to robotic gait rehabilitation. With the overall aim to find and target areas of hemiparetic gait linked to functional gait recovery using novel robotic rehabilitation methods, a detailed literature review was carried out to assess what goals current systems were able to achieve and their limitations. This highlighted several avenues that could be explored further in the hope of providing alternative methods of providing robotic gait rehabilitation.

The underlying work that would provide direction to future orthoses designs was the gait analysis of hemiparetic stroke survivors with regards to walking speed. However, it was noted from the literature review that there were few studies on how the targeting effect can affect the gait analysis of stroke survivors.

A full study was carried out and looked at healthy and stroke survivors' gait across a force plate target as well as beyond said target to evaluate if there were any differences in gait between these two points. While results indicated that there were significant differences in both populations for spatiotemporal data it was found that the kinematic joint data was largely unaffected, achieving **Objective 1**.

This allowed a second gait analysis study to be carried out that focused on the kinematic data without needing to factor in further study design considerations. This study examined the stroke survivors' gait and its variations with regards to walking speed using the Linear Fit

method to provide a more in-depth insight into the kinematic variations than previous studies.

It was found that there were significant relationships between various aspects of stroke survivors' gait and walking speed. Importantly, many of these relationships were found to not correspond to a healthy gait pattern and that significant asymmetry was still present in the stroke survivors' gait even when their gait speed became close to that of the healthy counterpart. This opens up the possibility of alternative goals for functional hemiparetic gait rehabilitation and fulfils **Objective 2**.

Following on from this work outlining potential targets for robotic gait rehabilitation systems the current trends and designs within the field were evaluated. It was found that while a variety of designs were being pursued there were still difficulties in providing increased walking speeds. Part of this was attributed to lack of user engagement with training and over-constraint of their joints.

Soft robotics provided a potential solution for this due to their compliant behaviour, contrasting against the rigid, fixed designs that have previously been implemented. Soft robotics came with their own problem though as most systems that currently use soft robotic actuators are tethered to stationary power supplies/mechanisms such as pumps. Smart materials were suggested as a potential solution to creating compact rehabilitation systems that users would not be inhibited by.

A magnetic fluid-based muscle utilising the working principle of pneumatic artificial muscles was proposed and an FEA model created to allow for further design iterations. This model

was tested and compared against a baseline experiment which found fairly close agreement between the model and reality.

This allowed the model to be utilised in optimising the design of the magnetic fluid muscle with the goal of providing a significant enough tensile force that the design could be utilised for rehabilitation. It was found that the final design has the potential to provide a holding force of 18.894 N and a contraction force of 6.838 N.

A basis for an orthosis design which used a set of these magnetic fluid muscles working in parallel was then laid out and found to have the potential to be able to account for between 15.54% and 42.94% of the torque disparity across the knee for extension and 25.71% and 71.03% of the torque for flexion, dependant on whether the holding force or contraction force was used. While further work would be needed to fully design and test an orthosis such as this the current research fulfils **Objective 3**.

7.2. Contributions

The key contributions of this research were:

- The targeting effect and its impact on gait analysis collection for hemiparetic stroke survivors has been quantified and found to be significant for spatiotemporal and kinetic parameters though no significant effect was found on kinematic parameters
- The relationships between walking speed and the hemiparetic gait pattern have been explored in further detail than previous studies due to application of the Linear Fit method. This has shown that some stroke survivors may be able to achieve higher walking speeds using compensatory gait patterns and these gait patterns can be described by comparing the joint's kinematic waveform against a healthy average.
- A simple and novel design for a magnetic fluid muscle has been introduced that builds upon the work already carried out on smart materials and PAM's.
- An FEA model has been designed and validated that can be used to examine the magnetic fluid muscle design, combining a magnetic field, the induced magnetic fluid boundary stress and hyperelastic materials modelling.
- An improved magnetic fluid muscle has been detailed and explored using the aforementioned FEA model, showing how such a design could be iterated on and giving initial insight into the muscle's potential for use in robotic gait rehabilitation

7.3. Future Work

Chapter 3 demonstrates that there is still dispute within the area of research of the targeting effect. Further work could be carried out with a larger sample size however, such work should also consider other populations of interest to gait analysis. As well hemiparesis, gait abnormalities caused by cerebral palsy, multiple sclerosis and spinal injuries could be misrepresented in gait analysis due to the targeting effect.

While Chapter 4 explored how compensatory hemiparetic gait patterns can be related to higher walking speeds there remains the potential for a more in-depth study. Research with a larger pool of participants would improve the study's power and if a wider range of stroke survivors were recruited then further breakdowns based off of time since stroke event, method of rehabilitation and hemiparesis side could be carried out.

Chapters 5 and 6 introduced the concept of the magnetic fluid muscle and demonstrated an FEA model that approximates its real-world behaviour. However, aspects of the current design remain unexplored, such as the impact of the braided sleeve on the change in length, that will be required to produce a full orthosis design based on this technology. Further improvements to the design itself could also be made.

The introduction of the enclosed electromagnet increased muscle deformation but removed the useful compliance of a length of the muscle. Designs that utilise flexible electromagnet cores or otherwise shorten the area of the muscle covered by the rigid electromagnet could increase the functionality of this device and are worth exploring.

Finally, testing with an orthosis based on this technology or other soft robotics with aims to target the areas highlighted in Chapter 4 would require a suitable control scheme to be implemented that works as an advanced form of Path Control and is personalised to the user's current abilities.

References

1. Mehrholz J, Thomas S, Kugler J, Pohl M, Elsner B. Electromechanical-assisted training for walking after stroke. Cochrane database of systematic reviews. 2020(10).
2. Pennycott A, Wyss D, Vallery H, Klamroth-Marganska V, Riener R. Towards more effective robotic gait training for stroke rehabilitation: a review. Journal of neuroengineering and rehabilitation. 2012;9(1):1-13.
3. Masiero S, Poli P, Rosati G, Zanotto D, Iosa M, Paolucci S, et al. The value of robotic systems in stroke rehabilitation. Expert review of medical devices. 2014;11(2):187-98.
4. Dobkin BH. Strategies for stroke rehabilitation. The Lancet Neurology. 2004;3(9):528-36.
5. Duschau-Wicke A, Von Zitzewitz J, Caprez A, Lunenburger L, Riener R. Path control: a method for patient-cooperative robot-aided gait rehabilitation. IEEE Transactions on Neural Systems and Rehabilitation Engineering. 2009;18(1):38-48.
6. Duschau-Wicke A, Zitzewitz Jv, Lünenburger L, Riener R, editors. Patient-driven cooperative gait training with the rehabilitation robot lokomat. 4th European Conference of the International Federation for Medical and Biological Engineering; 2009: Springer.
7. Hassid E, Rose D, Commisarow J, Guttry M, Dobkin BH. Improved gait symmetry in hemiparetic stroke patients induced during body weight-supported treadmill stepping. Journal of neurologic rehabilitation. 1997;11(1):21-6.
8. Balasubramanian CK, Bowden MG, Neptune RR, Kautz SA. Relationship between step length asymmetry and walking performance in subjects with chronic hemiparesis. Archives of physical medicine and rehabilitation. 2007;88(1):43-9.
9. Mayo NE, Wood-Dauphinee S, Coˆte R, Durcan L, Carlton J. Activity, participation, and quality of life 6 months poststroke. Archives of physical medicine and rehabilitation. 2002;83(8):1035-42.
10. Barclay R, Ripat J, Mayo N. Factors describing community ambulation after stroke: a mixed-methods study. Clinical rehabilitation. 2015;29(5):509-21.
11. Bijleveld-Uitman M, van de Port I, Kwakkel G. Is gait speed or walking distance a better predictor for community walking after stroke? Journal of rehabilitation medicine. 2013;45(6):535-40.
12. Michael KM, Allen JK, Macko RF. Reduced ambulatory activity after stroke: the role of balance, gait, and cardiovascular fitness. Archives of physical medicine and rehabilitation. 2005;86(8):1552-6.
13. van de Port IG, Kwakkel G, Lindeman E. Community ambulation in patients with chronic stroke: how is it related to gait speed? Journal of rehabilitation medicine. 2008;40(1):23-7.

14. Shin SY, Lee RK, Spicer P, Sulzer J. Does kinematic gait quality improve with functional gait recovery? A longitudinal pilot study on early post-stroke individuals. Journal of Biomechanics. 2020;105:109761.
15. Huitema RB, Hof AL, Mulder T, Brouwer WH, Dekker R, Postema K. Functional recovery of gait and joint kinematics after right hemispheric stroke. Archives of physical medicine and rehabilitation. 2004;85(12):1982-8.
16. Rastegarpanah A. A methodology for the lower limb robotic rehabilitation system: University of Birmingham; 2016.
17. Patla AE. Understanding the roles of vision in the control of human locomotion. Gait & posture. 1997;5(1):54-69.
18. Haufe FL, Schmidt K, Duarte JE, Wolf P, Riener R, Xiloyannis M. Activity-based training with the Myosuit: a safety and feasibility study across diverse gait disorders. Journal of neuroengineering and rehabilitation. 2020;17(1):1-11.
19. Awad LN, Esquenazi A, Francisco GE, Nolan KJ, Jayaraman A. The ReWalk ReStore™ soft robotic exosuit: a multi-site clinical trial of the safety, reliability, and feasibility of exosuit-augmented post-stroke gait rehabilitation. Journal of neuroengineering and rehabilitation. 2020;17(1):1-11.
20. Tu Cong T, Tran Thien P. - Neural Network Control of Pneumatic Artificial Muscle Manipulator for Knee Rehabilitation. 2008;- 11(- 3).
21. Nguyen HT, Trinh VC, Le TD. An Adaptive Fast Terminal Sliding Mode Controller of Exercise-Assisted Robotic Arm for Elbow Joint Rehabilitation Featuring Pneumatic Artificial Muscle Actuator. Actuators. 2020;9(4):118.
22. Beyl P, Van Damme M, Van Ham R, Vanderborght B, Lefeber D. Pleated pneumatic artificial muscle-based actuator system as a torque source for compliant lower limb exoskeletons. IEEE/ASME Transactions on Mechatronics. 2013;19(3):1046-56.
23. Xiloyannis M, Alicea R, Georgarakis A-M, Haufe FL, Wolf P, Masia L, et al. Soft robotic suits: State of the art, core technologies, and open challenges. IEEE Transactions on Robotics. 2021.
24. Iida F, Laschi C. Soft robotics: Challenges and perspectives. Procedia Computer Science. 2011;7:99-102.
25. Cianchetti M, Laschi C, Menciassi A, Dario P. Biomedical applications of soft robotics. Nature Reviews Materials. 2018;3(6):143-53.
26. Miller E, Kaufman K, Kingsbury T, Wolf E, Wilken J, Wyatt M. Mechanical testing for three-dimensional motion analysis reliability. Gait Posture. 2016;50:116-9.
27. Pfister A, West AM, Bronner S, Noah JA. Comparative abilities of Microsoft Kinect and Vicon 3D motion capture for gait analysis. J Med Eng Technol. 2014;38(5):274-80.
28. Simon SR. Quantification of human motion: gait analysis-benefits and limitations to its application to clinical problems. J Biomech. 2004;37(12):1869-80.

29. Oggero E, Pagnacco G, Morr DR, Simon SR, Berme N. Probability of valid gait data acquisition using currently available force plates. Biomedical sciences instrumentation. 1997;34:392-7.
30. Grabiner M, Feuerbach J, Lundin T, Davis B. Visual guidance to force plates does not influence ground reaction force variability. Journal of biomechanics. 1995;28(9):1115-7.
31. Wearing SC, Urry SR, Smeathers JE. The effect of visual targeting on ground reaction force and temporospatial parameters of gait. Clinical biomechanics. 2000;15(8):583-91.
32. Verniba D, Vergara ME, Gage WH. Force plate targeting has no effect on spatiotemporal gait measures and their variability in young and healthy population. Gait & posture. 2015;41(2):551-6.
33. Mendis S. Stroke disability and rehabilitation of stroke: World Health Organization perspective. Int J stroke. 2013;8(1):3-4.
34. Lawrence ES, Coshall C, Dundas R, Stewart J, Rudd AG, Howard R, et al. Estimates of the prevalence of acute stroke impairments and disability in a multiethnic population. Stroke. 2001;32(6):1279-84.
35. Party ISW, Henssge U, Hoffman A, Kavanagh S, Roughton M, Rudd A, et al. National sentinel stroke audit 2010 round 7. London, UK: Royal College of Physicians of London. 2011.
36. Hackett ML, Pickles K. Part I: frequency of depression after stroke: an updated systematic review and meta-analysis of observational studies. International Journal of Stroke. 2014;9(8):1017-25.
37. Kesikburun S, Yavuz F, Güzelküçük Ü, Yaşar E, Balaban B. Effect of ankle foot orthosis on gait parameters and functional ambulation in patients with stroke. Turkish Journal of Physical Medicine and Rehabilitation. 2017;63(2):143.
38. Wright RL, Bevins JW, Pratt D, Sackley CM, Wing AM. Metronome cueing of walking reduces gait variability after a cerebellar stroke. Frontiers in neurology. 2016;7:84.
39. Gama GL, Celestino ML, Barela JA, Forrester L, Whitall J, Barela AM. Effects of gait training with body weight support on a treadmill versus overground in individuals with stroke. Archives of physical medicine and rehabilitation. 2017;98(4):738-45.
40. Punt M, Bruijn SM, Wittink H, van de Port IG, Van Dieën JH. Do clinical assessments, steady-state or daily-life gait characteristics predict falls in ambulatory chronic stroke survivors? Journal of Rehabilitation Medicine. 2017;49(5):402-9.
41. Fulk GD, Reynolds C, Mondal S, Deutsch JE. Predicting home and community walking activity in people with stroke. Archives of physical medicine and rehabilitation. 2010;91(10):1582-6.
42. Husaini B, Levine R, Sharp L, Cain V, Novotny M, Hull P, et al. Depression increases stroke hospitalization cost: an analysis of 17,010 stroke patients in 2008 by race and gender. Stroke research and treatment. 2013;2013.

43. Kim CM, Eng JJ. Magnitude and pattern of 3D kinematic and kinetic gait profiles in persons with stroke: relationship to walking speed. Gait & posture. 2004;20(2):140-6.
44. Balaban B, Tok F. Gait disturbances in patients with stroke. Pm&r. 2014;6(7):635-42.
45. TekScan. The Gait Cycle: Phases, Parameters to Evaluate & Technology 2022 [Available from: https://www.tekscan.com/blog/medical/gait-cycle-phases-parameters-evaluate-technology.]
46. Jacquelin Perry M. Gait analysis: normal and pathological function. New Jersey: SLACK. 2010.
47. Cappellini G, Ivanenko YP, Poppele RE, Lacquaniti F. Motor patterns in human walking and running. Journal of neurophysiology. 2006;95(6):3426-37.
48. Chau T. A review of analytical techniques for gait data. Part 2: neural network and wavelet methods. Gait & posture. 2001;13(2):102-20.
49. Iosa M, Cereatti A, Merlo A, Campanini I, Paolucci S, Cappozzo A. Assessment of waveform similarity in clinical gait data: the linear fit method. BioMed Research International. 2014;2014.
50. Horsak B, Pobatschnig B, Baca A, Greber-Platzer S, Kreissl A, Nehrer S, et al. Within-assessor reliability and minimal detectable change of gait kinematics in a young obese demographic. Gait & Posture. 2017;54:112-8.
51. Castelli A, Paolini G, Cereatti A, Della Croce U. A 2D markerless gait analysis methodology: validation on healthy subjects. Computational and mathematical methods in medicine. 2015;2015.
52. Al-Amri M, Nicholas K, Button K, Sparkes V, Sheeran L, Davies JL. Inertial measurement units for clinical movement analysis: Reliability and concurrent validity. Sensors. 2018;18(3):719.
53. Díaz I, Gil JJ, Sánchez E. Lower-limb robotic rehabilitation: literature review and challenges. Journal of Robotics. 2011;2011.
54. Peshkin M, Brown DA, Santos-Munné JJ, Makhlin A, Lewis E, Colgate JE, et al., editors. KineAssist: A robotic overground gait and balance training device. 9th International Conference on Rehabilitation Robotics, 2005 ICORR 2005; 2005: IEEE.
55. Nelles G. Cortical reorganization–effects of intensive therapy. Restorative neurology and neuroscience. 2004;22(3-5):239-44.
56. Eng JJ, Tang P-F. Gait training strategies to optimize walking ability in people with stroke: a synthesis of the evidence. Expert review of neurotherapeutics. 2007;7(10):1417-36.
57. Belda-Lois J-M, Mena-del Horno S, Bermejo-Bosch I, Moreno JC, Pons JL, Farina D, et al. Rehabilitation of gait after stroke: a review towards a top-down approach. Journal of neuroengineering and rehabilitation. 2011;8(1):1-20.
58. Levack WM, Taylor K, Siegert RJ, Dean SG, McPherson KM, Weatherall M. Is goal planning in rehabilitation effective? A systematic review. Clinical rehabilitation. 2006;20(9):739-55.

59. Guadagnoli MA, Lee TD. Challenge point: a framework for conceptualizing the effects of various practice conditions in motor learning. Journal of motor behavior. 2004;36(2):212-24.
60. Hesse S, Uhlenbrock D. A mechanized gait trainer for restoration of gait. Journal of rehabilitation research and development. 2000;37(6):701-8.
61. Colombo G, Joerg M, Schreier R, Dietz V. Treadmill training of paraplegic patients using a robotic orthosis. Journal of rehabilitation research and development. 2000;37(6):693-700.
62. Jezernik S, Colombo G, Keller T, Frueh H, Morari M. Robotic orthosis lokomat: A rehabilitation and research tool. Neuromodulation: Technology at the neural interface. 2003;6(2):108-15.
63. Dobkin BH, Duncan PW. Should body weight–supported treadmill training and robotic-assistive steppers for locomotor training trot back to the starting gate? Neurorehabilitation and neural repair. 2012;26(4):308-17.
64. Takeuchi N, Izumi S-I. Rehabilitation with poststroke motor recovery: a review with a focus on neural plasticity. Stroke research and treatment. 2013;2013.
65. Langhorne P, Bernhardt J, Kwakkel G. Stroke rehabilitation. The Lancet. 2011;377(9778):1693-702.
66. Morone G, Paolucci S, Cherubini A, De Angelis D, Venturiero V, Coiro P, et al. Robot-assisted gait training for stroke patients: current state of the art and perspectives of robotics. Neuropsychiatric disease and treatment. 2017;13:1303.
67. Polygerinos P, Correll N, Morin SA, Mosadegh B, Onal CD, Petersen K, et al. Soft robotics: Review of fluid-driven intrinsically soft devices; manufacturing, sensing, control, and applications in human-robot interaction. Advanced Engineering Materials. 2017;19(12):1700016.
68. Joshi A, Kulkarni A, Tadesse Y. FludoJelly: Experimental study on jellyfish-like soft robot enabled by soft pneumatic composite (SPC). Robotics. 2019;8(3):56.
69. Tondu B. Modelling of the McKibben artificial muscle: A review. Journal of Intelligent Material Systems and Structures. 2012;23(3):225-53.
70. Belforte G, Eula G, Ivanov A, Sirolli S, editors. Soft pneumatic actuators for rehabilitation. Actuators; 2014: MDPI.
71. Takashima K, Rossiter J, Mukai T. McKibben artificial muscle using shape-memory polymer. Sensors and Actuators A: Physical. 2010;164(1-2):116-24.
72. Takosoglu JE, Laski PA, Blasiak S, Bracha G, Pietrala D. Determining the static characteristics of pneumatic muscles. Measurement and Control. 2016;49(2):62-71.
73. Yap HK, Lim JH, Nasrallah F, Cho Hong Goh J, Yeow CH. Characterisation and evaluation of soft elastomeric actuators for hand assistive and rehabilitation applications. J Med Eng Technol. 2016;40(4):199-209.
74. Whitesides GM. Soft robotics. Angewandte Chemie International Edition. 2018;57(16):4258-73.

75. Pan M, Yuan C, Liang X, Dong T, Liu T, Zhang J, et al. Soft Actuators and Robotic Devices for Rehabilitation and Assistance. Advanced Intelligent Systems. 2022;4(4):2100140.
76. Park G, Erturk A, Han J-H, editors. Active and Passive Smart Structures and Integrated Systems 2017. Proc of SPIE Vol; 2017.
77. Li Y, Hashimoto M. PVC gel soft actuator-based wearable assist wear for hip joint support during walking. Smart Materials and Structures. 2017;26(12):125003.
78. Bira N, Dhagat P, Davidson JR. A review of magnetic elastomers and their role in soft robotics. Frontiers in Robotics and AI. 2020;7:588391.
79. Ebrahimi N, Bi C, Cappelleri DJ, Ciuti G, Conn AT, Faivre D, et al. Magnetic actuation methods in bio/soft robotics. Advanced functional materials. 2021;31(11):2005137.
80. Stierstadt K, Liu M. Maxwell's stress tensor and the forces in magnetic liquids. ZAMM-Journal of Applied Mathematics and Mechanics/Zeitschrift für Angewandte Mathematik und Mechanik. 2015;95(1):4-37.
81. Zeng G, Xiang-yu Y, Yin H, Pei Y, Zhao S, Cao J, et al. Asynchronous machine with ferrofluid in gap: Modeling, simulation, and analysis. IEEE Transactions on Magnetics. 2019;56(1):1-4.
82. Fan X, Dong X, Karacakol AC, Xie H, Sitti M. Reconfigurable multifunctional ferrofluid droplet robots. Proceedings of the National Academy of Sciences. 2020;117(45):27916-26.
83. Ziegler M, Ochs K, Hansen M, Kohlstedt H. An electronic implementation of amoeba anticipation. Applied Physics A. 2014;114(2):565-70.
84. Chen B, Zhu Y, Zhao J, Cai H, editors. Design of a prototype of an adaptive soft robot based on ferrofluid. 2015 IEEE International Conference on Robotics and Biomimetics (ROBIO); 2015: IEEE.
85. Kirtley C. Clinical gait analysis: theory and practice: Elsevier Health Sciences; 2006.
86. Samson MM, Crowe A, De Vreede P, Dessens JA, Duursma SA, Verhaar HJ. Differences in gait parameters at a preferred walking speed in healthy subjects due to age, height and body weight. Aging clinical and experimental research. 2001;13(1):16-21.
87. Kim H, Jo G-Y, Han N, Eom M-J, editors. Analysis of vertical ground reaction force variables by Foot scan in hemiplegic patients. Journal of Foot and Ankle Research; 2014: BioMed Central.
88. Boudarham J, Roche N, Pradon D, Bonnyaud C, Bensmail D, Zory R. Variations in kinematics during clinical gait analysis in stroke patients. PloS one. 2013;8(6):e66421.
89. Olney SJ, Richards C. Hemiparetic gait following stroke. Part I: Characteristics. Gait & posture. 1996;4(2):136-48.
90. Davis III RB, Ounpuu S, Tyburski D, Gage JR. A gait analysis data collection and reduction technique. Human movement science. 1991;10(5):575-87.

91. Rastegarpanah A, Saadat M, Borboni A, Stolkin R, editors. Application of a parallel robot in lower limb rehabilitation: A brief capability study. 2016 International Conference on Robotics and Automation for Humanitarian Applications (RAHA); 2016: IEEE.
92. Maddalena M, Saadat M, Rastegarpanah A, Loureiro RC, editors. An optimized design of a parallel robot for gait training. 2017 International Conference on Rehabilitation Robotics (ICORR); 2017: IEEE.
93. FerroTec. EMG 900 Series - Safety Data Sheet. Rev. E ed2021.
94. Holzapfel GA. Nonlinear solid mechanics: a continuum approach for engineering science. Meccanica. 2002;37(4):489-90.
95. Pressman A. Switching power supply design: McGraw-Hill Education; 2009.
96. Patil A, Nordmark A, Eriksson A. Instabilities of wrinkled membranes with pressure loadings. Journal of the Mechanics and Physics of Solids. 2016;94:298-315.
97. Hunter IW, Lafontaine S, editors. A comparison of muscle with artificial actuators. Technical Digest IEEE solid-state sensor and actuator workshop; 1992: IEEE.
98. Blank AA, French JA, Pehlivan AU, O'Malley MK. Current trends in robot-assisted upper-limb stroke rehabilitation: promoting patient engagement in therapy. Current physical medicine and rehabilitation reports. 2014;2(3):184-95.
99. Kim CM, Eng JJ. The relationship of lower-extremity muscle torque to locomotor performance in people with stroke. Physical therapy. 2003;83(1):49-57.

Appendix A. Publications by the Author

Peer-reviewed Journal Papers

1 - Rastegarpanah A, Scone T, Saadat M, Rastegarpanah M, Taylor SJ, Sadeghein N. Targeting effect on gait parameters in healthy individuals and post-stroke hemiparetic individuals. Journal of Rehabilitation and Assistive Technologies Engineering. 2018 Apr;5:2055668318766710.

2 – Scone T, Saadat M, Barton H, Rastegarpanah A. Effects of Variations in Hemiparetic Gait Patterns on Improvements in Walking Speed. IRBM. 2023 Feb 1;44(1):100733.